DISSERTATION

CRYO-GEOHAZARDS IN A WARMING CLIMATE: GEOPHYSICAL, HYDROLOGICAL, AND REMOTELY SENSED INVESTIGATIONS OF GLACIAL LAKES, OUTBURST FLOODS, AND ROCK GLACIERS

Submitted by

Brianna Rick

Department of Geosciences

In partial fulfillment of the requirements

For the Degree of Doctor of Philosophy

Colorado State University

Fort Collins, Colorado

Fall 2022

Doctoral Committee:

Advisor: Daniel McGrath

Sara Rathburn
Julia Klein
Scott McCoy

ABSTRACT

CRYO-GEOHAZARDS IN A WARMING CLIMATE: GEOPHYSICAL, HYDROLOGICAL, AND REMOTELY SENSED INVESTIGATIONS OF GLACIAL LAKES, OUTBURST FLOODS, AND ROCK GLACIERS

Changes to the cryosphere impact both societal and ecological communities, and understanding where changes have occurred in the past allow us to predict changes in the future, and help in creating plans to minimize or alleviate potential societal stressors. The overarching goal of this dissertation was to explore changes to the cryosphere at varying spatial and temporal scales, utilizing a range of methods from in situ measurements to large-scale remote sensing, exploring seasonal to annual to decadal scale changes. I investigated ice-marginal lake changes in Alaska (Chapter 2), documented ice-dammed lake drainages in Alaska (Chapter 3), and explored the hydrological influence of the Lake Agnes rock glacier in Colorado (Chapter 4).

Ice-marginal lakes impact glacier mass balance, water resources, and ecosystem dynamics, and can produce catastrophic glacial lake outburst floods (GLOFs). Multitemporal inventories of ice-marginal lakes are a critical first step in understanding the drivers of historic change, predicting future lake evolution, and assessing GLOF hazards. In Chapter 2, I used Landsat satellite imagery and supervised classification to semi-automatically delineate lake outlines for four, ~5-year time periods between 1984 and 2019 in Alaska and northwest Canada. Overall, ice-marginal lakes in the region have grown in total number (+183 lakes, 38% increase) and area (+483 km^2, 59% increase) between the time periods of 1984–1988 and 2016–2019, though 56% of inventoried lakes did not experience detectable change. Changes in lake numbers

and area were notably unsteady and nonuniform. I demonstrated that lake area changes are connected to dam type (moraine, bedrock, ice, or supraglacial) and the spatial relationship to their source glacier (proglacial, detached, unconnected, ice, or supraglacial), with important differences in lake behavior between the sub-groups. In strong contrast to all other dam types, ice-dammed lakes decreased in number (–6, 9% decrease) and area (–51 km^2, 40% decrease), while moraine-dammed lakes increased (+56, 26% and +479 km^2, 87% for number and area, respectively) at a faster rate than the average when considering all dam types together. Proglacial lakes experienced the largest area changes and rate of change out of any lake position throughout the period of study, and moraine-dammed lakes experienced the largest increases. Moraine-dammed lakes with large growth are also associated with clean-ice glaciers (<19% debris cover). By tracking individual lakes through time and categorizing lakes by dam type, subregion, and location, I detected trends that would otherwise be obscured if these characteristics were not considered. Chapter 2 highlights the importance of including lake characteristics when performing ice-marginal lake inventories, and provides insight into the physical processes driving recent ice-marginal lake evolution.

Chapter 3 focuses specifically on ice-dammed lakes, as the glacial lake outburst flood record is dominated by these types of lakes, yet as I found in Chapter 2, ice-dammed lakes are decreasing in number and area. Rapid lake drainage (on the order of hours to days) can produce devastating outburst floods leading many to propose that hazards from glacial lakes are increasing. Outburst flood compilations do show an increase in number of events over time, however, recent studies attribute such trends to observational bias. This leaves large uncertainty about current and future glacial-lake hazards. Using multitemporal satellite imagery, I documented 1150 drainages from 106 lakes between 1985–2020, with an apparent increase in

event frequency from 5 in 1985 to 70 in 2020. However, accounting for the increasing number of satellite images throughout the record, I found no temporal trend in drainage frequency. Furthermore, I documented a loss of >75% of ice-dammed lakes since the 1960s. This suggests a decrease in regional flood hazard and motivates an unbiased look at other regions.

As the world deglaciates, rock glaciers are important headwater features that have a delayed response to warming. Over 10,000 rock glaciers have been mapped in the contiguous United States, and 38% of these rock glaciers are found in Colorado. North American rock glaciers are estimated to have the third largest water volume equivalent by region, though these features are an often-disregarded component of the water budget in alpine basins. In Chapter 4, I incorporated geophysical, hydrochemical, and remotely sensed data to investigate the ice presence, movement, and hydrologic influence of the Lake Agnes rock glacier in the northern Front Range, Colorado. I observed an average horizontal velocity of 17 ± 5 cm yr^{-1} between 2019 and 2021 for the active lobe. Rock glacier streams remained below 2.5 °C throughout the summer, mixed-source streams remained below 3.5 °C, and the non-rock glacier stream reached 13.5 °C. The geophysical surveys suggest an internal rock glacier structure of an active layer ~3 m thick, underlain by an ice-poor layer up to 10 m thick, underlain by an ice-rich layer up to 18 m thick, with total rock glacier thickness between 20–30 m. This study confirms the presence of ice within the Lake Agnes rock glacier and documents its influence on basin hydrochemistry, elevating ion concentrations, pH, and maintaining low stream temperatures. In basins such as the Lake Agnes basin, the reduced climate sensitivity of rock glaciers and their sustained cold-water input to mountain streams will likely provide a refuge for cold-water species in a warming climate.

ACKNOWLEDGEMENTS

This dissertation would not have been possible without immense support from colleagues, family, and friends. The work presented here is a culmination of collaborations to which I owe immense gratitude.

First and foremost, I'd like to thank my advisor, Dan McGrath, for taking a chance on me as your first PhD student and being willing to figure things out together. Thank you for being incredibly supportive throughout the entire process, trusting me to work independently, and for your never ending positive and forward outlook. I am incredibly grateful for all the experiences you helped facilitate and I could never thank you enough.

Thank you to my committee members, Scott McCoy, Sara Rathburn, and Julia Klein for your invaluable feedback and guidance at each step along the way. Thank you to Scott McCoy and Billy Armstrong for close collaborations—I have enjoyed working with both of you and your insight and discussions made Chapters 2 and 3 possible.

I'd also like to thank the CryoCrew, Randall Bonnell, Lucas Zeller, and Wyatt Reis for everything from figure feedback to days in the field to pleasant human interactions while in the midst of a pandemic. I have enjoyed working with each of you immensely.

Chapter 4 would not have been possible without a multitude of helpers. A special thank you to Russell Callahan, Megan Thompson-Munson, Brad Carr, and Randall Bonnell for help with the geophysics, Tim Fegel and Jeremy Caves Rugenstein for help processing and interpreting the hydrochemistry, and Benjamin Lehmann, Bob Anderson, and Susanne Anderson for many discussions about Colorado rock glaciers. Thank you to Hank Cole, Johanna Eidmann,

Arielle Koshkin, Caitlyn Florentine, Paddy Ball, Jessi Rick, Kathryn Moore, Holly Proulx, Anna Marshall, Leah Cromer, Lewis Faller, and many many others for help collecting water samples, carrying heavy equipment, and entertaining me in the field.

Thank you to both the Fort Collins and Laramie ultimate frisbee communities for keeping me active, entertained, and sane throughout this process.

Thank you to all my family and friends both near and far for the many phone calls (both answered and unanswered), the elaborate schemes to adventure with one another, and the constant support. To my sister, Jessi, for helping pave the way and providing guidance at nearly every step, including many Zoom calls working through my R code with me.

To my pup, Josie, who has been my constant companion the last 2.5 years, reminding me to play hard, nap hard, and always find moments to soak up the sun. And to my partner, Lewis, thank you for all your companionship and support.

I am incredibly grateful for the funding for my PhD, through the Ed Warner Graduate Research fellowship and the National Science Foundation Graduate Research Fellowship under Grant No. 006784-00002. My research was also funded by the American Alpine Club, the Geological Survey of America, and the Tobacco Root Geological Society.

TABLE OF CONTENTS

LIST OF TABLES

LIST OF FIGURES

1. INTRODUCTION

Over the past century, Arctic and alpine environments have warmed at among the fastest rates on the planet (Hansen et al., 2010; Pepin et al., 2015), leading to pronounced physical and ecological impacts (Nitze et al., 2018). Some of the most significant and visible of these changes have occurred in the cryosphere, including the loss of Arctic sea ice (Onarheim et al., 2018), decreasing extent of seasonal snow (Mote et al., 2018), mass losses from mountain glaciers (Hugonnet et al., 2021) and the Greenland Ice Sheet (Box et al., 2018), and widespread permafrost degradation (Gruber and Haeberli, 2007). Between 2000 and 2019, glaciers lost 267 ± 16 gigatons per year, contributing 0.74 ± 0.04 mm to sea level rise per year, which is equivalent to ~20% of observed sea level rise (Hugonnet et al., 2021). Additionally, winter Arctic sea ice loss has accelerated from –2.4% per decade between 1979 to 1999 to –3.4% per decade from 2000 to 2018 (Stroeve and Notz, 2018). While these environments are often far removed, the magnitude and rate of these changes have profound impacts at local to global scales, from local hazards to downstream water resource to global sea level rise (Huss et al., 2017).

Mountains are often referred to as the “water towers of the world”, storing important water supplies in snowpack, glaciers, and permafrost (Immerzeel et al., 2020). Mountain snowpack-derived meltwater sustains vibrant alpine ecosystems and provides key water resources to more than 1.2 billion people globally (Barnett et al., 2005). In many places, these snowpacks are diminishing in both total amount and duration due to warming air temperatures (Mote et al., 2018), creating a potential stressor for downstream communities and ecosystems. Similarly, glaciers provide key water resources, particularly after the melt of the seasonal snowpack (Immerzeel et al., 2020). In basins where glaciers are predicted to disappear, the

presence or absence of permafrost features, such as rock glaciers, will likely dictate the magnitude of ecological disturbance. Cryospheric features help regulate stream temperatures (e.g., Leopold et al., 2015), provide habitat (e.g., Millar and Westfall, 2010), and maintain late season streamflow (e.g., Caine, 2010). Additionally, as glaciers retreat, over-deepened basins or moraine dams can form lakes, creating sediment traps which alter downstream sediment and nutrient supply (Bogen et al., 2015). Conversely, if a lake dam fails and shifts from a lacustrine to fluvial system, downstream sediment and nutrient supply would increase (Milner et al., 2017). Changes in habitat test resilience, and the magnitude of these changes, as well as species adaptability, will likely determine the survival of species in a warming climate (Hotaling et al., 2019).

Mountain regions provide important ecosystem services to both local and distant communities (Klein et al., 2019). Changes to the cryosphere impact the immediate area through hazards which can threaten infrastructure, lives, and livelihoods, and to the downstream area through changes to energy production and water resources, which are relied upon for agriculture and therefore food security (Huss et al., 2017). Understanding where changes have occurred in the past allow us to predict changes in the future, and help in creating plans to minimize or alleviate potential societal stressors.

Ice is a key, and highly sensitive, component of the structural integrity of many landforms in Arctic and alpine environments, and thus warming temperatures have decreased the stability of these features (e.g., glaciers, permafrost, moraines, headwalls; Allen et al., 2017). Natural hazards resulting from this decreased stability are considered “cryo-geohazards” and include landslides, avalanches, rock glacier debris flows, rockfall events, and glacial lake outburst floods (GLOFs).

Cryo-geohazards have always existed where snow and ice are present, but frequency and magnitude have changed due to increasing temperatures, and societal perception has likely changed due to an increase in the volume of human traffic in remote areas (Allen et al., 2017). Events such as glacier detachments (e.g., Jacquemart et al., 2020), landslides, and rockfall may go unnoticed without any people or instruments to capture an event, but the increase in high-resolution satellite imagery, monitoring equipment, and even personal videoing capabilities increase our ability to document such events (e.g., Shugar et al., 2021) and result in a perceived, and often real, increase in dramatic scenarios.

For example, within one week in July 2022, two different glacier detachments were documented, one in the Dolomites in Italy (Phillis, 2022) and another in the Tian Shan mountains in Kyrgystan (Patel, 2022a). Both events occurred during heat waves, reaching 10–15 °C at the summit. The event in Italy killed 11 people, as this area is a popular tourist destination with hiking trails beneath the glacier. In early May 2022, a flood from a glacier-dammed lake in response to warm temperatures flooded a village, destroyed a bridge, and caused tens of million in property damages in Pakistan (Patel, 2022b). The heat dome of June 2021 in the Pacific Northwest and western Canada caused a large cryospheric response, with extreme melt features and hydrologic discharge exceeding seasonal records (Menounos et al., 2021). This event caused the rapid melting of snow and thawing of permafrost such that a large rock avalanche cascaded more than 5 km onto the Canoe Glacier (Menounos et al., 2021). While events such as glacier detachments, GLOFs, and rock avalanches are not new, heat waves — which are an impetus for each of these events — have steadily increased since the 1950s (Perkins-Kirkpatrick and Lewis, 2020). Our ability to observe has also improved, and remarkable videos and instantaneous monitoring lead to much larger global attention. While there have been documented and

predicted increases in the frequency of cryo-geohazards (e.g., Zheng et al., 2021; Veh et al., 2022), an important consideration is what role observational bias plays in documented increases.

We can observe the cryosphere at varying spatial and temporal scales, from in-situ small-scale measurements (e.g., Leopold et al., 2015) to multi-temporal worldwide monitoring and modeling (e.g., Farinotti et al., 2019; Hugonnet et al., 2021). Before the use of satellites to observe Earth, observations were limited to in-situ measurements or aerial imagery. Regional studies required manual interpretation of hundreds of images (e.g., Post and Mayo, 1971). The introduction of public access to satellite imagery in the 1970s made regional or global scale studies possible, but still required relatively large storage and computing power. In more recent years, increases in storage and computing efficiency, as well as the introduction of cloud-computing tools such as Google Earth Engine (e.g., Amani et al., 2020), allow researchers to investigate the full satellite timeseries, a uniquely long record with near-global spatial coverage. Even within this record, however, increases in spatial and temporal resolution create an observational bias, with increasing resolution and frequency towards the present (Veh et al., 2022). In addition to satellite imagery, ease and access to small-scale, high-resolution aerial imagery has greatly increased in the recent years. Rather than chartering a flight, researchers are able to acquire high resolution imagery from uncrewed aerial vehicles (UAVs), making high resolution and high accuracy models and repeat surveys more accessible (e.g., Dall'Asta et al., 2017; Kienholz et al., 2020).

Arctic and alpine environments are often in remote locations and can cover large spatial extents. For example, 22% of the Northern Hemisphere is underlain by permafrost (Obu et al., 2019), and over 87,000 km^2 of glacial ice persists just in Alaska and Northwest Canada (RGI, 2017). As these environments are changing at some of the fastest rates globally, the many

decades of satellite records allow access into the past for detecting change over time. Landscape changes include everything from vegetation growth to deforestation to urbanization to river channel migration. Cryo-geohazard events can also be detected as an event often results in a permanent change. For example, a landslide, glacier detachment, or rockfall are all mass movements, and the size of the movement (i.e., cm, m, km) and rate of change (i.e., hours, days, years) determines the spatial and temporal resolution necessary to detect such an event.

While remote sensing is an incredibly valuable tool for larger spatial and temporal extents, it cannot replace in-situ measurements for understanding what is occurring on the ground. Measurements of the cryosphere such as snow depth and snowpack stratigraphy (e.g., Nolin, 2010), water quality of glacier and rock glacier fed streams (e.g., Caine, 2010; Fegel et al., 2016), and depth to permafrost (e.g., Streletskiy et al., 2017) cannot (in some cases, yet) be completely replaced by remote sensing, and therefore choosing the correct tool to address a specific question is critical when observing the cryosphere.

Within this dissertation, I explore changes to the cryosphere at varying spatial and temporal scales, utilizing a range of methods from in situ measurements to large-scale remote sensing, exploring seasonal to annual to decadal scale changes. This work also spans geographically from the alpine of northern Colorado to the thousands of square kilometers adjacent to glaciers in Alaska.

Ice-marginal lakes impact glacier mass balance, water resources, and ecosystem dynamics, and can produce catastrophic glacial lake outburst floods (GLOFs). Chapter 2 examines decadal scale changes of ice-marginal lakes in Alaska, exploring the role of dam type and lake location in lake area changes. I used multi-temporal satellite imagery to semi-automatically delineate lake outlines between 1984 and 2019 in Alaska and northwest Canada, classifying each lake by dam

type and location. This chapter provides the first comprehensive multi-temporal inventory for the region, highlights the importance of lake characterizations when performing ice-marginal lake inventories, and provides insight into the physical processes driving recent ice-marginal lake evolution.

As ice retreats due to climate change, glacial lakes can form and grow. Rapid lake drainage can produce devastating outburst floods leading to downstream ecological and societal impacts. Chapter 3 focuses on ice-dammed lakes in Alaska and northwest Canada, using multi-temporal satellite imagery to document lake drainages between 1985–2020. However, these types of drainages can be difficult to observe, and the availability of satellite images since the 1980s and recent advancement in and accessibility of high-powered computing allow for large scale assessments over time. This chapter addresses the important question of observational bias in long term changes.

Rock glaciers are important headwater features in a deglaciating world, with a delayed response to current and future warming. Chapter 4 explores the influence of the Lake Agnes rock glacier in an alpine basin, combing geophysical, hydrological, and remotely sensed datasets to investigate the ice presence, movement, and hydrologic influence of this rock glacier in the northern Front Range, Colorado. As glaciers disappear, subterranean ice – such as is present within active rock glaciers—will likely play a greater role in maintaining cold streams in a warming climate and provide refuge for organisms dependent on such streams for habitat.

2. DAM TYPE AND LAKE POSITION CHARACTERIZE ICE-MARGINAL LAKE AREA CHANGE IN ALASKA AND NW CANADA BETWEEN 1984 AND 2019[1]

2.1 INTRODUCTION

Ice-marginal lakes are located adjacent to glaciers, commonly forming at glacier termini, tributary junctions, along glacier margins, or where glacially eroded bedrock or sediment creates topographic depressions (overdeepenings; Carrivick and Tweed, 2013; Cook and Quincey, 2015). These lakes can impact human societies in a multitude of ways, ranging from water resources (Immerzeel et al., 2020) and tourist attractions (Wang and Zhou, 2019; Welling et al., 2020) to destructive and lethal hazards (Carrivick and Tweed, 2016; Cook et al., 2016; Emmer, 2017). Formation or drainage of lakes can impact ecosystem dynamics by providing or removing a source of stored freshwater, altering the sediment flux within a basin, creating new habitat (e.g., Milner et al., 2008), or altering downstream flow characteristics (Tweed and Carrivick, 2015; Jacquet et al., 2017). Glacial lake outburst floods (GLOFs; when a lake dam fails or is overtopped; Clague and Evans, 2000) from ice-marginal lakes can have massive impacts on downstream river channel morphology and sediment supply (e.g., Jacquet et al., 2017), disrupt ecosystems (e.g., Meerhoff et al., 2018), destroy infrastructure, and cause the loss of human lives (e.g., Carrivick and Tweed, 2016). Time-varying inventories of ice-marginal lakes are a critical first step in predicting future lake evolution and assessing GLOF hazards.

Global (Shugar et al., 2020) and regional (Wang et al., 2013; Carrivick and Quincey, 2014; Glasser et al., 2016; Nie et al., 2017; Song et al., 2017; Emmer et al., 2020) lake

[1]Chapter published as Rick, B., McGrath, D., Armstrong, W., and McCoy, S. W.: Dam type and lake location characterize ice-marginal lake area change in Alaska and NW Canada between 1984 and 2019, *The Cryosphere*, 16, 297–314, https://doi.org/10.5194/tc-16-297-2022, 2022.

inventories document recent increases in ice-marginal lakes, however, many studies report solely on the change in total frequency and cumulative area of lakes within the study region, or consider only one type of lake (e.g., moraine-dammed or ice-dammed). By not accounting for individual lake characteristics and individual lake changes through time, important trends could be aliased and limits the understanding of processes controlling area change. For example, if a subset of lakes grow while other lakes drain, the positive and negative growth will offset one another, and the overall lake frequency and area change would be small and therefore misleading. Alternatively, if a few large lakes dominate the documented area change for a region, applying the regionally-averaged lake growth to all lakes would overestimate growth, therefore preventing an accurate physical understanding of this change. In addition, the ecological consequences of lake changes may differ based on where lake growth occurs: a change from no lake to a 1 km^2 lake could have larger ecological and hazard implications than a large lake (e.g., >10 km^2) expanding by a few square kilometers (Dorava and Milner, 2000). Cumulative regional studies provide a first-order estimate of regional changes, however, individual lake change must be analyzed to develop a process-based understanding of area change in order to predict future lake growth and watershed-scale impacts.

Recent studies parse lakes by characteristics which predict lake behavior, such as dam type and evolution phase (Emmer et al., 2015, 2020), or the spatial relationship to their source glacier (e.g., proglacial, supraglacial, unconnected, detached; Nie et al., 2017; Rounce et al., 2017; Chen et al., 2021). In the Himalaya, proglacial lakes (located at the glacier terminus, in contact with ice) contributed to 83% of the total lake area increase from 1990 to 2015, while only composing 55% of the lake population (Nie et al., 2017). In this same region, supraglacial lakes (located on debris-covered glacier surfaces) experienced the greatest percent increase in area

(367%) since 1990, though they only constitute 1.2% of total lake area in 2015 (Nie et al., 2017). Himalayan proglacial lakes tend to be persistent and contribute the most to regional area growth, whereas supraglacial lakes are small and experience large spatio-temporal variation in area and location (Nie et al., 2017; Rounce et al., 2017; Chen et al., 2021). In the Cordillera Blanca of Peru, many lakes shifted from proglacial to detached (no longer in contact with ice) and the dominant dam type for proglacial lakes shifted from moraine-dammed in 1948 to bedrock-dammed in 2017 (Emmer et al., 2020). In both the Himalaya and the Cordillera Blanca, dam type and lake position help characterize lake behavior; this variability would be lost if only cumulative changes were reported. These studies support the inclusion of dam type and topological position (used throughout to indicate spatial relationship of lakes to their source glacier) in comprehensive regional ice-marginal lake studies.

Alaska's large glacier extent (86,723 km^2; second largest area outside the ice sheets; Fig. 1; Kienholz et al., 2015; Zemp et al., 2019) and recent retreat (Larsen et al., 2015) allow for the presence of many ice-marginal lakes, while a wide range of climate zones (maritime, transitional, continental, and Arctic; Miller et al., 1999), glacier morphologies (valleys, cirques, debris, icefields) and bedrock lithologies/surficial deposits (Wilson et al., 2015) lead to a variety of lake characteristics (e.g., dam type and topological position; Fig. 2.1). Two unique aspects of the Alaska region are the numerous large, low-elevation coastal lakes (e.g., Bear Glacier Lake, Malaspina Lake, Grand Plateau Glacier Lake), and that lakes tend to be larger than ice-marginal lakes found around the world (e.g., High Mountain Asia, Central Europe, and Alaska have median lake areas of 0.11 km^2, 0.11 km^2, and 0.17 km^2, respectively; Shugar et al., 2020). In addition, the lakes in this region are quite dynamic, as both the largest number and highest

frequency of recorded GLOFs globally have occurred here, accounting for 25% of all recorded historical events (Carrivick and Tweed, 2016).

Previous studies of glacial lakes in Alaska have examined ice-dammed lakes (Post and Mayo, 1971; Wolfe et al., 2014), a subset of ice-marginal lakes (Field et al., 2021), individual case studies (e.g., Sturm and Benson, 1985; Anderson et al., 2003; Pelto et al., 2013; Kienholz et al., 2020), or as a regional subset within a global study (Shugar et al., 2020). These studies are limited in their ability to comprehensively characterize regional trends for all lakes. Glaciers in this region are losing mass on the order of –75 Gt/yr (Larsen et al., 2015; Zemp et al., 2019), which represents the largest mass change and one of the highest specific mass changes for any region of the world. This change underscores the need for a time-varying lake inventory, given that ice-marginal lakes with different dam types and topological positions respond differently to glacier mass loss (e.g., Field et al., 2021).

The aims of the current study are to systematically inventory and characterize all ice-marginal lakes in Alaska using Landsat satellite imagery between 1984 and 2019. I aim to: (i) characterize ice-marginal lakes and decadal scale lake area change in Alaska; (ii) determine whether factors such as dam type, topological position, and region can characterize area change; and (iii) explore the interplay between the spatial distribution of lakes and regional characteristics such as glacier area, glacier complexity, and debris cover.

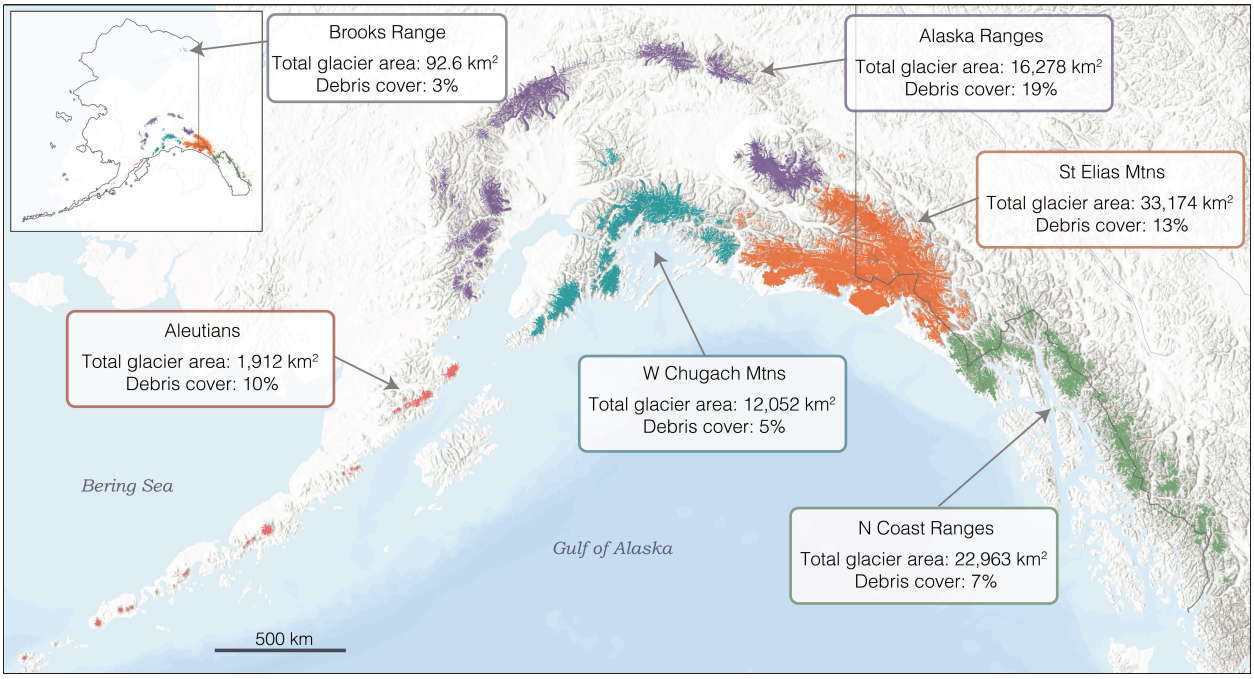

Figure 2.1. Distribution of glaciers as mapped by the Randolph Glacier Inventory (RGI Consortium, 2017) and subregions used to separate glaciated areas in Alaska and NW Canada (basemap provided by ESRI, 2021). Total glacier area (km^2) and percent debris cover (percent of glacier surface covered by debris; Herreid and Pellicciotti, 2020) are displayed for each subregion.

2.2 DATA AND METHODS

2.2.1 Imagery and datasets

Cloud-free mosaics were compiled in Google Earth Engine (GEE), an open source, web-based remote sensing platform. Landsat 5 Thematic Mapper (TM), Landsat 7 Thematic Mapper Plus (ETM+), and Landsat 8 Operational Land Imager (OLI) surface reflectance Tier 1 images were used to create 5-year composites (Table 2.1). Intervals were selected based on available imagery and to capture average lake outlines for a five-year period within each decade (1980s to 2010s). Few images are available for the late 1980s to early 1990s, and therefore this time period was excluded. Imagery was limited to a 10 km buffer around the Randolph Glacier Inventory, which was created with source imagery for glacier outlines mostly from 2004 to 2010 for Region 01 (RGI v6.0; RGI Consortium, 2017; Wang et al., 2012; Kienholz et al., 2015; Zhang et al.,

2018). For each pixel within the region of interest, the mosaicking algorithm calculates the median value of all cloud-free pixels between July 1st and September 31st for each year within the given time period (Fig. A1). Five-year mosaics minimize the impact of frequent cloud cover in Alaska, which complicates region-wide assessments on shorter timescales. In theory, 5-year composites allow for an average shoreline delineation, capturing longer term trends rather than seasonal variation. However, ice-dammed lakes are known to fill and drain on sub-annual (e.g., Lago Cachet Dos; Jacquet et al., 2017) to annual (e.g., Hidden Creek Lake; Anderson et al., 2003) timescales, so a lake may be characterized as persistent (present at every time step) even though it has undergone multiple fill/drain cycles between composites. Owing to this limitation, my focus here is on decadal changes in lake number and area, not sub-annual lake dynamics relevant for GLOF frequency.

Table 2.1. Dataset and the resolution of the dataset used for each time step.

Time interval	Dataset	Sensor	Resolution	# of images used
1984–1988	Landsat 5	ETM	30 m	683
1997–2001	Landsat 5 & 7	ETM/ETM +	30 m	1312
2007–2011	Landsat 5 & 7	ETM/ETM +	30 m	2630
2016–2019	Landsat 8	OLI	30 m	1754

2.2.2 Generating lake inventories 1984–2019

Image composites were classified in ArcGIS Pro using an object-based supervised classification (Support Vector Machine; Fig. 2.2). Manual training samples were selected for snow, ice, water, bedrock, supraglacial debris, and vegetation for each individual time step as

snow, ice, and water can vary from year to year. To reduce false positives from mountain shadows, which have a similar spectral signal as water (Fig. A3), a slope threshold of 10° was implemented (Zhang et al., 2018; Shugar et al., 2020; Chen et al., 2021). I used a digital elevation model (DEM) composed of the national elevation dataset (NED; 10 m resolution) and Worldview-derived DEMs (resampled to 10 m resolution; DEMs created by the Polar Geospatial Center from DigitalGlobe, Inc. imagery). A minimum area threshold of 0.05 km^2 (~55 pixels) excludes pixel-level noise and small lakes with minimal hydrological impact and GLOF potential (Carrivick and Quincey, 2014; How et al., 2021). Lakes with margins entirely outside a 1 km buffer from the RGI were eliminated to minimize the inclusion of lakes disconnected from a glacial system (Shugar et al., 2020). Wet, supraglacial debris bands are often misclassified as lakes, likely due to the presence of supraglacial water and therefore similar spectral properties (Fig. A4). A length to area threshold of 0.3 was implemented to remove these long and thin features with atypical lake shape. For this study, any lake within 1 km of the RGI was considered an ice-marginal lake, acknowledging that some low-lying lakes (e.g., Vitus Lake) may have tidal influence. Lakes which are within 1 km of the RGI and unconnected from a glacial system are noted (Sect. 2.2.3.2) and treated separately (Table 2.2).

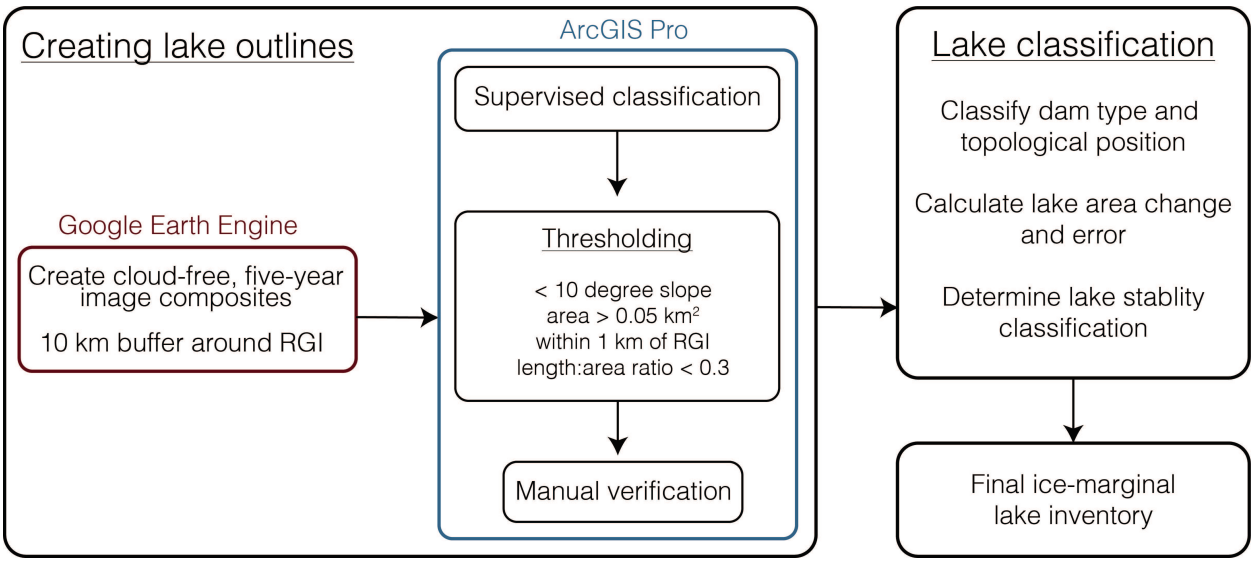

Figure 2.2. General workflow for creating the ice-marginal lake inventory for time periods 1984–1988, 1997–2001, 2007–2011, and 2016–2019.

All lake outlines were visually inspected and, if necessary, the lake margins were manually adjusted to produce a final delineation (Fig. A2). Lakes were added or excluded based on visual inspection and consideration of all four time steps together; lakes <0.05 km^2 were manually added back in if the lake grew in subsequent years to minimize false signals of lake formation. Lakes which coalesced or separated over time were given the same Lake ID to minimize misclassification of a lake forming or draining. Every lake in each time step was then classified by i) dam type (Sect. 2.2.3.1), ii) topological position (Sect. 2.2.3.2), and iii) stability (Sect. 2.2.3.3).

2.2.3 Lake characteristics

2.2.3.1 Dam type classification

Using a combination of DEMs and high-resolution satellite imagery (i.e., Maxar Technologies in Google Earth), each lake's dam type was visually interpreted and manually classified (Buckel et al., 2018). Four different dam types were identified in this study (Fig. 2.3):

i) Moraine-dammed lakes: most frequently located at the glacier terminus, impounded behind a terminal or lateral moraine (Otto, 2019);

ii) Ice-dammed lakes: located along glacier margins or within tributary valleys and blocked by glacier;

iii) Supraglacial lakes: found on the surface of the glacier, often dammed by glacier surface topography (ice or debris) within the ablation zone. For this study, I only observe supraglacial lakes within debris cover; and

iv) Bedrock-dammed lakes: frequently located in cirques with minimal remaining glacial ice, or in other overdeepenings created from glacial erosion (Otto, 2019).

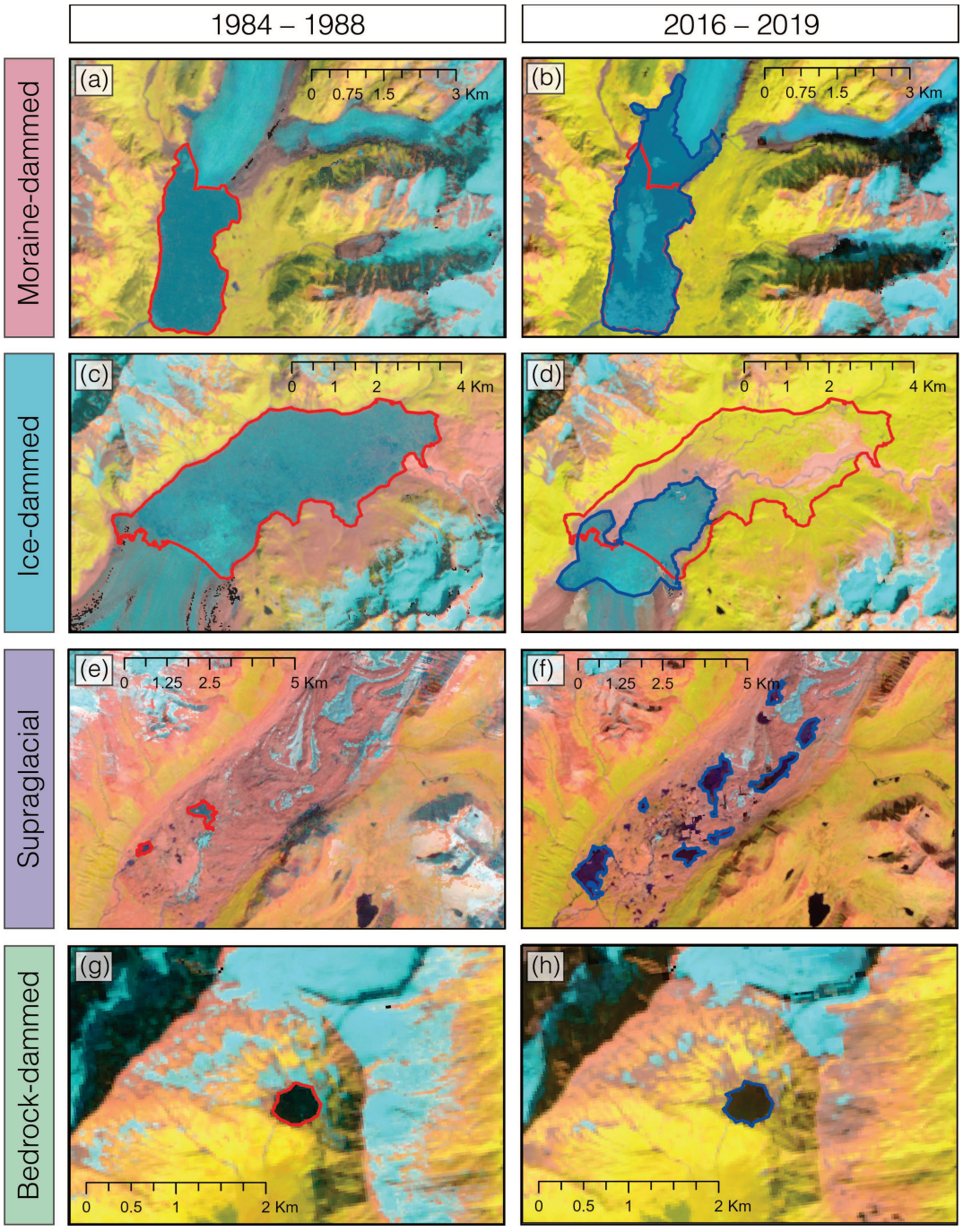

Figure 2.3. Examples of typical lake behavior for each dam type (moraine (a-b), ice (c-d), supraglacial (def), and bedrock(g-h)), and changes in lake area from 1984–1988 (left; red) and 2016–2019 (right; blue). False color images using Landsat bands for shortwave infrared (SWIR), near infrared (NIR), and red.

2.2.3.2 Topological position

In addition to dam type, all glacial lakes were classified based on their spatial relationship to their source glacier (Nie et al., 2017; Rounce et al., 2017), into one of the following categories:

i) Proglacial: lakes at the terminus of the glacier, in contact with the ice;

ii) Supraglacial: lakes on the surface of the glacier, most commonly within debris;

iii) Detached: lakes fed by glaciers but not in contact with ice;

iv) Unconnected: detached lakes not fed by glaciers; or

v) Ice: ice-dammed lakes located at ice margins or in tributary valleys.

2.2.3.3 Lake stability classification

Lake stability simply refers to whether or not a lake is present, rather than the stability of the lake shoreline. Five stability classifications are identified within this dataset:

i) Forms: lakes which appear after 1984–1988 and are present in every mosaic through 2016–2019;

ii) Forms-Drains: lakes which form after 1984–1988 and drain by 2016–2019;

iii) Drains: lakes which were present in 1984–1988 and disappear by 2016–2019;

iv) Drains-Refills: lakes which are present in 1984–1988, are not present for one or two time steps, then reappear by 2016–2019; or

v) Persistent: lakes which are present in all four time steps.

2.2.4 Lake area change

Absolute area change (ΔA) was calculated for all lakes present in the latest time step (2016–2019), taken as the difference between the last (2016–2019) and first (either 2007–2011, 1997–2001, or 1984–1988) outline for each lake. For lakes which first appear in the 2016–2019

composite, ΔA is equal to lake area in 2016–2019. Rate of change (km^2 per decade, calculated between the midpoint of each interval) was also calculated to minimize bias of longer standing lakes having a larger area change. Rate of change per time step was also calculated to compare rates of area change over time.

2.2.5 Error

Error in lake delineation was calculated assuming an error of ± 1 pixel for the entirety of each lake perimeter (Chen et al., 2021):

$$E = P * R, \qquad (1)$$

where P is the perimeter of the lake (km), R is the pixel resolution of the imagery (0.030 km for Landsat), and the resulting error (E) is in km^2. This error calculation is more generous than numerous lake inventories which assume ± 0.5 pixel error (e.g., Fujita et al., 2009; Salerno et al., 2012; Zhang et al., 2015; Nie et al., 2017; Rounce et al., 2017; Wang et al., 2020).

Error for the difference in areas was calculated using the theory of propagation of uncorrelated error:

$$E_{diff} = \sqrt{{E_x}^2 + {E_y}^2}. \qquad (2)$$

Where E_x and E_y are the error for the first and second lake outlines, respectively. Lakes where the area difference was greater than E_{diff} were determined to have detectable area change.

2.3 RESULTS

2.3.1 Lake evolution 1984–1988 to 2016–2019

The overall number of lakes in the Alaska region increased from 484 in 1984–1988 to 667 in 2016–2019, and total area grew from 815.5 km^2 in 1984–1988 to 1298.5 km^2 in 2016–2019 (Fig. 2.4). The distribution of lakes of each dam type has remained fairly consistent over

time, with 40–44% of all lakes being moraine-dammed, 26–30% bedrock-dammed, 9–14% ice-dammed, and 16–23% supraglacial. However, the contribution of each dam type to the total lake area has changed. The contribution of ice-dammed lakes decreased (16% in 1984–1988 to 6% in 2016–2019), while moraine-dammed lakes increased (67% in 1984–1988 to 79% in 2016–2019). While supraglacial lakes have increased in number over time, their contribution to total lake area has remained consistent around 2–3%. Supraglacial lakes accounted for 20% of lakes by number in 2016–2019, though they only contributed to 3% of the total area. Conversely, moraine-dammed lakes composed 41% of all lakes yet contributed to 79% of the total area.

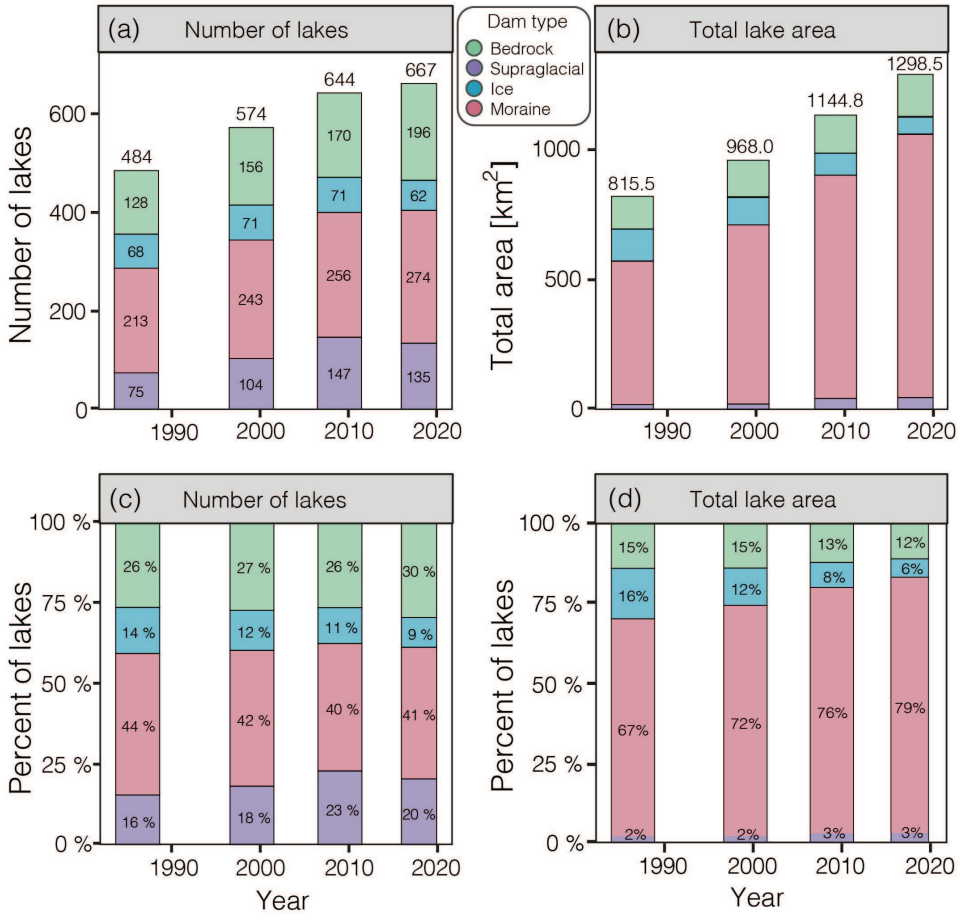

Figure 2.4. Time evolution of ice-marginal lakes in terms of (a) unscaled number of lakes, (b) unscaled lake area, (c) number of lakes scaled by total number of lakes in that timestep (percent), and (d) lake area scaled by the total lake area in that timestep (percent). Lakes are colored by lake dam type (legend between panels a and b). Bar widths correspond to imagery time intervals.

Lake stability describes whether a lake is persistent, or if it formed or drained during any of the four time intervals used for analysis. Lakes that appear in all four time intervals ("persistent lakes") dominate both the number and area of bedrock-, ice-, and moraine-dammed lakes (Fig. 2.5). Supraglacial lakes are the least stable, as this class is dominated by non-persistent lakes. Changes in the number of persistent lakes from interval to interval is due to lakes either splitting or merging. The rate of formation of new bedrock and moraine-dammed lakes appears relatively constant over time, with ~10–30 new lakes of each dam type first appearing in each time interval.

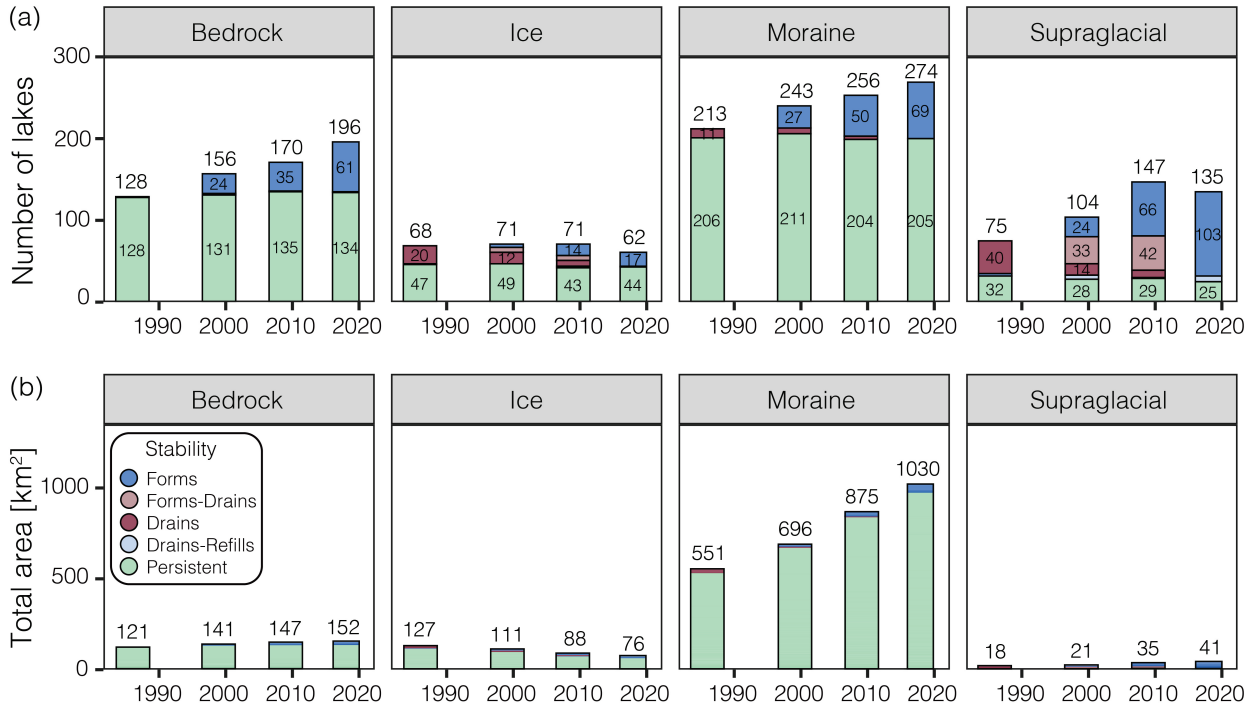

Figure 2.5. Number of lakes (a) and total area (b) of each dam type through time. The number of lakes in blue indicates the total number of lakes in that time period that were not present in 1984–1988; the number of lakes in red indicates the number of lakes present in that time period which drain in a subsequent time period. Light red indicates lakes which form after 1984–1988 but drain before 2016–2019. Bar widths correspond to imagery time intervals.

Moraine-dammed lakes added 56 lakes (+26%) and grew by 479 km^2 (+87%) from 1984–1988 to 2016–2019, while bedrock-dammed lakes added 68 lakes (+53%) and grew by 31.8 km^2 (+26%; Fig. 2.5). Though they added a similar number of lakes, moraine-dammed lakes increased in total area more rapidly than bedrock-dammed lakes, primarily through the growth of pre-existing lakes.

While bedrock and moraine-dammed lakes steadily increased in lake frequency and area, supraglacial lakes exhibited more variability. This class increased by 72 lakes from 1984–1988 to 2007–2011, yet lost 12 lakes from 2007–2011 to 2016–2019, resulting in an overall increase of 60 lakes (80% increase). Despite varying frequency, supraglacial lakes grew in total area between each time period, resulting in a total increase of 22.8 km^2 (+127%) from 1984–1988 to 2016–2019. Supraglacial lakes had the largest percent increase in area; however, they contributed the least (2–3%) to total lake area across different dam types.

Ice-dammed lakes are the only dam type with decreasing number and area, losing 6 lakes (–9%) and 51 km^2 (–40%) overall from 1984–1988 to 2016–2019. However, a total of 20 individual lakes drained and 17 formed throughout this time period, with an additional three lakes merging, resulting in an overall loss of six lakes.

Lake frequency, dam type, and area change distribution varies with lake area (Fig. 2.6). The majority of lakes (77%) in the region are less than 1 km^2, but collectively constitute only 9% of total lake area. Lakes greater than 1 km^2 thus constitute >90% of the total lake area and are dominated (69%) by moraine dams. The lake area change distribution by lake area from 1984–1988 to 2016–2019 closely reflects the total lake area distribution, with lakes greater than 1 km^2 experiencing 94% of the total lake area change. In particular, there are 19 lakes (17 moraine-dammed, one bedrock-dammed, and one ice-dammed; see Table S1), each with individual areas

greater than 10 km^2, that constitute ~60% of the total lake area and area growth. Of these 19 lakes, 14 occupy piedmont lobe depressions (defined here as a basin which is not constrained by valley walls), and about half are found within a coastal plain environment, with four lakes located within 2 m of sea level. Lake basin geometry and elevation have previously been linked to lake area change in Alaska, with low elevation lakes growing the most rapidly (Field et al., 2021). Excluding lakes greater than 10 km^2, the total lake area in the Alaska region grew by 42% (compared to the 59% area increase when considering all lakes).

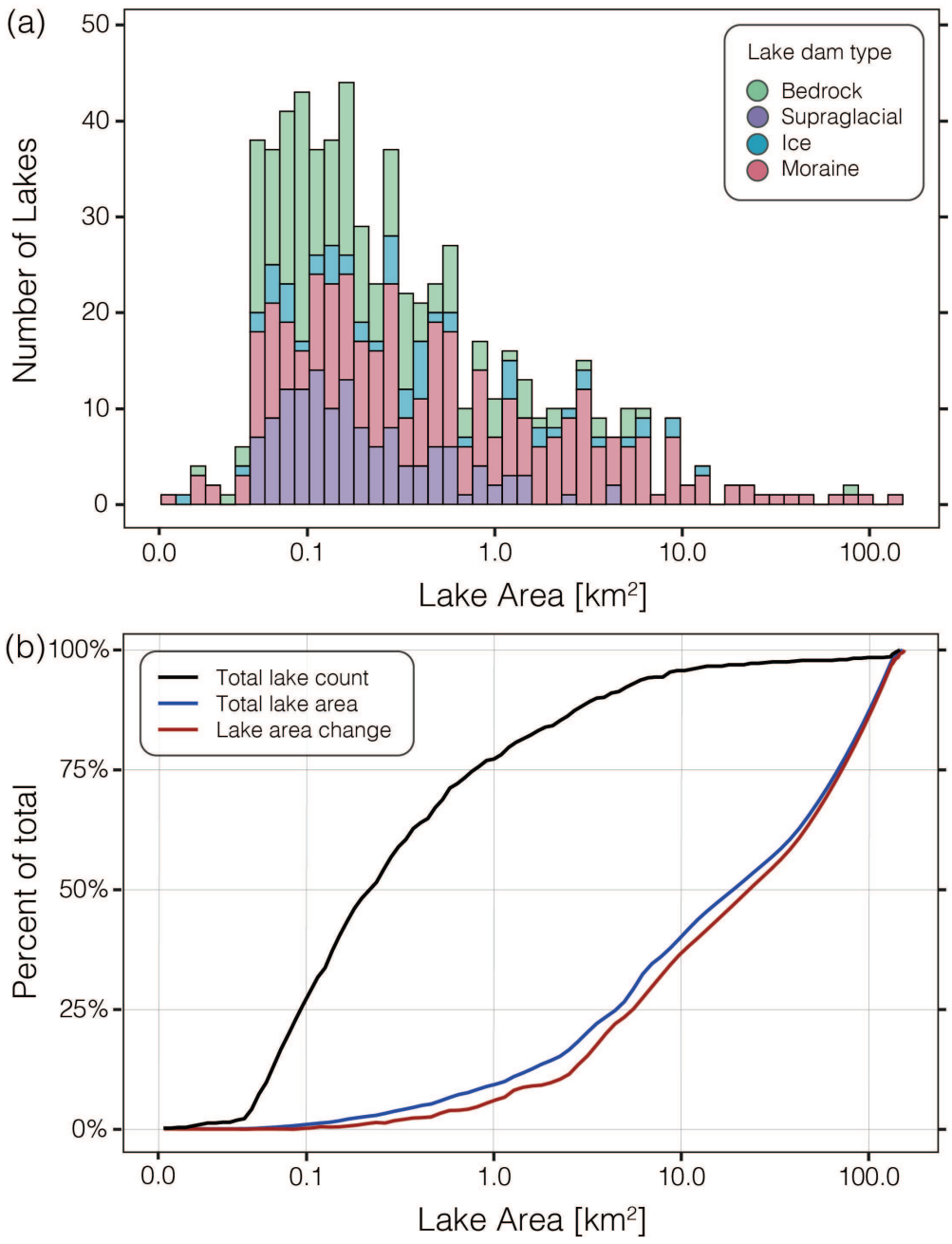

Figure 2.6. Distribution of lake area frequency in 2016–2019 by lake area (colored by dam type; a) and cumulative distribution function of total lake number, total lake area, and total lake area change (1984–1988 to 2016–2019; b). Note that the x-axis is logarithmic.

2.3.2 Individual lake area evolution

From 1984–1988 to 2016–2019, 791 distinct lakes were identified, 667 of which were still present in 2016–2019. Of the 124 lakes which drained, 97 (78%) were supraglacial, 20 (16%) were ice-dammed, and 7 (6%) were moraine-dammed. Absolute area change was

calculated for each individual lake, with drained lakes considered to have an area of zero km^2 after drainage (Fig. 2.7). Detectable change (error < area change) occurred for 334 of the total 791 lakes (44%). Within each dam type, 63% of moraine-dammed, 45% of ice-dammed, 39% of supraglacial, and 24% of bedrock-dammed lakes experienced detectable change.

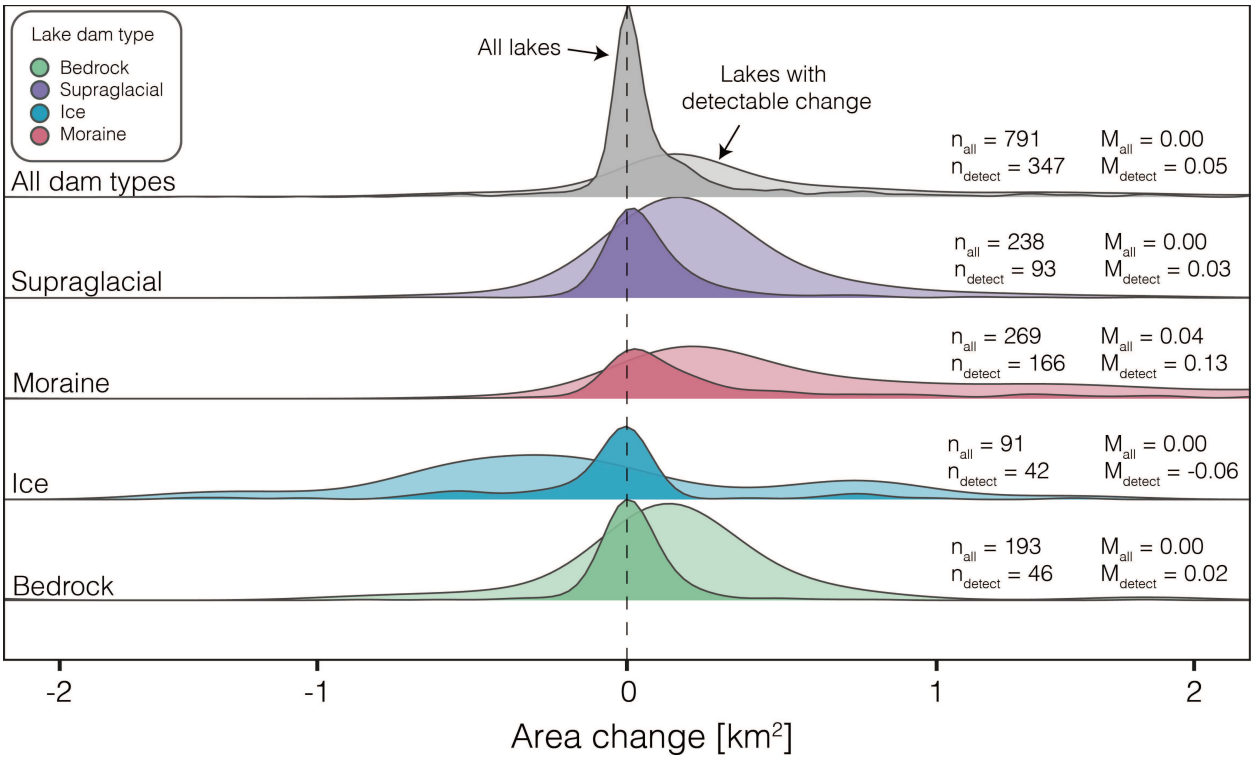

Figure 2.7. Smoothed density distribution (normalized to 1 for each dam type) of absolute lake area change for all lakes (dark curves) compared to that for only lakes with detectable change (light curves) for each dam type, with number of lakes (n) and median lake area change (M). Note that the x-axis has been limited to –2 and 2 km^2. For the full distribution, see Fig. A5.

The median area change for lakes of all dam types with detectable change (n = 344) is 0.05 km^2 between 1984–1988 and 2016–2019 (Fig. 2.7). Considering only lakes with detectable change, the median change for moraine-dammed lakes (n = 166) is 0.13 km^2, ice-dammed lakes (n = 42) is –0.06 km^2, supraglacial lakes (n = 93) is 0.03 km^2, and bedrock-dammed lakes (n =

46) is 0.02 km^2. Median change values remain relatively stable even when lakes > 10 km^2 are excluded from analysis (Fig. A6).

Proglacial lakes (moraine- and bedrock-dammed) experienced the largest median detectable change (0.14 km^2), while ice-dammed lakes are the only dam type to experience negative median detectable change (–0.06 km^2; Table 2.2; Fig. A7). Unconnected and detached lakes have a median change of 0.02 km^2 for lakes with a detectable change. Proglacial moraine-dammed lakes have a wider distribution and higher median change than detached or unconnected moraine-dammed lakes (Table 2.2). Proglacial moraine-dammed lakes also have a wider distribution and higher median change than proglacial bedrock-dammed lakes.

Table 2.2. Count (area, km^2) of glacial lakes by dam type and location between 1984 and 2019, as well as median area (km^2), range of areas (km^2), and median area change (km^2) for all lakes. Median area change for lakes with detectable change (km^2) are within the parentheses.

Dam Type	Location	1984–88	1997–2001	2007–11	2016–19	Change 1984–88 to 2016–19	Median area	Area range	Med change 1984–88 to 2016–19
Moraine	Proglacial	172 (539)	193 (674)	193 (849)	201 (999)	26 (460)	0.71	0.01–143.1	0.3 (0.75)
	Detached	37 (9.6)	46 (19.3)	59 (24.5)	69 (28.8)	32 (19.2)	0.12	0.02–5.9	0.0 (0.08)
	Unconnected	4 (2.1)	4 (2.2)	4 (2.0)	4 (2.0)	0 (–0.1)	0.40	0.05–1.2	0.0 (0.0)
Bedrock	Proglacial	12 (4.0)	10 (2.7)	13 (5.0)	16 (7.1)	4 (3.1)	0.19	0.04–2.2	0.1 (0.19)
	Detached	57 (92.6)	75 (103)	77 (105)	85 (106)	28 (13.4)	0.13	0.03–76.4	0.0 (0.11)
	Unconnected	59 (23.9)	71 (35)	80 (36.7)	95 (38.7)	36 (14.8)	0.16	0.02–5.6	0.0 (0.09)
Ice	Tributary	42 (113)	41 (96.0)	44 (71.3)	38 (66.2)	–4 (–46.8)	0.75	0.01–22.0	0.0 (–0.36)
	Margin	26 (13.4)	30 (14.9)	27 (16.9)	24 (9.6)	–2 (–3.8)	0.16	0.03–7.0	0.0 (–0.13)
Supraglacial		75 (17.8)	104 (21.1)	147 (34.7)	135 (40.7)	60 (22.9)	0.12	0.03–4.1	0.0 (0.03)
Total		**484 (815.5)**	**574 (968.0)**	**644 (1145)**	**667 (1298.5)**	**183 (483.0)**	**0.21**	**0.01–143.1**	**0.00 (0.21)**

Rate of area change (km^2 per decade) follows a similar distribution as absolute area change (Fig. A8). The median change rate for lakes of all dam types with detectable change (n = 344) is 0.02 km^2 per decade. When considering all lakes within each dam type, moraine-dammed lakes are the only dam type with a change rate greater than zero (0.05 km^2 per decade). Supraglacial and bedrock-dammed lakes experience very small changes on a decadal scale, with a median change rate of 0 for all lakes as well as the subset of detectable lakes. Ice-dammed lakes with detectable change experienced a median change rate of –0.02 km^2 per decade.

2.3.3 Regional lake distribution

Distribution of lake dam type and total lake area varies spatially by subregion (Table 2.3; Fig. 2.8), though median lake area change does not vary substantially when considering all lakes with detectable change per region (ranges from 0.04–0.06 km^2). Ice-dammed lakes occur most frequently in the St. Elias Mountains (n = 26 in 2016–2019) and least frequently in the W Chugach Mountains (n = 6 in 2016–2019), Brooks Range (n = 0), and the Aleutians (n = 0). The N Coast Ranges are dominated by moraine- and bedrock-dammed lakes, whereas the Alaska Ranges and St. Elias Mountains are dominated in number by supraglacial lakes. Supraglacial lakes occur in the regions with the highest debris cover (19% of glacier area in the Alaska Ranges, and 13% in the St. Elias Mountains; Herreid and Pellicciotti, 2020). However, supraglacial lakes contribute little to the total lake area. The number of lakes within a region does not directly predict lake area; the N Coast Ranges host the highest number of lakes (n = 234, 382.5 km^2), yet the St. Elias Mountains have the greatest total lake area (n = 181, 545.5 km^2).

Table 2.3. Number of lakes, glacierized area, debris covered area, percent debris cover, normalized lake frequency, normalized lake area, normalized lake area change, and specific glacier mass balance (from Jakob et al., 2021) per subregion.

Region	# of lakes 2016–19	Total glacier area (km^2)	Total debris cover (km^2)	Total lake area (km^2)	Percent debris cover	Normalized lake freq (# per 100 km^2 ice)	Normalized lake area (km^2 per 100 km^2 ice)	Normalized lake area change (km^2 per 100 km^2 ice)	Specific mass balance (m w.e. yr^{-1})
Brooks Range	11	346	10.3	0.7	3.0	3.2	0.2	0.1	N/A
Alaska Ranges	103	16278	3135.5	143.0	19.3	0.6	0.9	0.2	–0.41 ± 0.05
Aleutians	25	1912	198.7	30.0	10.4	1.3	1.6	0.6	–0.64 ± 0.10
Chugach Mtns	107	12052	586.2	182.8	4.9	0.9	1.5	0.6	–0.80 ± 0.09
St. Elias Mtns	181	33174	4446.3	545.5	13.4	0.5	1.6	0.6	–1.03 ± 0.10
N Coast Ranges	234	22963	1553.8	382.5	6.8	1.0	1.7	0.6	–1.08 ± 0.09

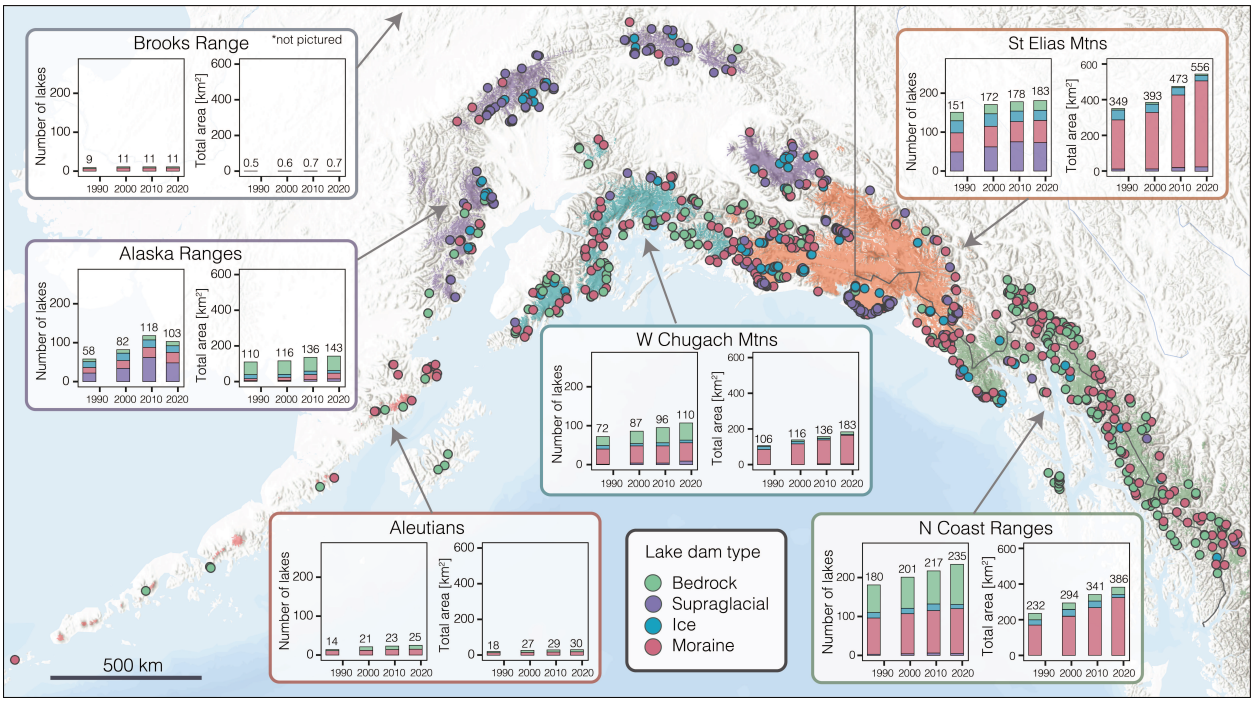

Figure 2.8. Dam type distribution (spatial, frequency, and total area) for each Alaska subregion. Note: Brooks Range not pictured on map; see Fig. 1. Basemap provided by ESRI, 2021.

Persistent lakes dominate the total area for each subregion, likely because new lakes tend to be small. The N Coast Ranges have the most persistent lakes (n = 175 in 2016–2019), with 57 lakes forming yet contributing little to the total area (Fig. A9). Changes in persistent lake numbers between time steps is due to lakes splitting or coalescing through time. The Alaska Ranges and St. Elias Mountains have the largest number of lakes that ultimately drain, likely due to the high frequency of supraglacial lakes in these regions and their spatial and temporal heterogeneity.

2.4 DISCUSSION

My inventory of ice-marginal lakes in Alaska from 1984 to 2019 demonstrates that lake area changes vary based on lake dam type and a lake's topological position. By tracking individual lakes through time and categorizing lakes by dam type, region, and spatial relationship to their source glacier, I am able to identify trends that would otherwise be overlooked if lakes within Alaska were considered as a whole.

Overall, ice-marginal lakes in Alaska have grown in both number and area between 1984 and 2019, following the trend in both regional (Wang et al., 2013; Carrivick and Quincey, 2014; Nie et al., 2017; Song et al., 2017; Emmer et al., 2020) and global (Shugar et al., 2020) studies. However, ice-dammed lakes have decreased in number and area whereas moraine-dammed lakes have increased at a faster rate than the average when considering all dam types together. By examining individual lakes, I identify that the majority (56%) of lakes have not experienced a detectable area change over the period of study, and that 19 large (>10 km^2), primarily moraine-dammed lakes contributed to 60% of total area growth. Analyzing all dam types together would fail to identify decreases in number and area of ice-dammed lakes, underestimate the increases in

proglacial moraine-dammed lakes, and likely overestimate the importance of the appearance of small, supraglacial lakes.

2.4.1 Alaska's ice-marginal lakes

Lake position and dam type, which are often linked, provide a simple, physically-based metric for parsing ice-marginal lakes in Alaska. The majority of moraine-dammed lakes are proglacial, located behind a Little Ice Age (LIA; ~1250–1850 AD) moraine at the front of a retreating glacier (e.g., Wiles et al., 1999; Santos and Córdova, 2009; Solomina et al., 2015, 2016). They tend to be associated with clean-ice glaciers (82%), defined by Brun et al. (2019) as <19% debris cover (Fig. 2.9). The growth rate of moraine dammed lakes appears to be coupled to the amount of debris cover, as the lakes with the largest area increase are associated with clean-ice glaciers, with the exception of Vitus Lake at Bering Glacier (Fig. 2.9). Moraine-dammed lakes occur with both large and small glaciers, as most temperate glaciers can form a moraine during a period of advancement (e.g., the LIA), as long as sediment supply to the terminus is high. Basin geometry and glacier hypsometry likely play a large role in determining the lake expansion rate and maximum lake area, as the underlying bed slope influences how quickly the glacier retreats (depending on glacier mass balance; see Sect. 2.4.5). For example, large, coastal proglacial lakes can fill piedmont lobe basins (such as Vitus Lake, Malaspina Lake, and Grand Plateau Glacier Lake), which accommodate larger lake expansion than proglacial lakes confined to smaller, steeper valleys (Field et al., 2021). Basin geometry also determines the maximum lake level and the point at which the glacier detaches from the lake.

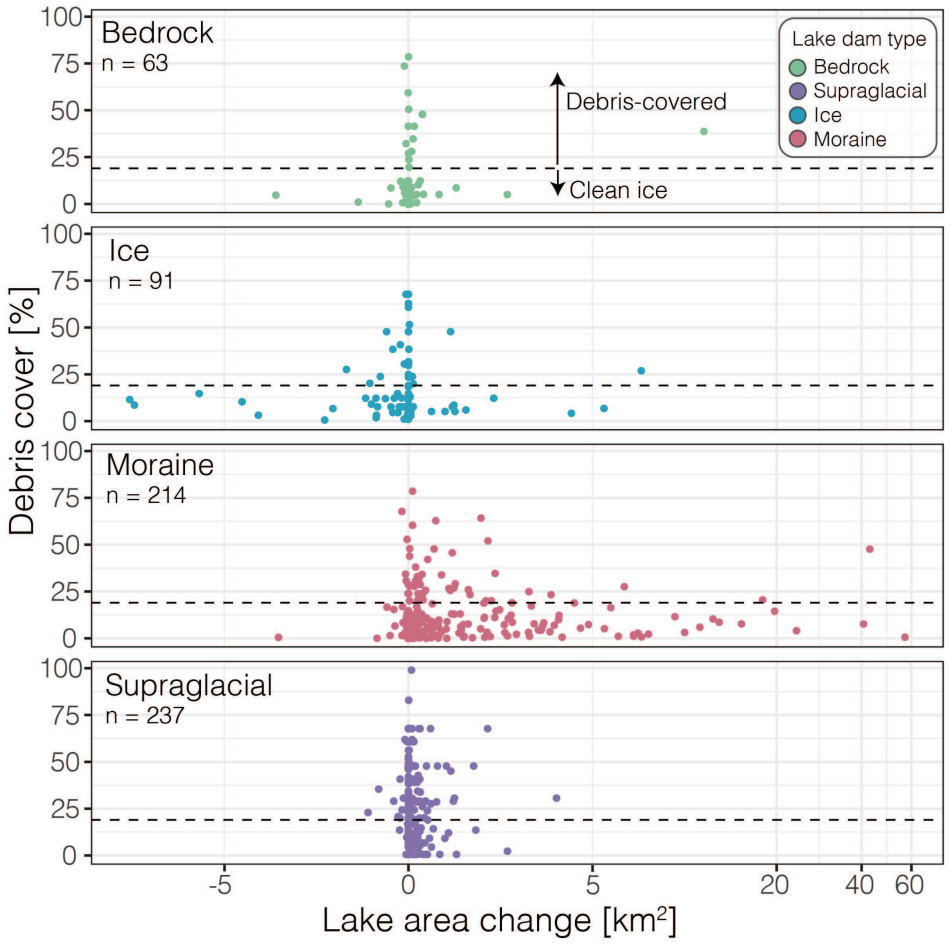

Figure 2.9. Percent glacier debris cover vs lake area change (km^2) for lakes associated with glaciers > 2 km^2. Each dot represents an individual lake. Dashed line is at 19%, above which is considered debris-covered ice and below is considered clean ice (Brun et al., 2019).

Ice-dammed lakes are primarily located next to clean-ice glaciers (65%), with larger, lower slope areas and positive hypsometric indices (bottom-heavy; Fig. 2.10), such as are found adjacent to Brady Glacier (Capps et al., 2011; Pelto et al., 2013). The largest lakes occur in tributary valleys, dammed by main branch ice, while many small lakes are found in pockets between glacier margins and valley walls. The decrease in ice-dammed lake number and area is likely due to the down-wasting of glacier surfaces (e.g., Larsen et al., 2015; Jakob et al., 2021), decreasing the height of the ice dam and therefore decreasing maximum area (and volume) of the

lake (e.g., Kienholz et al., 2020). The formation of new conduits alongside or beneath the glacier could also be influencing ice-dammed lake drainage (e.g., Tulsequah Glacier; Neal, 2007; Post and Mayo, 1971). Previous work documented ice thinning as the primary factor in the loss of an ice dam for 82% of lakes lost from land-terminating glaciers and 62% of loss from lake terminating glaciers between 1971 and 2008 (Wolfe et al., 2014).

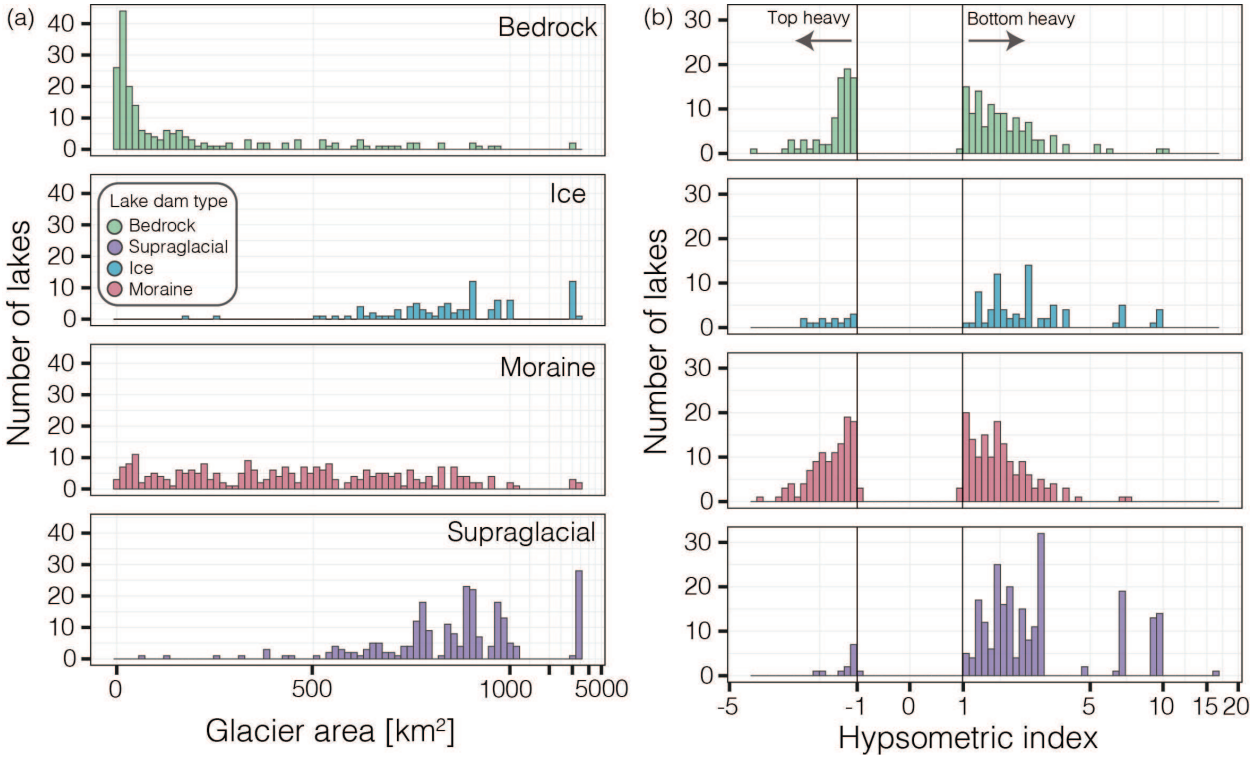

Figure 2.10. Histogram of number of lakes and associated glacier area, separated by dam type (a) and histogram showing number of lakes within each hypsometric index (HI) bin, separated by dam type (b). Hypsometric index was calculated by McGrath et al. (2017). HI values greater than 1 indicate a bottom heavy glacier, HI values less than –1 indicate a top heavy glacier. Note the logarithmic x-axis scales.

An overwhelming majority (>80%) of bedrock-dammed lakes are associated with clean-ice glaciers less than 10 km^2 in area (Figs. 2.9 and 2.10). These types of lakes generally form within cirques, where a small glacier has retreated and exposed an overdeepening. Bedrock-

dammed lakes can indicate an advanced stage of lake development (Emmer et al., 2020), such as is found in parts of the N Coast Ranges. Most bedrock-dammed lakes (>90%) are either detached or unconnected, with minimal influence from ice-water contact. The small changes in area of unconnected bedrock-dammed lakes could be due to changes in the regional water balance rather than glacier dynamics.

Supraglacial lakes generally form on low-sloped debris-covered tongues of glaciers (Reynolds, 2000), where thin debris enhances melt and thick debris insulates ice and reduces surface melt (Östrem, 1959), often leading to heterogeneous surficial topography. Debris cover tends to reduce ice discharge and surface melt, leading to longer glaciers (Anderson and Anderson, 2016). The inventoried supraglacial lakes in Alaska follow these trends, with their distribution strongly skewed towards flat, bottom-heavy glaciers, as is characteristic of debris-covered glaciers (Reynolds, 2000). These lakes can occur on glaciers with any amount of debris cover, though have the highest concentration (64%) out of any lake dam type on glaciers with >19% debris cover (Fig. 2.9). A majority of supraglacial lakes are located on a few large, heavily debris covered glaciers. For example, 95% of supraglacial lakes in the St. Elias Mountain region are located on two large, piedmont glaciers (Malaspina and Bering glaciers). Although these lakes are abundant, they exhibit high spatiotemporal variability and contribute minimally to total lake area (2–3%; Fig. 2.5).

Although additional factors are required to comprehensively assess GLOF hazards, a lake inventory that captures area and dam type provides a foundation for this type of assessment, as dam type influences stability, lake volume scales with area (e.g., Huggel et al., 2002; Cook and Quincey, 2015), and peak flood discharge scales with volume (e.g., Walder and Costa, 1996; Veh et al., 2020). Ice-dammed lakes are known to undergo multiple fill/drain cycles

with the capability of producing multiple GLOFs (e.g., Anderson et al., 2003; Jacquet et al., 2017), whereas moraine-dammed lakes tend to only GLOF once, as their dam is typically compromised in the process. The observed decrease in number and area of ice-dammed lakes in Alaska suggests an overall decrease in GLOF hazards from these types of lakes, although the specifics of remaining lakes need to be evaluated individually (e.g., Suicide Basin, Kienholz et al., 2020; Tulsequh Glacier, Neal, 2007; Bear Glacier, Wilcox et al., 2014). The increase in number and area of moraine-dammed lakes provides a greater number of potential source lakes and a larger potential flood volume, however, factors such as surrounding slope stability (e.g., landslides, rockfalls, permafrost), moraine geometry and stability (e.g., slope, presence of an ice core), and downstream impacts must be evaluated first to determine GLOF potential and hazard (e.g., Worni et al., 2013; Rounce et al., 2017). As the nature of the dam type influences lake stability, the opposing trends of ice-dammed and moraine-dammed lakes complicates a region-wide assessment of changing GLOF hazards in the Alaska region.

2.4.2 Regional trends

The Alaska region of the RGI is separated into six second-order regions (see Fig. 2.8), used here as subregions for analysis. Lakes are most numerous in the N Coast Ranges (35% of all lakes) and St. Elias Mountains (27%), though these ranges also have the largest glacier area (24% and 41% of total ice in Alaska, respectively). Normalized lake frequency (number of lakes per 100 km^2 of glaciers) is highest in the Brooks Range, though it has the lowest normalized lake area (lake area per 100 km^2 of glaciers; 0.2) as total lake area sums to just 0.7 km^2 (Table 3). I interpret these normalized lake statistics as reflecting the late stage of ice-marginal lake development, minimal LIA glacier advance, as well as the relatively small glacier extent in the Brooks Range even during the Last Glacial Maximum (Kaufman and Manley, 2004).

Normalized lake area is highest in the N Coast Ranges (1.7 km^2 per 100 km^2 of glaciers) due to the abundance of smaller glaciers and many proglacial lakes. The St. Elias Mountains have the largest total lake area; however, it also contains large icefields, which results in a similar normalized lake area as the Aleutians and the Chugach Mountains (1.5–1.6 km^2 per 100 km^2 of glaciers). This suggests that the area of ice-marginal lakes scales with glacier area in the coastal ranges (i.e., excluding the Brooks Range and Alaska Ranges), with normalized lake area ranging from 1.5 to 1.7.

Accounting for lake area change, the Brooks Range and Alaska Ranges have a small normalized lake area change (0.1–0.2; lake area change between 1984 and 2019 per 100 km^2 of glaciers). The Chugach, Aleutians, St. Elias, and N Coast Ranges, however, each have a higher normalized lake area change (0.6). These numbers suggest a dichotomy in which coastal glacier-lake systems are changing faster than those in more interior settings, in agreement with recent work investigating physical controls on ice-marginal lake area change (Field et al., 2021). The Alaska Ranges have the highest percent debris cover (19%), which could be a factor in the low normalized lake area and normalized lake area change seen in this region. Supraglacial lakes are the most abundant dam type in the Alaska Ranges (47% in 2016–2019), characterized by small areas and area changes (Table 2).

2.4.3 Temporal trends

Rate of lake area change (km^2 per decade) through time indicates whether ice-marginal lake evolution has remained constant between different time periods, or whether the lakes have experienced periods of accelerated or decelerated change. Bedrock dammed lakes experienced little variation in rate of area change throughout the period of study (Fig. 2.11), with a rate that hovers around zero, likely due to the fact that a majority (>90%) of bedrock-dammed lakes are

either detached from their associated glacier or unconnected to any glacier. Ice-dammed lakes consistently experienced a negative median rate of area change, with the most negative rate of growth between 2007–2011 and 2016–2019. This implies drainage of ice-dammed lakes may be accelerating, which could be due to an increased rate of glacier thinning since 2013–2014 (Jakob et al., 2021), though this link requires further investigation. Supraglacial lakes exhibit the opposite trend, growing at a faster rate after 2007–2011 than they did prior. Moraine-dammed lakes experienced the largest median rate of change between 1984–1988 and 1997–2001. A decreasing median rate of change for moraine-dammed lakes yet large total area growth is likely due to the growth of a few large, outlier lakes whose influence is minimized by comparing median rather than mean rates of change. Proglacial lakes experienced the overall largest rate of growth, even when compared to all moraine-dammed lakes, suggesting that topological position, rather than strictly dam type, is a better indicator for rate of ice-marginal lake area change. Together, these data suggest the ice-marginal lakes of Alaska and northwestern Canada could be undergoing a transition, with an increased role of supraglacial lakes driving regional lake area expansion.

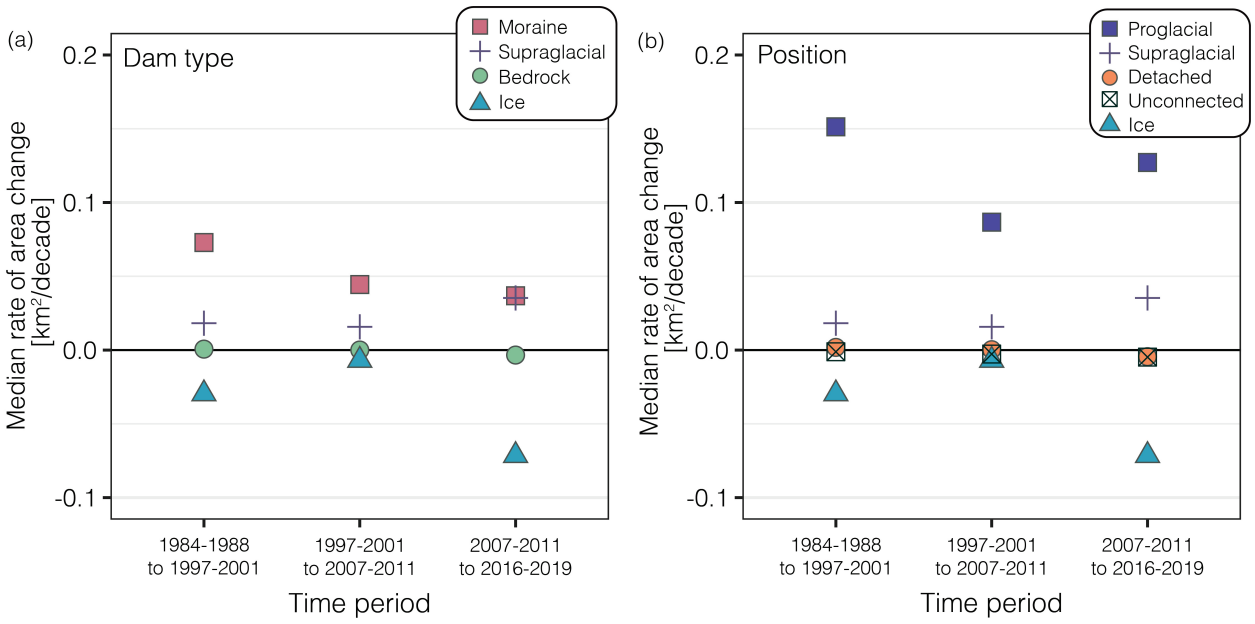

Figure 2.11. Median rate of area change between each time step, categorized by dam type (a) and topological position (b).

2.4.4 Comparison to other regions

Alaska's glaciers cover a large spatial extent, spanning different climatic, geologic, and glacial environments (Section 2.1). This makes the region particularly unique in relation to other glacierized regions, though the best analogue region depends on which Alaskan mountain range is considered. The heavily debris-covered areas (e.g., Alaska Ranges) have similar debris cover to the Himalaya, areas with clean-ice valley glaciers (e.g., N Coast Ranges) could behave similar to the Peruvian Andes, and the large and complex glaciers/icefields (e.g., St. Elias Mountains) have similar glacier and lake dynamics as the Patagonian Icefields. Dynamics within these Alaska subregions could shed light on ice-marginal lake behavior in comparable mountain ranges, and vice versa.

Many studies on ice-marginal lakes concentrate on High Mountain Asia (e.g., Nie et al., 2017; Zhang et al., 2018; Veh et al., 2020; Wang et al., 2020; Chen et al., 2021), a region with abundant proglacial and supraglacial lakes, though HMA lakes tend to be smaller than Alaskan

lakes (median lake area of 0.11 km^2 and 0.17 km^2, respectively; Shugar et al., 2020). Alaska and the Himalaya regions (RGI regions 14, 15) have a similar percent debris cover (~15%), though Alaska contains larger glacier and debris-covered areas (Herreid and Pellicciotti, 2020). Herreid and Pellicciotti (2020) calculated a debris stage for each RGI region from 0 to 1, where 1 indicates the ablation zone is entirely covered in debris. Debris stage is slightly higher in the Himalaya (~0.6–0.7) than Alaska (~0.5), though Alaska has a higher debris expansion potential (Herreid and Pellicciotti, 2020). This suggests that if debris cover expands in Alaska, these areas could become more similar to the heavily debris-covered areas in the Himalaya. Supraglacial lakes in the Himalaya vary considerably in location, shape and size, appearing, disappearing, and coalescing through time (Benn et al., 2001; Gardelle et al., 2011; Nie et al., 2017), behavior exhibited in Alaska as well. These similarities indicate that supraglacial lakes within these two regions have similar characteristics, and that understanding one region could aid in understanding the other.

Glacierized mountain ranges around the world exhibit varying stages of glacial retreat. The Peruvian Andes are considered to be in a late stage of glacier retreat with little potential for further lake expansion, as ice generally remains in steep, high elevation parts of the study area (Emmer et al., 2020). In Peru, glaciers have retreated far off their LIA moraines, such that the majority of proglacial lakes shifted from moraine dammed in 1948 to bedrock dammed in 2017 as glaciers retreated and exposed bedrock overdeepenings (Colonia et al., 2017; Emmer et al., 2020). Though ice remains in many main valleys in the N Coast Ranges, glaciers are smaller, steeper, cleaner, and less complex than other subregions in Alaska, apart from the Juneau Icefield. Though lakes in the N Coast Ranges are on average larger than those found in the low-latitude Andes (median lake area of 0.21 km^2 and 0.12 km^2, respectively; Shugar et al., 2020),

the abundance of moraine dammed proglacial lakes and increasing proportion of bedrock dammed lakes (39% in 1984–1988 to 44% in 2016–2019) suggests the N Coast Ranges could follow a similar trajectory as the Cordillera Blanca, producing a shift in dominant dam type from moraine to bedrock in the future.

Ice-marginal lake increases have been documented throughout the world, though characteristics such as dam type, lake location, and associated glacier behavior vary widely. Examining ice-marginal lake behavior at different stages in various mountain ranges can help predict how these lakes might evolve in the future, though such analysis is outside the scope of this study.

2.4.5 Feedbacks on glacier mass balance

Lake geometry likely dictates the impact a proglacial lake has on glacier mass balance. Large, deep lakes can impede a glacier from reaching equilibrium by holding the terminus at lake elevation until it has retreated out of the lake basin (Larsen et al., 2015). Ice-water contact can also enhance calving, resulting in mass loss and lake expansion through terminus retreat (Carrivick and Tweed, 2013). Larsen et al. (2015) found that lake-terminating glaciers in Alaska have a more negative median mass balance in coastal regions where large, proglacial lakes have developed. Lake-terminating glaciers also experienced more rapid thinning near their terminus than land-terminating glaciers, and appear to be less directly coupled to climate variations (Larsen et al., 2015). In the Himalaya, lake-terminating glaciers have been linked with increased glacier mass loss through enhanced terminal retreat and surface lowering (King et al., 2019; Maurer et al., 2019), and center flow line velocities that are more than twice that of glaciers which terminate on land (Pronk et al., 2021). I therefore expect that as glaciers continue to retreat in Alaska, proglacial lake presence, formation, or detachment will influence glacier mass

balance, increasing thinning and glacier velocity where lakes are present, though variations in thinning have been observed (e.g., the Juneau and Stikine icefields; Melkonian et al., 2014, 2016).

Regional glacier thinning and mass loss rates appear to mimic lake area change in parts of Alaska. The N Coast Ranges and St. Elias Mountains are thinning (–1.27 ± 0.11 m yr^{-1} and –1.21 ± 0.12 m yr^{-1}, respectively) and losing mass (–1.08 ± 0.09 m w.e. yr^{-1} and –1.03 ± 0.10 m w.e. yr^{-1}) at a greater rate than other subregions from 2011–2019 (Jakob et al., 2021). These regions also experienced the largest normalized lake area growth (see Sect. 4.2). The high thinning rate in the Aleutians (–0.75 ± 0.06 m yr^{-1}) does not appear to be reflected in the low normalized lake area growth documented in my survey. This is likely due to the fact that 60% of lakes in the Aleutians subregion are either detached or unconnected and therefore not directly influenced by glacier dynamics. The Alaska Ranges are thinning (–0.48 ± 0.06 m yr^{-1}) and losing mass (–0.41 ± 0.05 m w.e. yr^{-1}) at the lowest average rates per region (Jakob et al., 2021) likely due to extensive debris cover, and is accompanied by the lowest normalized lake area change outside the Brooks Range.

2.4.6 Future change in ice-marginal lakes

As global temperatures continue to rise and glaciers thin and retreat (Zemp et al., 2019), Alaska's glaciated landscape will change, as will the nature of ice-marginal lakes. Alaskan glaciers have retreated off their LIA moraines, and therefore it is unlikely that new moraine-dammed lakes will form without a sustained period of glacial advance or surge. However, proglacial lake expansion is expected to continue as glacier retreat accommodates lake growth, dependent on basin geometry. Using the Cordillera Blanca as an analogue for later stages of lake development (Emmer et al., 2020), I hypothesize a future shift in new proglacial lakes to mostly

bedrock dammed lakes, as glaciers retreat into higher, steeper terrain (e.g., Linsbauer et al., 2016; Furian et al., 2021), though it is uncertain how long the present stage of moraine-dammed lake growth will persist before glaciers leave their terminal overdeepenings. Alaska's glacier complexity and relative abundance of ice-dammed lakes poses an interesting question as to whether these lakes will continue to drain as they have since 1970 (Wolfe et al., 2014), or whether new ice-dammed lakes will form if tributary valley ice retreats faster than main branch ice, such as has occurred in Suicide Basin since 2011 (Kienholz et al., 2020). Modeling basin geometry and future ice extent would provide insight into where ice-marginal lakes in Alaska are likely to form in the future.

2.4.7 Inventory challenges

Two primary challenges were encountered while creating the inventory, which should be understood before using this dataset or applying its findings. Due to the use of spectrally-based supervised classification for lake identification, only lakes that have the spectral characteristics of water appear within my inventory. This limitation results in the exclusion of some ice-dammed lakes which are either iceberg filled, or lake basins which appear dry in the five-year mosaics due to a lake that is more often drained than filled. Therefore, this inventory is a clear minimum of ice marginal lakes, with several known omitted lakes. Known lakes which were not identified in my inventory include Suicide Basin, Valdez Lake, Snow Lake, Lake Linda, and Summit Lake, all of which are ice-dammed. These lakes, which have experienced multiple drainage events (e.g., Jones and Wolken, 2019; Kienholz et al., 2020), are important for individual GLOF hazard assessments, though they have little impact (0.4% of total lake area) on my assessment of regional decadal scale lake area trends by dam type.

Dam type classification was performed using manual visual interpretation for all lakes, with the most likely dam type identified in cases that are uncertain due to poor image resolution and/or possible mixed dam types (i.e., bedrock with moraine material; Emmer et al., 2017). A shift in dam type (e.g., ice dammed to bedrock dammed) was also documented for a few lakes, particularly where a lake becomes bedrock dammed after the loss of an ice dam (e.g., Terentiev Lake which was formerly dammed by Columbia Glacier). These lakes were classified by their most recent dam type when performing analysis on change over time. The small number of cases of transitioning dam types suggests this process is not particularly important for understanding the regional scale behavior of Alaska ice-marginal lakes discussed here.

2.5 CONCLUSIONS

As the second largest glacierized region outside the ice sheets, characterizing Alaska's ice-marginal lakes and their evolution has important implications for glacier mass balance, ecosystem dynamics, and GLOF hazards. Varying topographic settings (valleys, cirques, debris, icefields) and a wide range of glacier complexities allow for an abundance of ice-marginal lakes of varying dam type and position. Overall, ice-marginal lakes in Alaska have grown in both number (+183 lakes, 38% increase) and area (+483 km^2, 59% increase) between 1984–1988 and 2016–2019, though 56% of inventoried lakes did not experience detectable change. I demonstrate that lakes with different dam types and positions relative to their source glacier behave differently. Moraine-dammed, proglacial lakes experienced the largest growth likely due to clean-ice glacier retreat, while ice-dammed lakes experienced an overall loss in both number and area, likely due to thinning or disappearance of ice dams. This study highlights the value of parsing ice marginal lakes by dam type and location in comprehensive ice-marginal lake studies to clarify important lake dynamics that are obscured by coarser regional averages. A clear understanding of which lakes are growing, and which are

shrinking, as quantified here in a classified multitemporal ice-marginal lake inventory, is a crucial first step to understanding the drivers of historic change, predicting future lake evolution, and assessing GLOF hazard potential in icy mountainous regions.

3. DECREASING HAZARDS FROM GLACIAL LAKES IN ALASKA SINCE THE 1960s[2]

3.1 INTRODUCTION

Glacial lake outburst floods (GLOFs) occur when a lake dam fails or is overtopped, releasing a large volume of water to downstream environments (Clague and Evans, 2000). GLOFs can cause devastating impacts to downstream infrastructure, ecosystems, and communities (Milner et al., 2008; Carrivick and Tweed, 2016; Cook et al., 2016; Emmer, 2017; Meerhoff et al., 2018). The number of GLOFs per year that a region experiences is a fundamental measure of GLOF hazard, with a change in frequency potentially impacting the sustainability of communities and large infrastructure projects. Glacial lakes have been rapidly increasing in area and number (Shugar et al., 2020), and it has often been predicted that with continued climate change and glacier mass loss the frequency and hazards associated with GLOFs will also increase (Richardson and Reynolds, 2000; Carrivick and Tweed, 2013; Otto, 2019; Shugar et al., 2020). Indeed, a recent global compilation of historical GLOFs shows GLOF frequency increases from ~1900 towards the present (Veh et al., 2022). However, much of the observed increase in frequency could be explained by an observational bias, leaving actual trends in frequency in question (Veh et al., 2022).

The most common dam types of flood-originating glacial lakes are moraines and glacial ice. Dam type in turn influences the nature of the flood as well as likelihood for repeat events

[2] Chapter under review and available as a preprint: Rick, B., McGrath, D., McCoy, S., and Armstrong, W. Decreasing hazards from glacial lakes in Alaska since the 1960s, 19 August 2022, PREPRINT (Version 1) available at Research Square [https://doi.org/10.21203/rs.3.rs-1859425/v1]

(Carrivick and Tweed, 2016; Veh et al., 2022). Ice-dammed lakes are impounded behind a glacier dam, and drainage results from flotation of the ice dam, the opening of subglacial conduits, complete ice-dam failure, or flow over or along the ice margin (Post and Mayo, 1971; Walder and Costa, 1996; O'Connor et al., 2020). Because subsequent ice flow can effectively repair and reseal the ice dam, ice-dammed lakes can experience multiple fill and drain cycles. Drainage from ice-dammed lakes most commonly occur every 1–3 years (Alaska GDL Main Page, 2022), though some lakes can experience multiple events per year (e.g. Lake Nolake; Neal, 2007). In contrast, moraine dammed lakes typically drain only once as permanent damage to the dam is common in the drainage process. Thus, some discrepancy in frequency trends between regions might be attributable to the predominance of one dam type over another.

In Alaska, moraine-dammed lakes are the most common type of ice-marginal lake, composing over 40% of the lake population by number and nearly 80% of total lake area (Rick et al., 2022). However, since the 1980s, only four moraine-dammed lake drainage events have been documented (Harrison et al., 2018). In contrast, ice-dammed lakes compose 9% of the lake population and 6% of total lake area in the 2010s (Rick et al., 2022), yet over 330 events have previously been documented from these lakes between 1985 and 2020 (Veh et al., 2022). Thus, ice-dammed lakes have caused a disproportionately high number of GLOF events in Alaska and pose the greatest hazard to infrastructure and communities.

Whereas there are Alaska-wide inventories of ice-dammed lakes that provide a basis for analyzing changes in lake location through time (Post and Mayo, 1971; Rick et al., 2022), the dynamics of ice-dammed lake drainages have not seen similar systematic study, likely due to a lack of widespread data availability with sufficient spatial and temporal resolution. Current understanding regarding the numbers, frequency, and characteristic initiation date of lake

drainage events comes primarily from case studies of individual ice-dammed lakes (Sturm and Benson, 1985; Anderson et al., 2003; Wilcox et al., 2014; Kienholz et al., 2020), and from compilations of opportunistic observations with reporting bias towards events with societal impacts or lakes in more easily accessible locations (Veh et al., 2022). This lack of systematic and spatially explicit observations of lake drainage events poses challenges to accurately determine robust measures of lake drainage frequency and timing that are critical for accurate hazard assessments.

Rapid glacier retreat and thinning across Alaska (Hugonnet et al., 2021; Jakob et al., 2021) have contributed to the disappearance of over 70% of ice-dammed lakes in the region since the 1960s (Wolfe et al., 2014; Rick et al., 2022). Although ice-dammed lakes in Alaska have decreased in both number and area since the 1980s (Rick et al., 2022), there has been a documented increase in the number of reported GLOF events (Veh et al., 2022), suggesting that more ice-dammed drainages are produced by fewer lakes. However, no comprehensive and systematic inventory of ice-dammed lake drainages exists at a regional or global scale, and drainages from these lakes account for 72% of recorded outburst floods globally (Veh et al., 2022).

Here, I document all identifiable ice-dammed lake drainage events in the Alaska region using satellite imagery (Landsat and Sentinel-2) from 1985 to 2020 to determine robust measures of drainage-event frequency, timing, and size. I focus solely on ice-dammed lakes as they dominate the drainage event record and thus pose the greatest hazards to infrastructure and communities in Alaska.

3.2 METHODS

My study includes ice-dammed lakes within the Randolph Glacier Inventory Region 01 (Alaska and NW Canada) identified in a satellite-image-derived ice-marginal lake inventory (Rick et al., 2022), lakes which remain from a 1960s aerial-image-derived ice-dammed lake inventory (Post and Mayo, 1971), as well as lakes that have observed drainage events (Alaska GDL Main Page, 2022). In total, 118 ice-dammed lakes with an area > 0.1 km^2 were investigated, and 106 of these lakes experienced one or more drainage event.

3.2.1 Imagery dataset

For each lake, I created a true color time-lapse video in Google Earth Engine using all available Landsat 5 (Thematic Mapper, TM), Landsat 7 (Thematic Mapper Plus, ETM+), Landsat 8 (Operational Land Imager, OLI), and Sentinel-2 (Multi-Spectral Instrument, MSI) imagery with less than 20% cloud cover from May 30 to November 1 of each year, from 1985 to 2020. In total, over 14000 satellite images were analyzed. Over the entire study period, there was an average of 3.4 images per lake per year (min = 0, max = 35). The average number of images available tripled for the 2013–2020 period following the launches of Landsat 8 and Sentinel 2 (Fig. 1c), with an average of 10.6 images per lake per year. This study is limited by the availability of cloud-free satellite imagery, particularly before the launch of Landsat 8 in 2013 (see Fig. 1c).

For each image, the lake was manually classified as full, partially full, or drained. A drainage event was considered to have occurred between images when the lake was full in one image and partially or fully drained in the subsequent image, or a change from partially full to drained (see Fig. B5 for examples). I know the drainage occurred between these two images,

though not the precise drainage date (Fig. B6). When the two images (full, drained) are from different years, the event is assigned to the year when the lake was observed drained. In this study, I use the term "drainage event" rather than GLOF as I cannot identify the nature and rate of drainage for any particular event, and the term GLOF implies fast release and catastrophic drainage.

3.2.2 Determining drainage frequency over time

To address changes in imagery availability over the study period, I determined whether a lake had adequate imagery to possibly detect an event in any given year. In my record, the distribution of days between images that captured a drainage event indicates an average of 28 days between images, and the empirical probability distribution indicates 18, 32, and 48 days for the 25%, 50%, and 75% quantiles, respectively (Fig. B2).

I used three different criteria of "adequate imagery" to constrain whether I see a significant change in frequency over time (Fig. B3). Criteria one (least restrictive) described detection using the 25% quantile, requiring that for any given year and any given lake, there had to be at least two images that were 18 or more days apart. Criteria two (medium restrictive) was the middle ground scenario using the 50% quantile, requiring at least two images that were 32 or more days apart (> 50% chance of capturing an event; Fig. B7). Criteria three (most restrictive) used the 50% quantile and considered the timing of the images, requiring at least two images that were 32 or more days apart and their dates bracketing ± 20 days of the median drainage day of year (calculated using the midpoint between date full and date drained for each event per lake). The ratio of number of events detected to number of lakes with adequate imagery per year was used to normalize for imagery availability in each criteria (Fig. 3.1d).

3.2.3 Trend in release timing

Trend in drainage day over time for each individual lake was assessed by Monte Carlo methods to account for the unknown exact date of release. For each lake, 10,000 simulations were run in which a time series was constructed by randomly selecting a day of year between the last date full and first date drained for each year to be the exact drainage date (using uniform distribution within the window). I then performed linear regressions on the synthetic datasets to determine whether a temporal trend in lake drainage date exists at the 95% confidence level.

3.2.4 Lake area and volume

Lake area and lake area change are based on outlines from Rick et al. (2022), and more detailed records of lake area for the five largest lakes were manually outlined before and after each drainage event (Fig. B8 and B9).

Lake volume estimates were calculated using the power scaling described by Shugar et al. (2020),

$$V = k_1 A^{k_2}$$

Where V is lake volume (x 10^6 m^3), A is lake area (m^2), coefficient k_1 has an estimated value of 4.66 x 10^{-11} and coefficient k_2 has an estimated value of 1.76.

3.2.5 Challenges and limitations

This study is limited by satellite imagery availability and the spatial and temporal resolution of this imagery. Due to limited imagery frequency, I am unable to detect more than one drainage event per year, though lakes such as Lake Nolake and Suicide Basin have experienced multiple drainages in a single year (Neal, 2007; Kienholz et al., 2020). The ice-filled nature of many ice-dammed lakes also complicates the distinction between a full and drained

lake, as sometimes the only indicator that a lake drained is a small depression in the lake ice (Fig. B5). I am also unable to detect if a lake drains after snow cover onset. For example, Snow Lake tends to drain in the fall, often after snow cover onset and has been observed through hydrological methods to drain every 2–3 years since the 1950s (Alaska GDL Main Page, 2022) (Fig. B10). However, my methods only capture three events since 2015, likely due to the heavily iceberg-filled nature of the lake as well as its drainage timing. The 30 m resolution of Landsat imagery is not sufficient to see small changes in ice topography when the lake drains (Fig. B11), and I am only able detect Snow Lake events with Sentinel-2 imagery (10 m resolution). Thus, the reported findings here are a clear minimum of the number of ice-dammed lake drainage events that occurred between 1985 and 2020.

3.3 INCREASE IN DETECTED DRAINAGE EVENTS OVER TIME ATTRIBUTABLE TO IMAGERY BIAS

Ice-dammed lakes in Alaska are often located in remote locations and their drainage may go undetected. However, understanding release characteristics such as return interval, timing, volume, and changes over time facilitate the prediction of flood events and characterization of hazards. I document 1150 drainage events from 106 individual ice-dammed lakes across the Alaska region between 1985 and 2020. This is approximately three times the 339 events previously documented in the region (Veh et al., 2022). Furthermore, I document an increase in the number of *detected* drainage events over time (Fig. 3.1b). This striking increase with time, however, appears attributable to the increase in satellite imagery availability over the study period. Suitable imagery increased markedly with the launches of Landsat 7, Landsat 8, and Sentinel-2 in 1999, 2013, and 2015, respectively (Fig. 3.1c). I find a strong positive correlation ($R^2 = 0.95$; Fig. B1) between the number of lakes with adequate imagery to detect a drainage

event (see Methods) and the number of events detected, suggesting that increased image availability is the primary driver of the apparent increase in drainage events.

3.4 UNCHANGED PROPORTION OF LAKES DRAINING OVER TIME AT THE REGIONAL SCALE

To correct for this first-order bias stemming from imagery availability, I only consider lakes in each year with adequate imagery to detect an event. With imagery bias removed, I find no significant trend over time in the proportion of lakes that drain each year (Fig. 3.1d). Best-fit linear trends in time have slopes approaching zero (trends of –0.00003 events/year with p-value = 0.99, 0.0009 events/year with p-value = 0.62, and 0.0009 events/year with p-value of 0.57, for the most restrictive, medium restrictive, and least restrictive criteria, respectively. See Methods and Supplementary Fig. B2 and B3 for details). This suggests that although glaciers have rapidly thinned and retreated in Alaska (Hugonnet et al., 2021) and ice-dammed lakes have decreased in both number and area (Rick et al., 2022), the proportion of ice-dammed lakes that drain each year (ratio of number of events detected to number of lakes with adequate imagery) has remained unchanged at ~50% over the past 35 years. Thus, when averaged across the Alaska region it is expected that ~50% of ice-dammed lakes drain in any given year, and that the average reoccurrence interval of a drainage event for an individual ice-dammed lake is approximately two years.

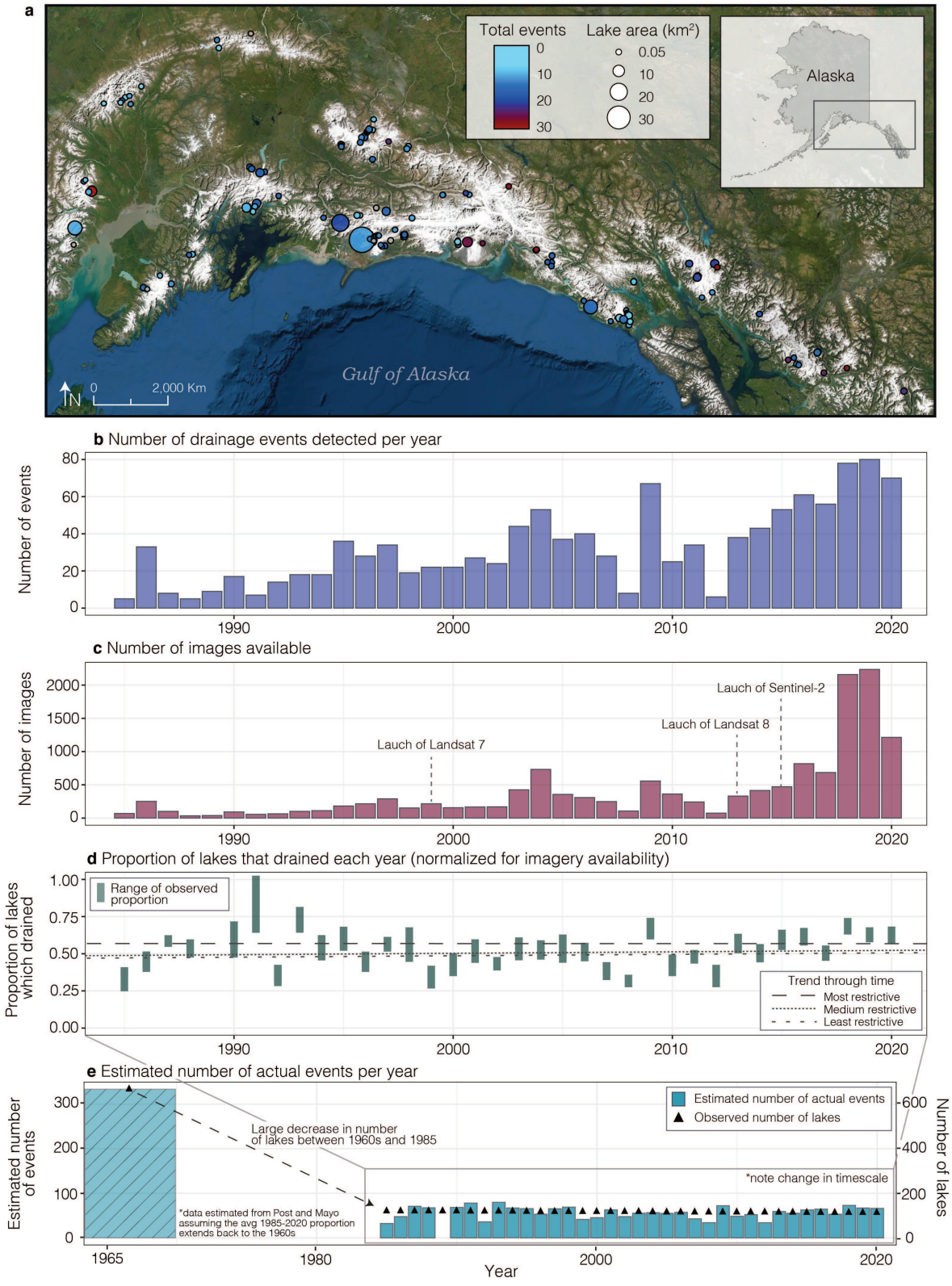

Figure 3.1. Ice-dammed lake locations and drainage events through time. a) Spatial distribution of ice-dammed lakes colored by total number of events documented between 1985 and 2020, sized by area. b) Total number of detected drainage events per year. c) Total number of cloud-

free images available per year. d) Range of proportion of lakes that drained each year calculated as the ratio of number of events detected to number of lakes determined to have the possibility of detection given three different criteria (see Methods or Fig. B3): Least restrictive — two images with at least an 18 day gap; Medium restrictive —two images with at least a 32 day gap; and Most restrictive —two images with at least a 32 day gap and dates bracketing the median drainage day. Dashed lines represent the trend through time for the most restrictive criteria (trend = –0.00003 events/year, p-value = 0.99), medium restrictive criteria (trend = 0.0009 events/year, p-value = 0.62), and the least restrictive criteria (trend = 0.0009 events/year, p-value = 0.57). e) Estimated number of actual drainage events per year (blue bars) calculated by multiplying the number of lakes present (triangles) by the stationary proportion of lakes that drained (mean value from d). Estimate for the 1960s was calculated assuming the mean proportion extends back to the 1960s.

3.5 NOTABLE VARIABILITY IN THE DRAINAGE FREQEUNCY AND TIMING OF INDIVIDUAL LAKES

Although the regionally averaged proportion of lakes that drain each year appears stationary across the record, the drainage frequency and timing of individual lakes shows substantial variability (Figs. 3.2, 3.3 and B4). One notable pattern seen for individual lakes was a changing date of drainage. Whereas over half of the observed lakes do not have a clear trend in the timing of drainage events, 30% of lakes experienced an earlier release over time and 9% experienced a later release over time. The trend in progressively earlier draining has been recorded at a global scale as well, with two thirds of lakes draining five or more times exhibiting this trend (Carrivick and Tweed, 2016). Release date is thought to be influenced by when the lake fills, lake water temperature, dam strength, and ice dynamics (Jacquet et al., 2017). As ice dams are thinned and weakened, it requires less pressure to destabilize the ice and produce a flood, suggesting that drainage events should occur earlier in the season if water inputs to the lake are constant in time. Earlier onset of snow and ice melt likely contributes to earlier drainage dates as well.

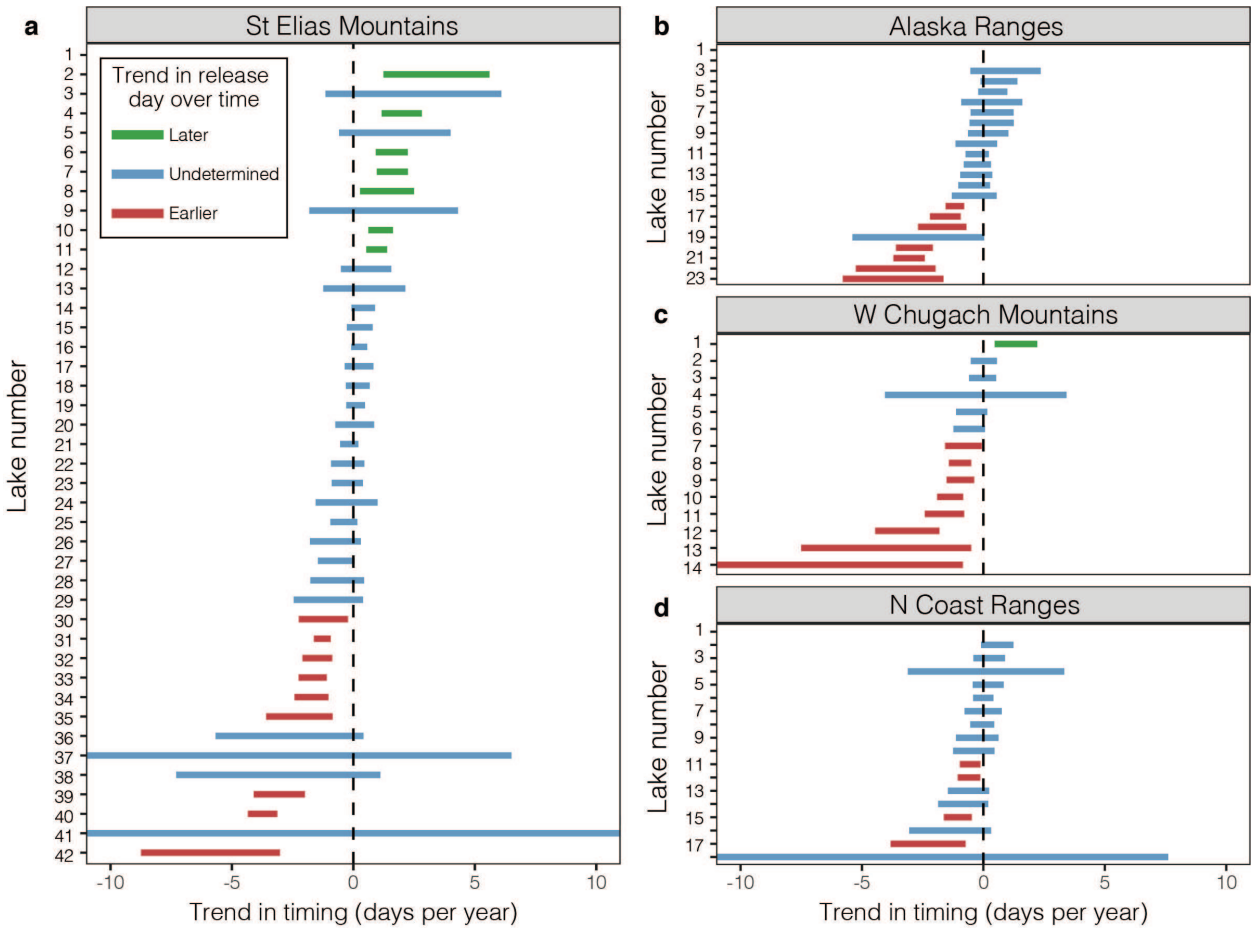

Figure 3.2. Trend in lake release date over time. Ninety-five percent confidence interval for the trend in drainage event timing (in days per year) for each lake which experienced two or more drainage events, separated by RGI subregion (a–d) and colored by whether the trend indicates an earlier (red), later (green), or undeterminable (blue) release over time. Corresponding lake IDs to the lake number (y-axis) can be found in Table B1.

Another notable pattern of drainage events seen at individual lakes was an increase in frequency with time. Summit Lake is an example of a lake which has been observed since its first outburst flood in 1961 (Mathews, 1965; Gilbert, 1972; Mathews and Clague, 1993). This lake progressed from a stable state to a regular draining state in 1961, with increasingly earlier and smaller flood events as the volume of the lake has decreased over time (Mathews and Clague, 1993). Summit Lake has drained annually since 1970, but has lost over 4 km^2 (~80%) in surface area since then (Post and Mayo, 1971). Summit Lake continues to drain annually, though

the lake is now ~1 km^2. Strandline Lake also exhibits increased drainage frequency (Fig. 3.3). It drained every 2–3 years between 2000 and 2010, but every year between 2013 and 2020. Additionally, the volume of water released from Strandline Lake has decreased over time as the maximum lake area has decreased.

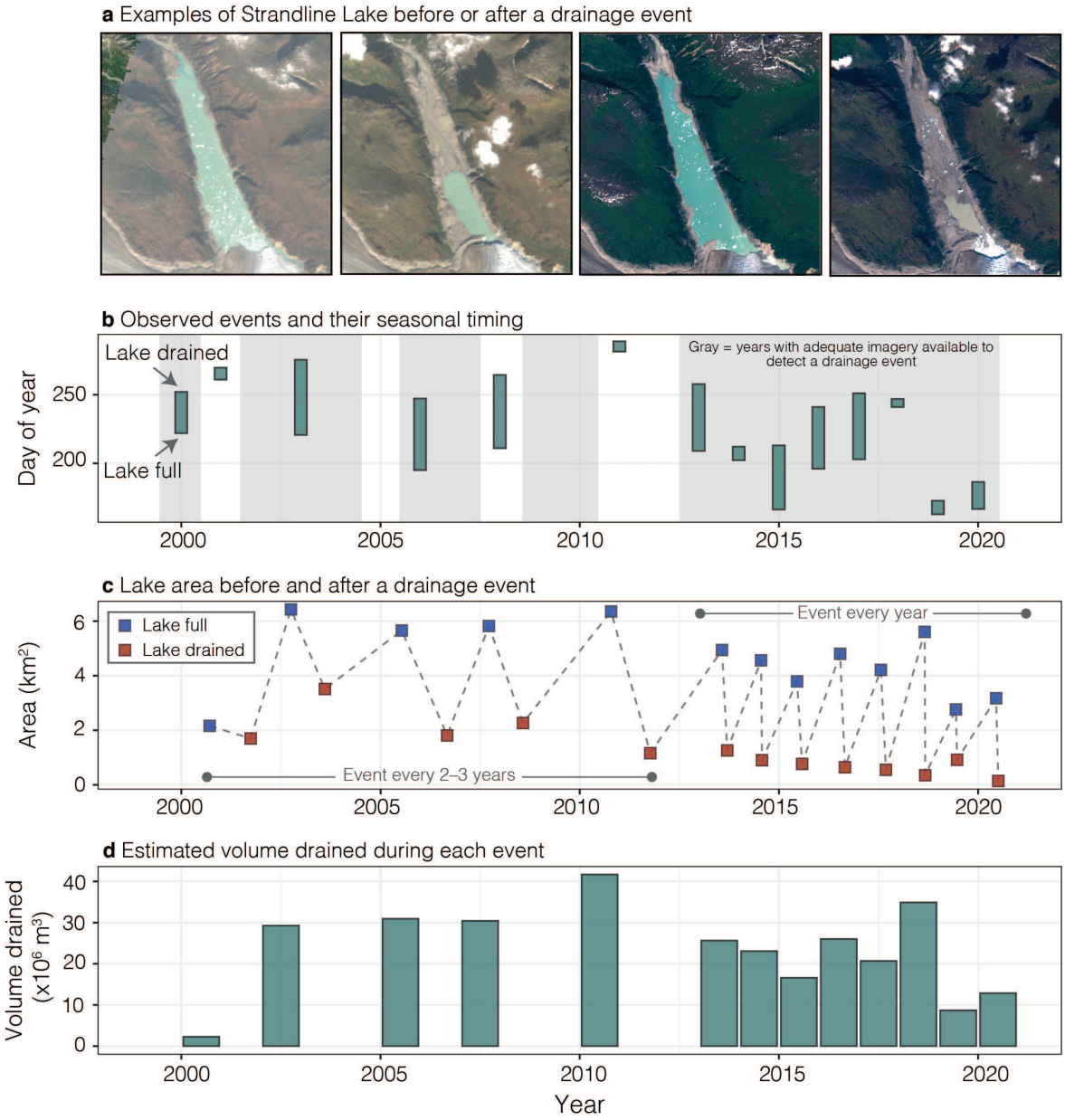

Figure 3.3. Strandline Lake exhibits trends of increasing frequency of drainage events and decreasing area and volume over time. a, Examples of images when Strandline Lake was full or drained from the early 2000s and mid-2010s. b, Observed events with the bottom of the segment representing the last image when the lake was full, and the top representing the first image the

lake was drained, indicating that the lake must have drained between those two dates. Gray bars indicate years with adequate imagery to detect an event given the medium restrictive criteria (32+ days between images). c, Area of the lake before (blue) and after (red) each drainage event. d, Estimated volume drained for each drainage event.

As glaciers continue to thin and retreat, I expect lakes that fill and drain to move upwards in elevation along the glaciers (Wolfe et al., 2014), as glacier network structure in Alaska should allow for the creation of new lakes as tributary valleys deglaciate. The lifespan of a lake depends on the height and thinning rate of the ice dam, as a dam's height limits its ability to impound water (Tweed and Russell, 1999). An interesting question for future work is whether accelerating rates of ice loss (Hugonnet et al., 2021) will shorten the life cycle of persistent and newly formed ice-dammed lakes.

3.6 THE ROLE OF DAM TYPE IN DRAINAGE FREQUENCY

The documented yearly average of ~66 events per year during the period of most comprehensive imagery coverage (2015–2020; Fig. 3.1b and c) is 55 times greater than the regional rate of GLOFs from moraine-dammed lakes documented in the Himalaya (average of 1.3 events per year (Veh et al., 2019)). This striking difference in frequency between Alaska and the Himalaya can largely be attributed to the abundance of ice-dammed lakes in Alaska as compared to the predominance of moraine-dammed lakes in the Himalaya.

Although moraine-dammed lakes make up the majority of glacial lakes in Alaska, only four GLOFs have been documented from moraine-dammed lakes since 1985 (Harrison et al., 2018). The relatively low frequency of moraine-dammed lake drainage events in Alaska is likely related to the structure and location of Little Ice Age moraines (LIA; ~1350–1850 AD in the Northern Hemisphere; Solomina et al., 2015). In many instances, LIA moraines are located in large, flat valleys, rather than the steeper settings found in the Himalaya or Tropical Andes. The

triggering mechanism for moraine-dammed lake floods are often ice or rock fall into the lake, which initiate from steep adjacent slopes (O'Connor et al., 2020). Few moraine-dammed lakes in Alaska are currently surrounded by these types of steep, triggering slopes, which reduces the likelihood of moraine-dam failure from such a trigger. Additionally, some moraine dams remain stable due to low-gradient outlet channels draining the lake, maintaining a stable lake level (Clague and Evans, 2000). Other moraine-dammed lakes may disappear due to sediment infill (as occurred for the seven lakes lost between 1984–2019; Rick et al., 2022), which results in lake displacement and a low likelihood of an outburst flood (O'Connor et al., 2020).

3.7 REGIONAL REDUCTION OF HAZARDS DUE TO THE LOSS OF ICE-DAMMED LAKES SINCE THE 1960S

An inventory created with areal imagery in the 1960s documented 750 ice-dammed lakes in Alaska (Post and Mayo, 1971), 667 of which were lakes larger than 0.1 km^2. Nearly sixty years later, only 195 of these lakes remain in modern imagery, indicating that over 70% of ice-dammed lakes have disappeared since the 1960s (Fig. 3.4). An additional 44 lakes within the inventory transitioned to a more stable dam type (e.g., from ice-dammed to bedrock- or moraine-dammed; Fig. 3.4c) such that only 23% of the ice-dammed lakes present in the 1960s remain as ice-dammed lakes. Of the lakes that were lost, 63% of lakes were < 0.5 km^2, while over 70% of persistent lakes were > 0.5 km^2. My inventory identifies 22 ice-dammed lakes which formed after the 1960s, though this is likely an undercount as my semi-automated, spectrally based method misses many small, marginal lakes which are iceberg-choked and therefore spectrally indistinct from glacier ice. Regardless, the number of newly formed lakes is a small fraction of the 472 that have been lost.

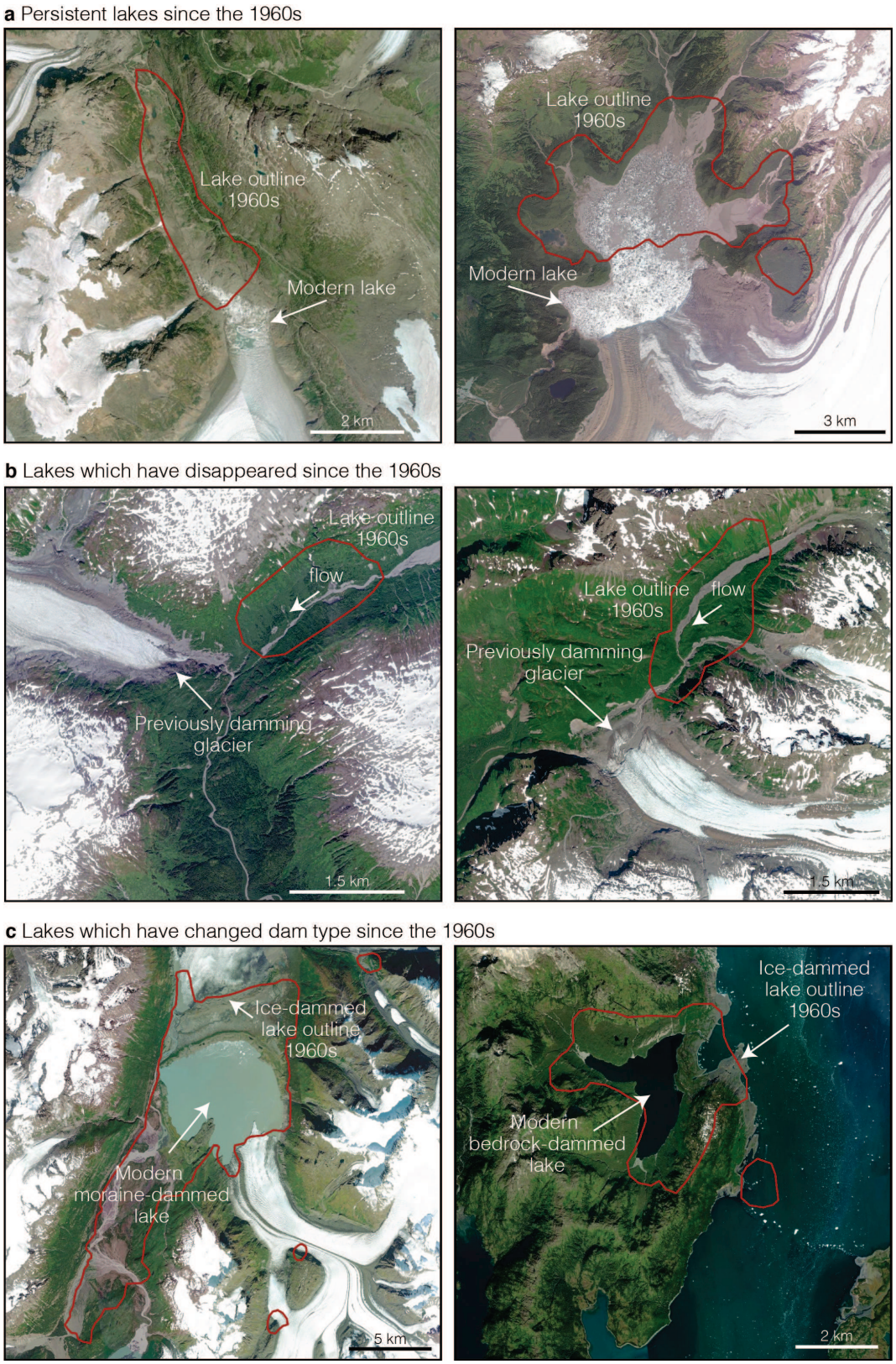

Figure 3.4. Examples of lake outlines from the 1960s. a, Examples of persistent lakes with Summit Lake on the left and Berg Lake on the right. Red outlines were digitized from the map

produced by Post and Mayo(Post and Mayo, 1971), overlayed on modern imagery. b, Examples of two lakes that have been lost since the 1960s due to the retreat of the damming glacier. c, Examples of lakes that have changed dam type since the 1960s, with Lake George on the left (now moraine-dammed) and Terentiev Lake on the right (now bedrock-dammed).

Assuming that the unchanging proportion of ice-dammed lakes that drain each year (Fig. 3.1d) documented here for 1985–2020 extends back to the 1960s, I infer a nearly 70% reduction in ice-dammed lake related drainages. These changes suggest a substantial reduction in hazards in the region as a whole owing directly to the dramatic loss of ice-dammed lakes over time.

Post and Mayo (1971) identified 32 of the most hazardous or unique ice-dammed lakes in their inventory, based on lake size, location, and historical flood records. At present, 20 of these 32 (63%) lakes remain, though four have transitioned to a more stable dam type. This means that 16 of 32 ice-dammed lakes remain – this fact, combined with the unchanged proportion of ice-dammed lakes that drain each year, implies a 50% reduction in the most hazardous lakes since the 1960s. Of the lakes that remain, nearly all have seen a decrease in volume (inferred from area), likely reducing the maximum peak discharge possible for any modern drainage event.

Although the frequency of drainage events that a region experiences is a fundamental measure of GLOF hazard, the peak discharge of each event, which scales with drainage duration, is of similar importance. Unfortunately, I was unable to measure drainage duration in the current analysis, as a typical lake drains on the order of hours to days. This timing is much shorter than the average 28 days between images capturing an event in the current analysis. Additionally, the sensitivity of event magnitude to drainage duration precludes a simple relationship between lake volume and flood impact (Walder and Costa, 1996). Thus, even though the total area, and therefore volume, of ice-dammed lakes has decreased in Alaska since the 1960s (Rick et al., 2022), no certain statements can be made regarding characteristic event magnitude based on

these easily-measured lake properties. For example, a small lake that drains quickly can have a large peak discharge, and conversely, a large lake which drains slowly could have a smaller peak discharge and little to no downstream impacts.

Furthermore, the size and characteristics of the river into which a lake drains also factors into the impact of an event, as a large river can mute the downstream signal of a lake draining (Jacquet et al., 2017). For example, Van Cleve Lake is a large (5.5 km^2 in 2016–2019) ice-dammed lake which drains through Miles Lake and into the Copper River. Due to the Copper River's large mean annual flow (~1755 m^3/s; Granato et al., 2017), these drainage events are presently difficult to detect within the Copper River hydrograph. Conversely, Suicide Basin, located adjacent to the Mendenhall Glacier, has an area of only 0.5 km^2 and impacts homes and roads downstream due to the lake's proximity to settled areas and its drainage discharge being large relative to typical flows in the Mendenhall River (Kienholz et al., 2020).

Taken together, it is clear that determining regional relationships for event magnitude and impact are critical next steps to fully characterize hazards from glacial lakes, albeit challenging ones (Carrivick and Tweed, 2016). However, this study takes an important step towards a more accurate characterization of glacial-lake hazards across Alaska by determining the characteristic tempo of lake-drainage events. The observed decrease in number of ice-dammed lakes, combined with unchanged proportion of lakes which drain, suggests that the overall frequency of events has decreased, and barring some exceptional increase in flood magnitude, so has the regional flood hazard presented by ice-dammed lakes.

3.8 CONCLUSIONS

Alaska is losing ice mass at one of the fastest rates globally and this rate is accelerating, causing profound physical changes to the region's glaciers and downstream environments. Ice-

dammed lakes are impacted by glacier thinning and mass loss as their volume and stability is determined by dam height and integrity. My study triples the previous estimate of ice-dammed lake drainage events over the satellite record in Alaska, with 1150 identified drainage events from 106 individual ice-dammed lakes. Nearly a third of lakes with two or more events experienced a progressively earlier release date over time. Whereas the proportion of lakes that drain each year between 1985 and 2020 has remained unchanged, the number and area of ice-dammed lakes have dramatically decreased between the 1960s and 2020, implying a large decrease in hazards related to ice-dammed lakes in the Alaska region. Understanding when and where lake drainage events occurred in the past is critical for predicting future lake behavior, with hazard implications for floods producing large societal and ecological impacts.

4. HYDROLOGICAL INFLUENCE OF AN ACTIVE ROCK GLACIER IN THE FRONT RANGE, COLORADO[3]

4.1 INTRODUCTION

As global and high mountain environments experience air temperatures increases, these temperature changes affect mountain ecosystems, hydrology, biodiversity, and cryospheric systems (Pepin et al., 2015; Huss et al., 2017). Warming impacts to glaciers, snowpack, snowmelt timing, and stream temperatures influence the presence and survival of certain cold-water alpine species (Huss et al., 2017; Brighenti et al., 2021). As glaciers disappear, particularly in the Southern Rocky Mountains, subterranean ice – such as is present within active rock glaciers—will likely play a greater role in maintaining cold streams in a warming climate and providing refuge for microbial communities to aquatic macroinvertebrates to fish, which can be dependent on such streams for habitat (Isaak et al., 2015; Hotaling et al., 2019; Tronstad et al., 2019; Muhlfeld et al., 2020; Brighenti et al., 2021). However, these long-term cold-water stores are relatively understudied and are often disregarded in future climate scenarios (Leopold et al., 2011; Rangecroft et al., 2015; Janke et al., 2017; Colombo et al., 2018; Munroe, 2018; Jones et al., 2019).

Rock glaciers are lobate- or tongue-shaped landforms comprised of rock and ice found in mountain environments (Giardino and Vitek, 1988; Barsch, 1996). While rock glacier origins have been heavily debated surrounding periglacial/permafrost origins (e.g., Haeberli, 1985) vs glacial origins (e.g., Potter, 1972), recent studies describe a spectrum of rock glaciers, dependent

[3]Chapter in preparation as Rick, B., McGrath, D., Lehmann, B., Fegel, T., and Williams, K. Hydrological influence of an active rock glacier in the Front Range, Colorado.

on individual slope, glaciological, and climatic controls (Berthling, 2011; Anderson et al., 2018; Jones et al., 2019; Knight et al., 2019). Glaciogenic origin is generally evidenced by a massive glacier ice core, and is considered to be the end member of the glacier—debris-covered glacier—rock glacier continuum (Monnier and Kinnard, 2015; Anderson et al., 2018). The periglacial model describes how interstitial ice or ice lenses are formed from freezing rain, meltwater, groundwater, and/or snow and ice accumulations, which are buried by rock and eventually induce permafrost creep (Wahrhaftig and Cox, 1959; Haeberli, 1985; Burger, Jr and Giardino, 1999; Haeberli et al., 2006; Jones et al., 2019). These two origin models have distinct internal rock glacier structure (massive glacial ice vs interstitial ice) which aids in interpreting origin as well as ice content for hydrological estimations and runoff implications (Jones et al., 2019).

Downslope movement results from internal ice deformation, conveying rocky debris downslope (RGIK, 2022). Rock glaciers are categorized into three different categories based on inferred movement: *active, transitional*, and *relict* (RGIK, 2022). *Active* rock glaciers contain ice and show geomorphological evidence of downslope movement over most of its surface, such as ridge-and-furrow features and steep frontal and lateral margins (Haeberli et al., 2006; Jones et al., 2019; RGIK, 2022). *Transitional* rock glaciers have reduced ice content and little to no detectable movement over most of their surface, displaying less distinct geomorphological evidence of current downslope movement. A *relict* rock glacier, or a former rock glacier, contains little to no ice and shows no geomorphological evidence of recent movement, characterized by gentler and rounder slopes, extensive vegetation or lichen cover, and oftentimes surface collapse features such as thermokarst ponds (Martin and Whalley, 1987; Barsch, 1996; Baroni et al., 2004; Harrison et al., 2008; Jones et al., 2019; RGIK, 2022).

Rock glaciers can be difficult to study due to their coarse, blocky, and unstable surfaces which conceal ice present beneath the surface. Geophysical imaging allows for subsurface interpretation, and is the main tool used to estimate rock glacier depth to ice, bedrock, and internal structure (Maurer and Hauck, 2007; Leopold et al., 2011; Florentine et al., 2014; Merz et al., 2016; Petersen et al., 2020). For example, ground-penetrating radar (GPR) can help determine whether a rock glacier is composed of massive or interstitial ice, the depth of the active layer, and internal layers (Florentine et al., 2014; Harrington et al., 2018; Petersen et al., 2020). Seismic refraction is similarly used to identify internal structure based on changes in seismic velocity which correspond to changes in material (e.g., rock and air in the active layer, ice or rock and ice mixture, bedrock, etc.; Maurer and Hauck, 2007; Merz et al., 2016). The thick surface debris layer which makes rock glaciers difficult to study is also what makes them more resilient to warming temperatures, as the debris partially decouples the ice from external climate forcings (Liu et al., 2013; Anderson et al., 2018). Rock glaciers are able to persist even when the equilibrium line altitude is above local topography, and have persisted and experienced pulses of activity throughout the Holocene (Refsnider and Brugger, 2007; Anderson et al., 2018; Larsen et al., 2020).

The presence or absence of a rock glacier within a basin can impact short-, intermediate-, and long-term water storage due to impacts on snowmelt and precipitation runoff, seasonal ice melt, and internal ice melt (Geiger et al., 2014; Jones et al., 2018). In the La Sal Mountains, Utah, rock glaciers were found to act as an impervious surface and increase runoff from alpine basins, representing 15–30% of total basin runoff (Geiger et al., 2014). Work in the Green Lakes Valley, CO documented substantial contribution of rock glaciers to late summer/early fall (September-October) streamflow, and an increase in late season discharge over an ~30-year

timespan (1982–2009; Caine, 2010). Water samples from a rock glacier in the Uinta Mountains, Utah were aged from 0–2 years, suggesting a mixture of water from snowmelt/annual ice melt and older ice from the rock glacier interior (Munroe, 2018). These studies illustrate the range of hydrological contributions from rock glaciers, from precipitation runoff to late season discharge.

In addition, streamflow characteristics and water chemistry are important in determining ecosystem function and capacity (Williams et al., 2006; Fegel et al., 2016; Harrington et al., 2017). Rock glaciers contribute significantly to the biogeochemistry of alpine headwaters, and support a higher microbial richness and diversity than ice glaciers (Fegel et al., 2016). Rock glacier streams tend to have elevated pH, ion concentrations, and lower temperatures as compared to non-rock glacier basins, though ion concentrations are mountain range or even basin specific, and are dependent on local lithology (Williams et al., 2006; Caine, 2010; Fegel et al., 2016; Munroe, 2018). Rock glaciers which maintain even very low discharge streams late in the summer can sustain aquatic life where ephemeral streams cannot (Brighenti et al., 2021). In certain basins, the reduced climate sensitivity of rock glaciers and their sustained cold-water input to mountain streams could help mitigate predicted habitat loss for endemic species (Millar and Westfall, 2010; Isaak et al., 2015; Wallis et al., 2016; Hotaling et al., 2019; Tronstad et al., 2019; Muhlfeld et al., 2020; Brighenti et al., 2021).

In addition to a providing a cold-water resource, rock glaciers can be hazardous to mountain travelers and downslope infrastructure. Destabilization and debris flows have been documented in the European Alps (Bodin et al., 2017; Marcer et al., 2021; RGIK, 2022), and the June 28, 2022 rockslide near Hallet Peak in Rocky Mountain National Park was possibly related to interstitial ice detachment or destabilization. Understanding where ice and permafrost are present within alpine landscapes is important for being able to predict hazardous conditions,

from thaw induced rockfall to rock glacier destabilization to glacier collapses (Allen et al., 2017).

Colorado is home to over 3800 rock glaciers, vastly outnumbering the ~16 traditional ice glaciers present today (Johnson et al., 2020). Rock glaciers cover a much larger spatial extent, occupying nearly 13 times more area in the Front Range than glaciers (Janke, 2007), suggesting that rock glaciers contain a larger volume of ice. Previous studies in Colorado have documented displacement rates, hydrological impacts, and internal structure of a few individual rock glaciers, though these studies are limited spatially and temporally. Photogrammetric analysis documented average horizontal rock glacier velocities from 14 to 20 cm yr^{-1} in the Front Range (Janke, 2005), while in-situ measurements ranged from 5 to 10 cm yr^{-1} (White, 1971; Janke, 2005, p.a). Displacement in rock glaciers indicates ice presence, which has been confirmed in the Green Lake 5 rock glacier through geophysical surveys, observing 4–5 m depth of the active layer and 16–18 m total rock glacier thickness (Leopold et al., 2011, 2015). This ice presence also influences basin hydrology, with water temperatures draining from this same rock glacier rarely exceeding 2.5 °C (Leopold et al., 2015), and rock glacier baseflow constituting 38% of the hydrograph (Williams et al., 2006). Late season streamflow increased between 1982 and 2009, likely due to the melting of permafrost ice (Caine, 2010). While the Green Lakes Valley has received concentrated attention thus far, little has been done to understand the spatial and temporal distribution of rock glacier influence on basin hydrology in the greater Colorado area.

In the present study, I incorporate geophysical, hydrochemical, and remotely sensed data to investigate the ice presence, movement, and hydrologic influence of the Lake Agnes rock glacier in the northern Front Range, Colorado. Though rock glacier influence varies between

individual landforms, a detailed case study of the Lake Agnes rock glacier will expand the scarce data available concerning the hydrologic role of rock glaciers in alpine watersheds.

4.2 STUDY AREA

The Lake Agnes rock glacier is located in a north-facing basin within the Never Summer Mountain Range of northern Colorado (40°28'34.14"N, 105°54'8.22"W; Fig. 4.1). The rock glacier is 700 m long, ranging from 3260 to 3525 m asl with an average slope of 30%, and is classified as active (Janke, 2007; Johnson et al., 2020). Mean annual air temperature (MAAT) at the rock glacier is ~0.2 °C, as calculated by applying a standard lapse rate (0.55°C per 100 m) to temperature observations from the Joe Wright SNOTEL station (Site 551, 3085 m asl, 6.2 km from Lake Agnes). The surrounding bedrock and rock glacier source material are granodiorite of Miocene age, with principal minerals of andesine, potash feldspar, quartz, hornblende, biotite, and minor pyroxene (USGS, 1981).

Lake Agnes is located just west of the Continental Divide, draining naturally as a headwater into the North Platte Basin. However, Lake Agnes is also the headwaters of the Michigan Ditch. This trans-mountain diversion moves nearly 3 million cubic meters of water from the North Platte Basin to the Poudre River annually, supplying water to the Joe Wright Reservoir which stores and supplies water for communities along Colorado's Front Range (NSOS, 2017). Consequently, Lake Agnes is an important headwater for both the North Platte Basin and the Poudre River Basin.

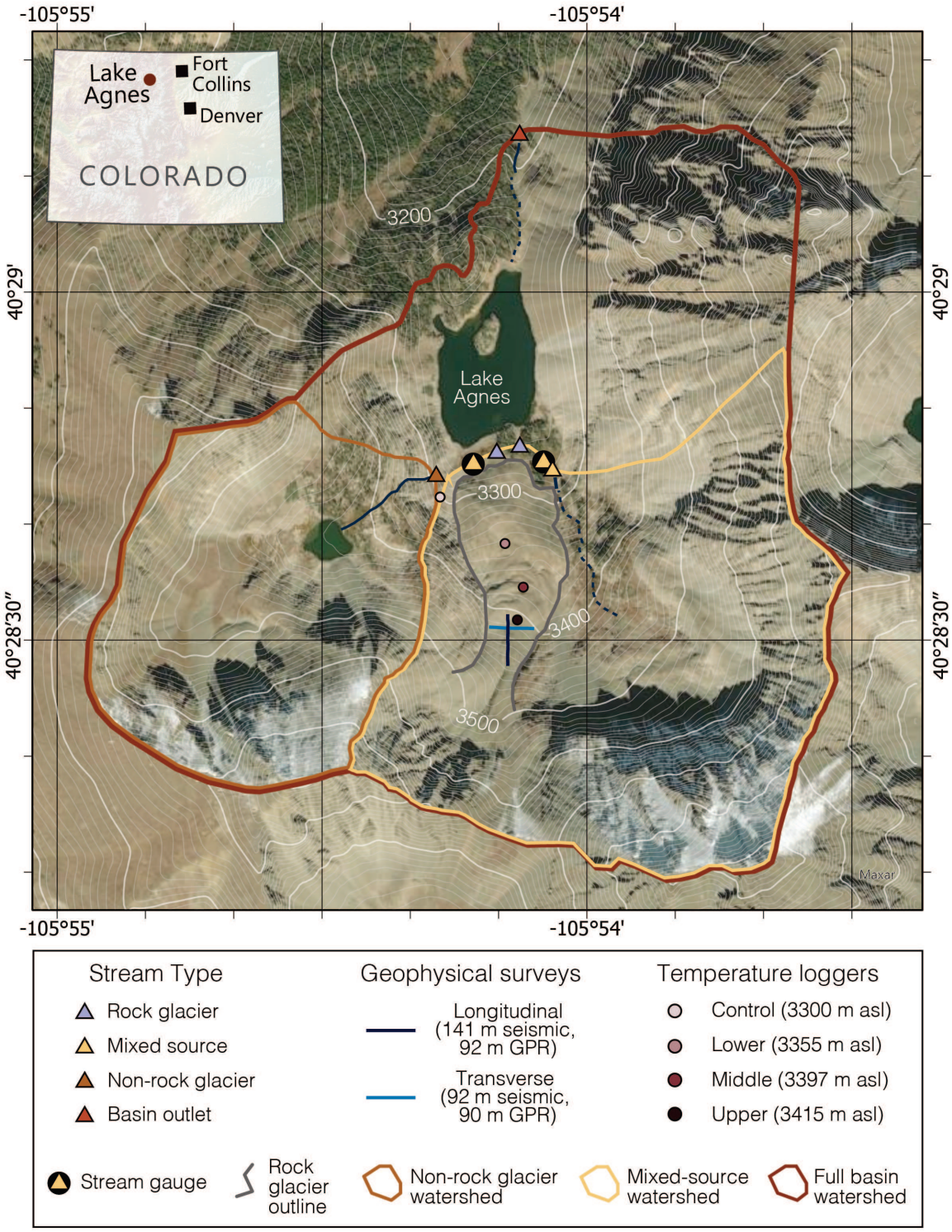

Figure 4.1. Location of the Lake Agnes rock glacier with watersheds outlined for the non-rock glacier (orange), mixed-source (yellow), and basin outlet (red) streams. Location of temperature loggers (circles), geophysical surveys (blue lines), and stream sites (triangles) are also present. Dark blue lines represent streams, with dashed lines indicating intermittent or below surface streams.

4.3 METHODS

This study incorporates geophysical, hydrochemical, and remotely sensed data from summers 2019, 2020, and 2021 to investigate the ice presence, movement, and hydrologic contribution to late-season streamflow from the Lake Agnes rock glacier (Fig. 4.2). Field campaigns in late summer 2020 were impacted by the Cameron Peak fire as the field site was inaccessible.

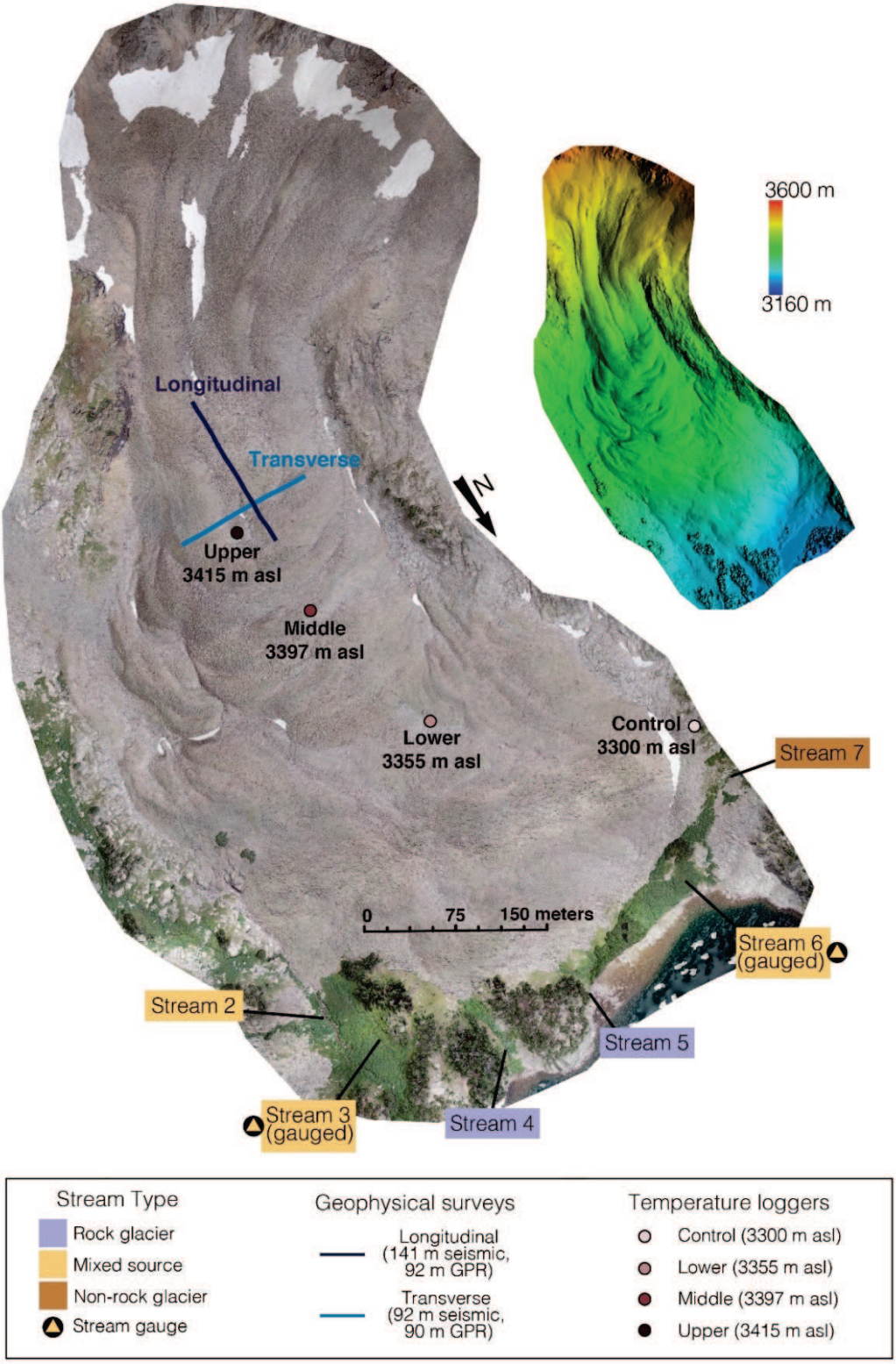

Figure 4.2. Summary of locations of sampled streams with stream type, geophysical surveys, and temperature loggers. Upper right shows surface topography and elevation of the rock glacier. Note that basin outlet is not shown on this figure—see Fig. 4.1 for location.

4.3.1 Water quality and streamflow

Water samples were collected and filtered (0.45 μm Restek Syringe filters) at seven stream locations (two pure rock glacier, three mixed-source, one non-rock glacier, and one basin outlet; Fig. 4.2) throughout the 2019, 2020, and 2021 summer seasons. Samples were processed for stable isotopes (δ^2H and $\delta^{18}O$) in 2019 at the University of Wyoming Stable Isotopes Lab, and in 2020–2021 at the Colorado State University NREL EcoCore Lab. Ion concentrations were analyzed at the Rocky Mountain Research Station's Biogeochemistry Lab (Ca^{2+}, Mg^{2+}, Na^+, K^+, NH_4^+, Cl-, NO_3-, PO_4^{3-}, SO_4^{2-}) via ion chromatography. Temperature, pH, and electrical conductivity (EC) were collected in-situ using a handheld sensor (Apera PC400S) at the time of sampling. Two stream gauges (TruTrack WT-HR data logger) recorded stream stage at 15-minute intervals at mixed source streams (Streams 3 and 6; Fig. 4.2) draining the rock glacier and upper basin throughout the snow-free period.

In-situ discharge measurements were collected using the tracer dilution method (Hudson and Fraser, 2005). By conducting these measurements at different stream heights, I created a rating curve to convert the stage record into a hydrograph for each gauge location (Fig. C1 and C2). A total of seven manual discharge measurements were used to create the rating curve for the stream gauge at the eastern rock glacier outflow (Stream 3), and five measurements were used for the western rock glacier outflow (Stream 6).

4.3.2 Geophysics: Seismic refraction and ground-penetrating radar (GPR)

Geophysical techniques are well-established for gathering information about the internal structure of rock glaciers (Maurer and Hauck, 2007). GPR measures variations in dielectric properties, and for rock glaciers specifically, these properties vary for air, ice, and rock. Seismic

refraction tomography (SRT) uses changes in seismic velocity to infer internal layering. Typically, rock glacier structure consists of a surface layer of rock and air (active layer) with velocities ranging 500–1500 m/s, a heterogenous layer of rock and ice with intermediate velocities ranging ~3000–4000 m/s, and bedrock below with high velocities (>4500 m/s), though velocities are dependent on rock type and ice content (Maurer and Hauck, 2007; Merz et al., 2016).

Two seismic refraction surveys were conducted in October 2019 using a Geometrics Geode data acquisition system, one longitudinal profile (141 m, 3 m spacing) and one transverse to flow (92 m, 4 m spacing). After removing the spikes, the geophones were attached directly to boulders using plumber's putty to increase contact. The energy source was a sledgehammer, and traces were stacked 8 times per location to improve the signal to noise ratio. First arrivals were manually picked, and the data were inverted using Geogiga Seismic Pro software, with inversion velocities constrained between 300 and 6000 m/s.

I used a Sensors & Software Pulse Ekko Pro 100 MHz GPR in common-offset configuration to survey two transects coinciding with the seismic transects in July 2020. Antennas were separated by 1 m and traces were collected every 25 cm, with a time-sampling interval of 100 ps and 32 stacks at each survey location. An Emlid Reach RS2 RTK system was used for geolocating GPR traces for the longitudinal line, and GPS points were collected every 10 m along the transverse line. The slight discrepancy in elevation profiles for GPR and SRT is likely due to small horizonal offsets during surveys to find more suitable ground.

Radargrams were processed in ReflexW software (Sandmeier Geophysical Research, 2014) with the following steps: (1) move start time, (2) dewow filter, (3) divergence compensation, (4) butterworth bandpass filter, and (5) running average filter. An electromagnetic

wave velocity of 0.13 m/ns was assumed from previous studies working in a similar environment (Langston et al., 2011; Harrington et al., 2018).

One electrical resistivity survey was attempted using a SuperSting-R8 for an along-flow profile (167 m, 3 m spacing), but poor coupling between electrodes and boulders resulted in frequent high voltage errors and insufficient data collection. Placing saline water-soaked sponges between electrodes and boulders (Maurer and Hauck, 2007) did not improve coupling sufficiently to produce usable data.

4.3.3 Structure from motion (SfM)

Uncrewed aerial vehicle (UAV) surveys were conducted August 31, 2019 and September 24, 2021 using a DJI Phantom Pro 4 and DJI Mavic Pro 2, respectively. Flights were flown in a grid pattern with 80% overlap and at an average height of 60 m above the surface. These images were used for Structure from Motion (SfM), creating an orthomosaic and digital elevation model (DEM) of the rock glacier for each year using Agisoft Metashape software (Version 1.7.6). Ground control points (n=10; 0.05 m accuracy) consisted of 1 m square black and white targets. An additional five "natural" GCPs (i.e. distinct rock fractures, corners, features) were used for consistency and coregistration between years. Center coordinates for GCPs were measured using two Emlid Reach RS2 GPS units (one as a base station and one as a rover) for a post-processed kinematic (PPK) survey. Post-processing was performed using the RTK Library and documentation (RTKLib version 2.4.3; Takasu and Yasuda, 2009).

Orthomosaics from 2019 and 2021 were used to estimate 2D horizontal displacement using the feature-tracking IMCORR module (Scambos et al., 1992) within the SAGA toolbox in QGIS. This module identifies pixel patterns between two georeferenced images and estimates displacement between small subsections of the images. I used the following parameters within

IMCORR: a search window size of 64 x 64 pixels, a reference window size of 16 x 16 pixels, and a grid spacing of 1 m. An error threshold of 10 pixels was applied in the x- and y- directions, removing ~3% of the calculated points.

4.3.4 Bottom temperature of snow (BTS)

I placed three Hobo Tidbit temperature loggers (± 0.21°C uncertainty) longitudinally along the rock glacier at elevations of 3415 m asl (upper), 3397 m asl (middle), and 3355 m asl (lower), and one logger off the rock glacier as a control (3300 m asl; Fig. 4.1). Loggers were place just beneath the ground or rock glacier surface, and recorded temperatures throughout winters 2018–2019 and 2019–2020.

4.4 RESULTS

4.4.1 Water quality and streamflow

Hydrochemical results (pH, temperature, ion concentrations, $\delta^{18}O$) of stream samples distinguish between rock glacier, non-rock glacier, and mixed source streams (Fig. 4.3). Rock glacier fed streams were elevated in Na^{+}, Mg^{2+}, Ca^{+}, K^{+}, SO_4^{2-}, EC and pH, while stream temperatures remained low (< 2.5 °C) throughout the summer. The non-rock glacier stream maintained low EC throughout the summer, never exceeding 40 µS/cm. While the non-rock glacier stream had consistently lower EC values and the rock glacier streams had consistently higher EC values (>100 µS/cm), the mixed-source streams and basin outlet recorded increasing values throughout the summer, with a maximum of 85 µS/cm and 58 µS/cm in October, respectively. Rock glacier streams were slightly more alkaline than the other streams with a median pH of 8.1, while the median pH for non-rock glacier, mixed, and outlet streams were 7.6, 7.5, and 7.6, respectively.

The non-rock glacier stream experienced variable temperature throughout the season, ranging from 1.8 °C during snowmelt to 13.5 °C in August 2021 (Fig. 4.3). The basin outlet stream also had variable temperatures, ranging from 1.8 °C to 8.6 °C. The mixed-source streams ranged in temperatures from 0.6 °C to 3.6°C, while the rock glacier streams ranged from 0.6°C to 2.5°C.

The $\delta^{18}O$ from the rock glacier streams was similar to all other types of streams during the beginning of summer during snowmelt but displayed little variation throughout the year, with values ranging between –17.3 and –16.0 ‰ (Fig. 4.4). The basin outlet showed a similar range in $\delta^{18}O$ values. The mixed-source streams and non-rock glacier stream behaved similar to one another, with depleted $\delta^{18}O$ values early in the summer during snowmelt (~ –18 ‰), and with increasing values throughout the summer (to ~ –15 ‰).

Discharge from mixed-source Streams 3 and 6 exhibit seasonal and annual variability in runoff, influenced by snowpack, snowmelt, and precipitation (Fig. 4.5). Stream 3 had consistently larger discharge (an average of 3.7 times higher in July), though diurnal oscillations in Stream 6 in the second half of July in 2019 exceeded the discharge of Stream 3. Stream 3 had low yet persistent flow throughout the entire summer, whereas Stream 6 ran dry in late September and early October in 2020 and 2021. However, Stream 6 is a short reach (approximately 30 m between the front of the rock glacier and the lake) with large boulders such that flow could be heard subsurface even when the surface stream was dry. Discharge in the second half of July was the greatest in 2019, followed by 2020, then 2021, reflected by the July snow cover in the Lake Agnes basin (Fig. 4.6).

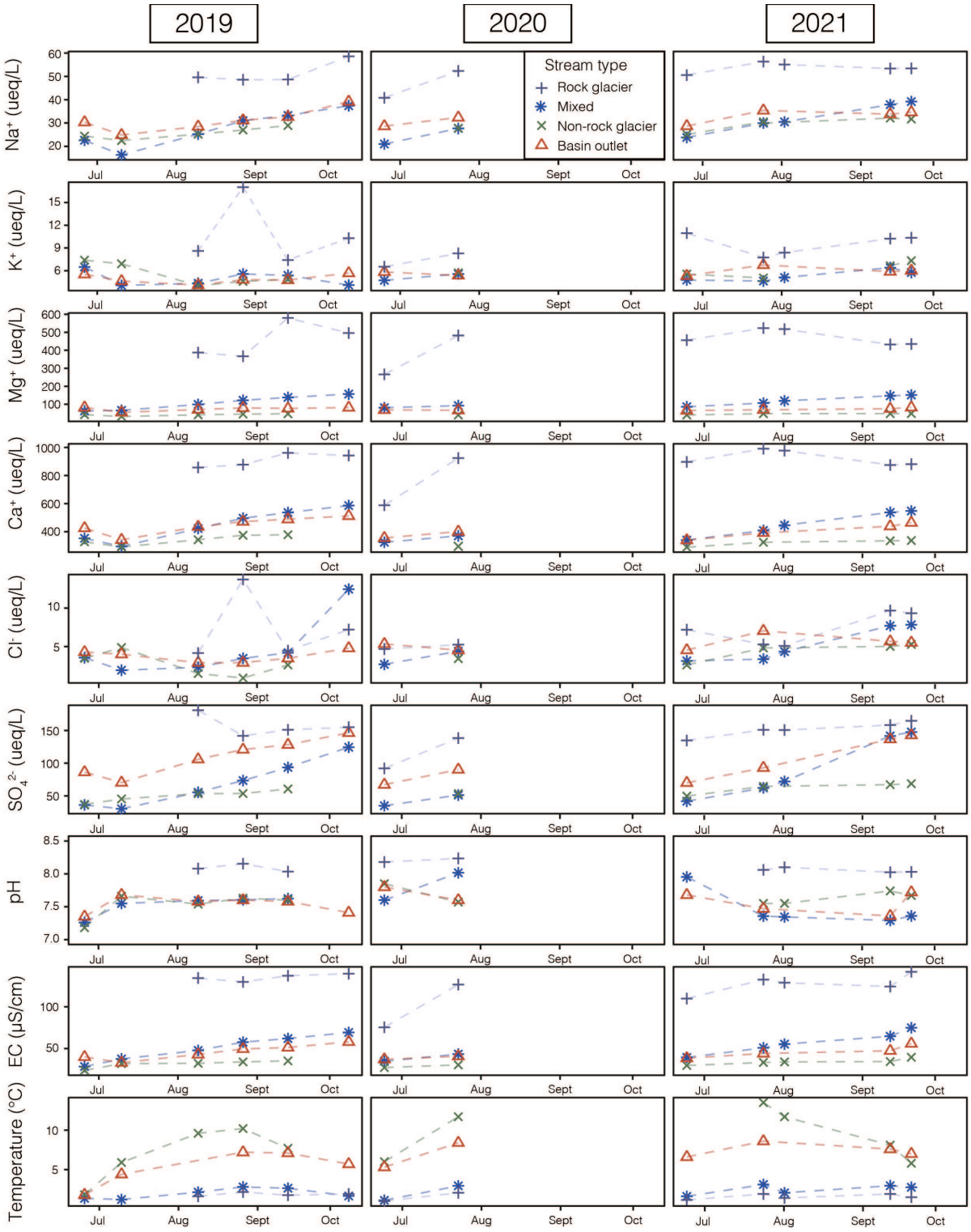

Figure 4.3. Time series for 2019, 2020, and 2021 of water quality for rock glacier, non-rock glacier, mixed source, and basin outlet streams. Values for the two rock glacier and two mixed source streams were averaged per sample date. EC stands for electrical conductivity. Water samples in Aug, Sept, and Oct 2020 were unable to be collected due to the nearby Cameron Peak fire.

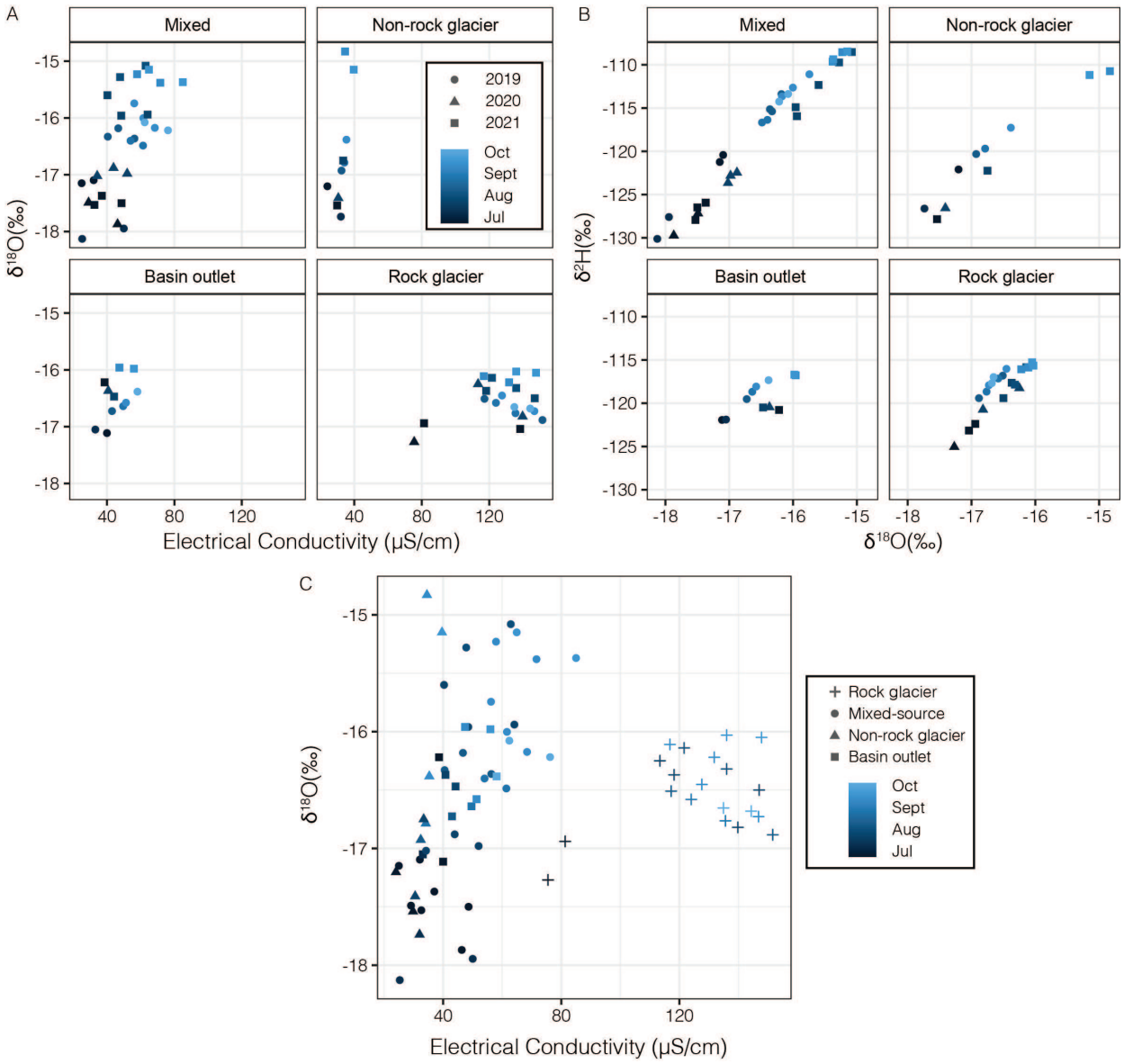

Figure 4.4. Electrical conductivity vs $\delta^{18}O$ values for all water samples (A), separated by stream type and colored by date collected, with shape representing the year the sample was collected. $\delta^{18}O$ vs $\delta^{2}H$ values for all water samples (B), separated by stream type and colored by date collected, with shape representing the year the sample was collected. Electrical conductivity vs $\delta^{18}O$ values for all water samples (C), colored by date collected, with shape representing the stream type.

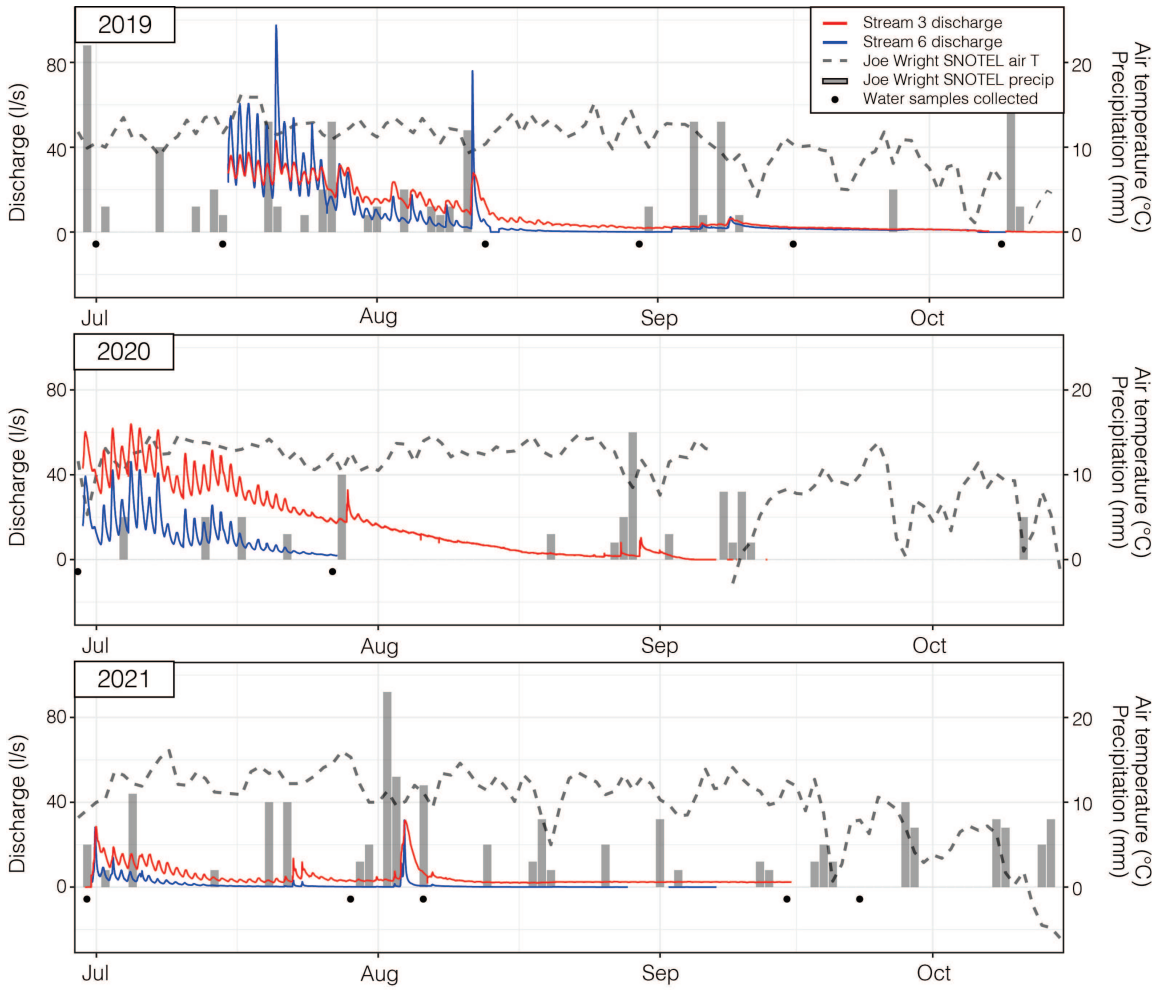

Figure 4.5. Discharge (l/s) from mixed-source Streams 3 (red) and 6 (blue) from June 29 to October 15 in 2019 (top), 2020 (middle), and 2021 (bottom). Gray bars represent precipitation (mm) recorded at the nearby Joe Wright SNOTEL site. The dashed line represents the air temperature (°C) recorded at the Joe Wright SNOTEL site. Black dots indicate when water samples were collected each year.

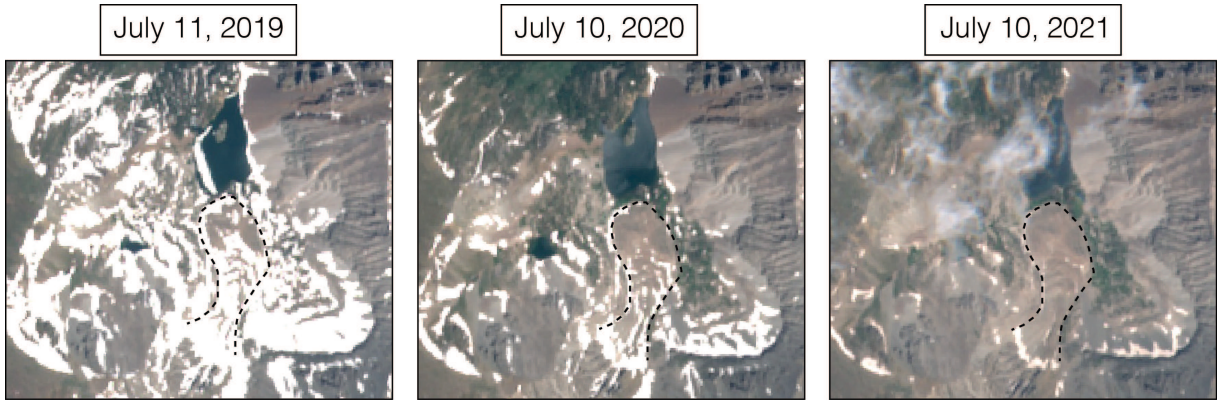

Figure 4.6. Sentinel-2 imagery from July 11, 2019, July 10, 2020, and July 10, 2021 comparing snow cover in the Lake Agnes basin. The rock glacier is outlined by a black dashed line.

4.4.2 Geophysics: Seismic refraction and ground-penetrating radar (GPR)

The seismic velocity model estimated for the Lake Agnes rock glacier is composed of a low velocity layer adjacent to the surface with velocities ranging from 300–2000 m/s, a medium velocity layer beneath this with velocities ranging from 2000–3500 m/s, and a high velocity layer even deeper with velocities >4000 m/s (Fig. 4.7). In the longitudinal profile, the low velocity layer ranges in thickness from 4 m at 42 m along the profile to 10 m at 70 m along the profile. From 36 m to 64 m along the profile, a high velocity layer is indicated about 8-10 m below the surface. However, this high velocity layer is not identified from 0–36 m and 70–141 m along the profile.

In the transverse profile, the seismic profile follows a similar structure, with a low-velocity layer consistently ~3 m thick, though this layer thickens to ~6 m from 20 to 30 m along the profile as well as from 74 to 88 m along the profile. The higher velocity (>4000 m/s) layer appears between 48 and 66 m along the profile at about 12 m depth.

The longitudinal GPR radargram is characterized by a relatively consistent reflector at 3 m depth, underlain by a layer containing many reflectors to about 10 m depth. Below this is a zone where reflectors are of a much lower magnitude. This package is underlain by a high magnitude reflector at 30 m depth seen from 74–96 m along the profile and is interpreted as the bottom of the rock glacier.

The transverse GPR radargram is similarly characterized by a relatively consistent reflector at 3 m depth, underlain by a layer containing many reflectors, followed by a layer of low magnitude reflectors. A strong reflector is identified at ~20 m depth from 0–10 m and 63–70 m along the profile, and at ~15 m depth from 79–89 m along the profile. The estimated rock

glacier thickness at the east end of transverse line of ~20 m corresponds to the elevation difference measured between off-glacier and the start of the line as measured using a DEM. A furrow is present in the transect at about 45 m along the profile, with topography too challenging to collect GPR traces. At 20 m along the profile is the top of a small ridge, with shallow, downward-dipping reflectors angled away from the high point roughly parallel to the surface slope.

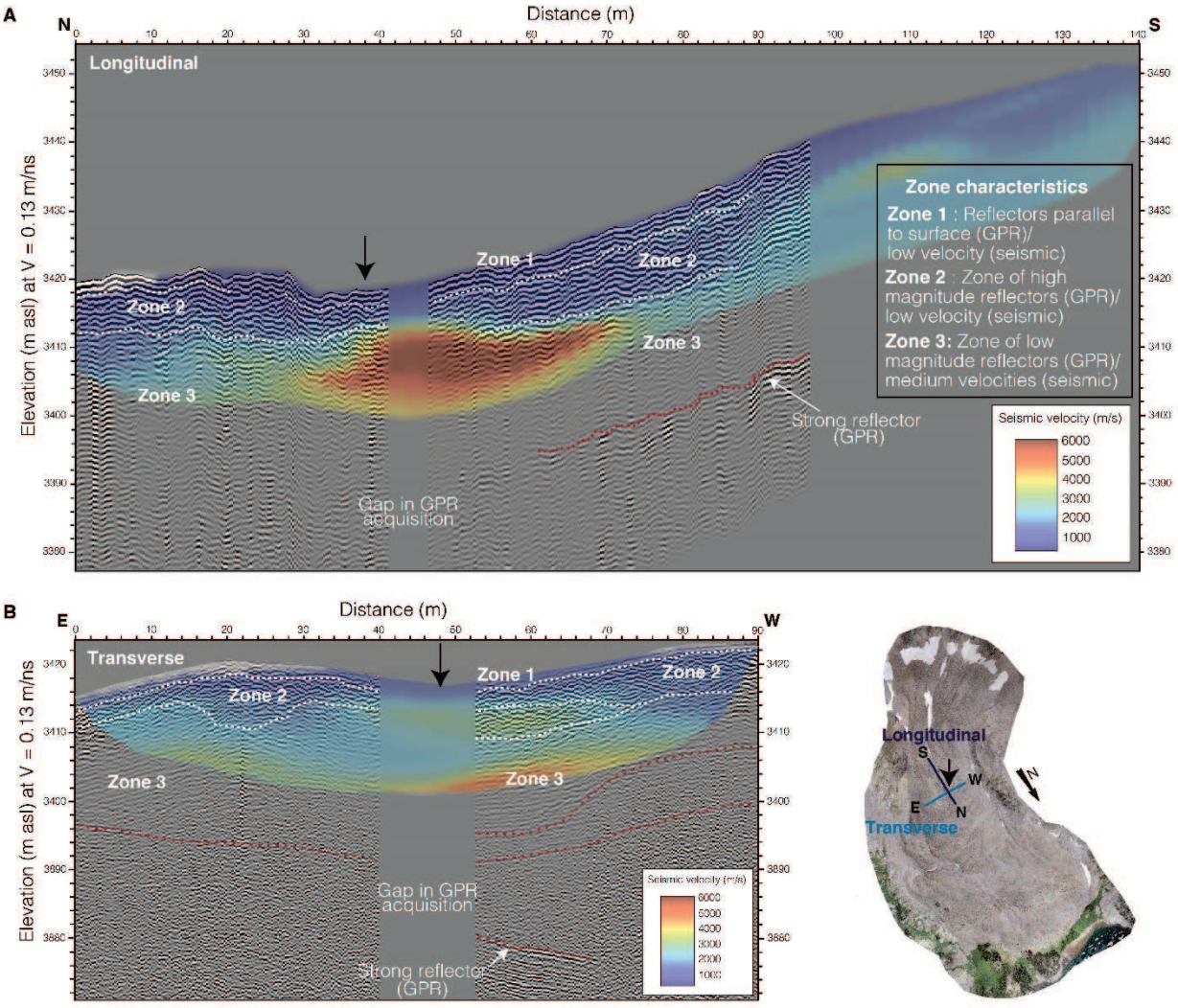

Figure 4.7. Seismic velocity models overlain upon GPR radargrams for longitudinal (A) and transverse profiles (B) on the Lake Agnes Rock glacier. The black arrows indicate where the two lines intersect. The white dashed line delineates layers within the rock glacier, and the red dashed lines outline other strong reflectors at depth.

4.4.3 Structure from motion (SfM)

Displacement between orthomosaics from 2019 and 2021 confirm movement in the upper 400 m of the rock glacier, while the lower half of the landform experiences little to no detectable movement (Fig. 4.8A). The average velocity in areas where there should be no movement (i.e. bedrock) was 5 cm yr^{-1}, and therefore this value was used as the uncertainty for the velocity calculated between the two years. Average horizontal velocity of the active lobe was 17 ± 5 cm yr^{-1}, with maximum velocities up to 36 ± 5 cm yr^{-1}. The displacement detected in the northeast and northwest corners of the model is due to vegetation growth between the two years at the edge of the rock glacier. Slower velocities found in the middle of the upper tongue could be due to complex deformation that is not captured in simple horizontal displacements (e.g., if rocks are moving up or down a ridge, etc).

The rock glacier displacement confirms the presence of ice within the upper reaches of the rock glacier, supported by the geomorphology of ridge and furrow features, and a steep lateral margin on the eastern side of the upper rock glacier (Fig. 4.8B).

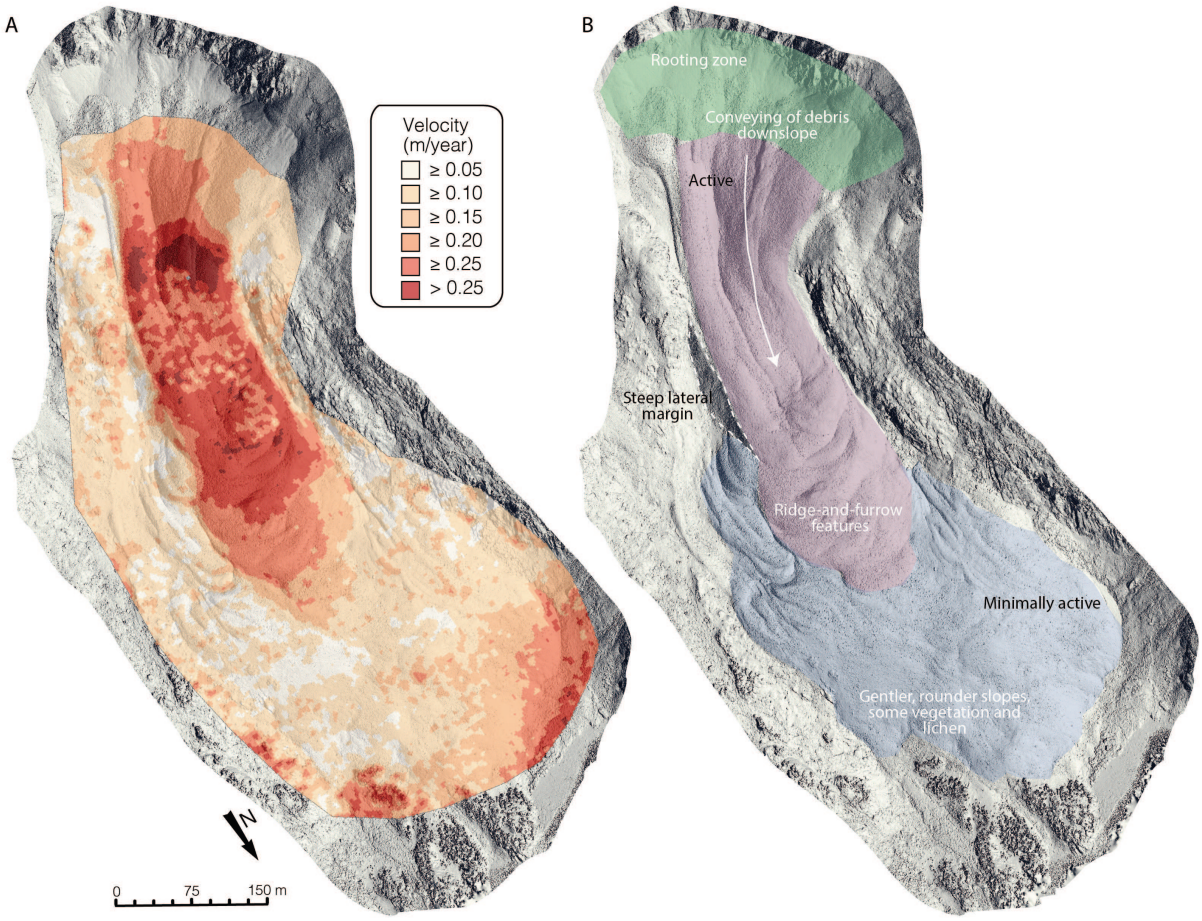

Figure 4.8. Rock glacier velocities calculated between 2019 and 2021 (A) and geomorphology (B) of the Lake Agnes rock glacier.

4.4.4 Bottom temperature of snow (BTS)

BTS is a useful proxy for the presence of permafrost as BTS underlain by permafrost can reach < -3 °C, whereas BTS in the absence of permafrost typically remains around 0°C (Haeberli, 1973). Temperatures between –2 and –3 °C suggest possible permafrost, and temperatures below –3 °C indicate probable permafrost (Haeberli, 1973). The off-RG control (3300 m asl) recorded an average winter (December 1 to March 31) BTS of 0.19 °C in 2018–2019 and 0.07 °C in 2019–2020, as is expected of ground without permafrost (Fig. 4.9). The upper logger (3415 m asl) recorded average winter temperatures of –3.40 °C and –3.45 °C in

2018–2019 and 2019–2020, respectively, indicating that permafrost is probable in the location. The middle logger (3397 m asl) recorded an average of –1.11 °C in 2018–2019 and –2.07 °C in 2019-2020, providing ambiguous evidence of permafrost. The lower logger (3355 m asl) recorded an average of –8.24 °C in 2018–2019 and –8.59 °C in 2019–2020. These temperatures observed in the lower rock glacier are much lower than expected, and are likely due to the fact that this location was not fully snow covered until mid-January, and therefore the averages reflect winter air temperatures. In addition, this section of the rock glacier is characterized by big boulders with large voids, and therefore temperatures could additionally be influenced by winter air circulation beneath the logger (Wicky and Hauck, 2020).

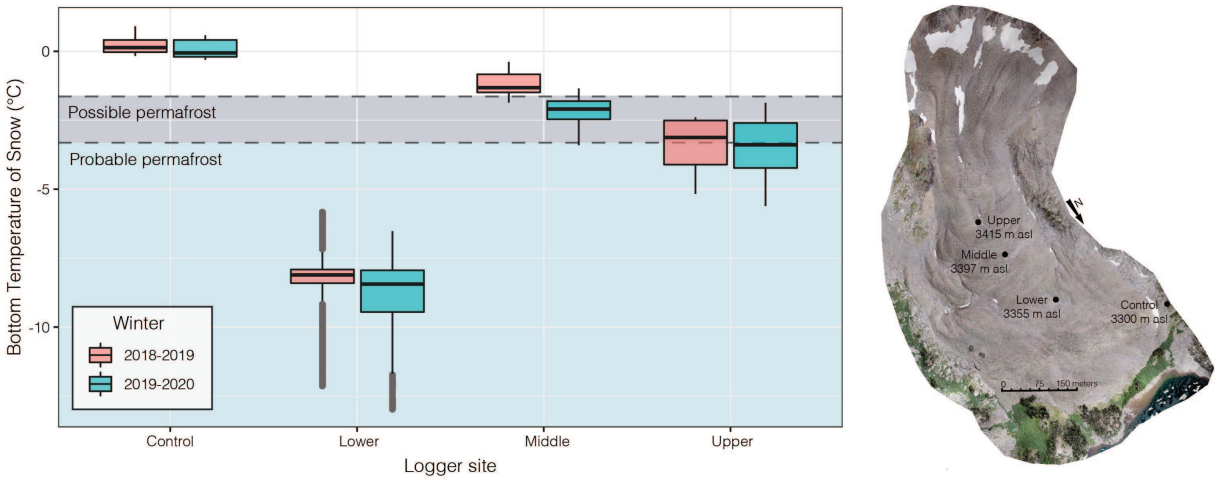

Figure 12. Boxplots of bottom temperature of snow (BTS; °C) recorded for winters (December 1 to March 31) 2018–2019 (left) and 2019–2020 (right).

4.5 DISCUSSION

4.5.1 Geochemistry

Elevated pH and ion concentrations in rock glacier-sourced streams draining the Lake Agnes rock glacier are consistent with previous studies (Williams et al., 2006; Caine, 2010;

Fegel et al., 2016; Munroe, 2018). These elevated weathering products can be explained through the breakdown of granodiorite, a rock composed mainly of Na and Ca rich feldspars, which constitutes the source material for the rock glacier. Substantial contact between rock surfaces and ice within the rock glacier increases chemical weathering, while rock glacier movement increases mechanical weathering (Ilyashuk et al., 2014).

Using EC as a proxy for the sum of ion concentrations, rock glacier-fed streams sustained relatively high concentrations throughout the summer (mean = 129 μS/cm) while the non-rock glacier sourced stream remained low (< 40 μS/cm). The increasing EC throughout the season for mixed-source and basin outlet streams suggests an increase in rock glacier contribution towards the end of the summer. In addition, the Lake Agnes rock glacier plays an important role in maintaining low temperatures throughout the summer. The non-rock glacier fed stream reached a maximum temperature of 13.5 °C, whereas maximum temperature recorded in a pure rock glacier stream was 2.5 °C. The mixed streams recorded a maximum temperature of 3.6 °C, implying that the rock glacier reduced the maximum water temperature by 10°C, a large decrease during the peak heat of summer. Rock glaciers elsewhere in North America have documented a similar muting of summer stream temperature increases (Williams et al., 2006; Liu et al., 2013; Harrington et al., 2018; Munroe, 2018).

Rock glacier-fed water tends to have a higher pH, higher conductivity, lower temperature, and minimal diurnal variations in discharge as compared to non-rock glacier streams, all of which were observed in the Lake Agnes basin (Fegel et al., 2016; Munroe, 2018). The hydrographs observed for two mixed-source streams follow a similar shape to what was documented in the La Sal Mountains, Utah (Geiger et al., 2014), with large diurnal pulses

corresponding to snowmelt within the basin, followed by low flow with muted diurnal fluctuations and large peaks following precipitation events.

The low temperatures, in conjunction with minimal diurnal fluctuations, found within the rock glacier and mixed-source streams creates a stable environment for cold-water aquatic communities to thrive. Elevated rock glacier meltwater solute concentrations can impact biological community assemblages and therefore change the characteristics of the water chemistry in alpine watersheds (Williams et al., 2006). These key differences make it possible to distinguish meltwater sourced from rock glaciers and are important in determining ecosystem function and capacity.

4.5.2 Horizontal velocity

A photogrammetric study of rock glaciers in the Front Range found that long term velocities averaged between 14 and 20 cm yr^{-1} from 1978 to 1999 (Janke, 2005), and this rate is consistent with what I observed at the Lake Agnes rock glacier (Fig. 4.8). The average rate of the active Lake Agnes lobe (upper ~ 400 m), 17 ± 5 cm yr^{-1}, is higher than InSAR-derived velocities in the Uinta Mountains, Utah, which ranged from 0.4 to 6 cm yr^{-1} (Brencher et al., 2021). The lack of movement in the lower half of the Lake Agnes rock glacier indicates that while the upper half of the rock glacier is active, the bottom half should be classified as transitional (RGIK, 2022). Movement of the rock glacier indicates the presence of ice within the feature, which has implications for short-, intermediate-, and long-term water storage.

4.5.3 Rock glacier structure

Seismic refraction and GPR results provide insight into the internal structure of the Lake Agnes rock glacier, and by combining the seismic tomography with interpretations from radargrams I can reduce some ambiguities associated with these geophysical methods. The

geophysical results suggest a typical layered structure to the rock glacier, with an ~3 m top layer of slow velocities interpreted to be the active layer composed of large rocks and air space observed in both longitudinal and transverse profiles. In both the longitudinal and transverse profiles, beneath the active layer is a package of high reflectivity underlain by a package with weak reflectivity, interpreted to be a layer of low ice content transitioning to high ice content (Leopold et al., 2011). This package of weak reflectivity is characterized by intermediate seismic velocities ranging from 2000–4500 m/s, consistent with permafrost layers observed in other rock glaciers as well (Maurer and Hauck, 2007; Harrington et al., 2018).

Unlike the radargrams of the Galena Creek rock glacier, WY (Petersen et al., 2020), I did not see a layer void of reflectors indicating a high purity glacial ice core. The radargrams for the Lake Agnes rock glacier look similar to that of the Green Lake 5 rock glacier (Leopold et al., 2011), and thus similarly interpret the less reflective zone as debris with ice or very high ice content. A borehole would be beneficial to aid in interpretation (Maurer and Hock, 2007; Merz et al., 2015), but unfortunately was not possible on the Lake Agnes rock glacier. Rock glacier thickness is estimated to be ~20 m in the transverse profile, with thickness up to 30 m in the longitudinal profile. The high seismic velocities (>4500 m/s) indicated from 40 to 64 m along the longitudinal profile suggest bedrock is present 8–10 m below the surface. This could indicate thinning of the rock glacier as it flows up and over a bedrock topographic high point. However, the seismic model and radargram appear to be at odds, making interpretation ambiguous.

4.5.4 Rock glacier influence

Geophysical imaging, bottom temperature of snow, and remote sensing all confirm the presence of ice within the Lake Agnes rock glacier, while water quality measurements document the impact of this ice on streams within the basin. By comparing rock glacier sourced streams to

non-rock glacier sourced streams, I conclude that the Lake Agnes rock glacier increases ion concentrations and pH while maintaining streams <2.5 °C during the snow free period.

Streamflow characteristics and water chemistry are important in determining ecosystem function and capacity, and therefore influence the presence and survival of alpine species. Biologists have recently identified the importance of "icy seeps" (i.e. rock glacier fed streams) in maintaining aquatic biodiversity in alpine basins and creating a cold-water refuge for species in a warming climate (Fegel et al., 2016; Harrington et al., 2017; Tronstad et al., 2019; Brighenti et al., 2021). Rock glaciers are important headwater features in a deglaciating world, with a delayed response to current and future warming. Basins containing rock glaciers, such as Lake Agnes, are predicted to dampen the impacts of warming temperatures for as long as these features persist (Jones et al., 2019).

4.6 CONCLUSIONS

This detailed study improves our knowledge of the Lake Agnes rock glacier and provides a framework for studying the thousands of other rock glaciers in Colorado and the western US, to better understand the extent and influence of subterranean ice in alpine ecosystems. I confirm the presence of ice within the Lake Agnes rock glacier and document its influence on basin hydrochemistry, elevating ion concentrations, pH, and maintaining low stream temperatures. I estimate an active layer depth of ~3 m, and a total rock glacier thickness of 20–30 m. I observe an average velocity of 17 ± 5 cm yr^{-1} between 2019 and 2021 for the active lobe. In certain basins, the reduced climate sensitivity of rock glaciers and their sustained cold-water input to mountain streams will likely provide a refuge for cold-water species in a warming climate. The data collected here adds to the sparse record of rock glacier hydrochemistry, particularly outside of the European Alps.

5. CONCLUSIONS

Within this dissertation, I demonstrated that the impacts of a changing cryosphere on cryo-geohazards are not as simple as previously suggested (e.g., Richardson and Reynolds, 2000; Carrivick and Tweed, 2013; Shugar et al., 2020), but is rather complex and nuanced. I found that while ice-marginal lakes have overall increased in area in Alaska and northwest Canada over the past 35 years, changes are dependent on the lake's location and damming mechanism. Most notably, moraine-dammed lakes increased in total area by 87%, while ice-dammed lakes decreased in total area by 40%. Ice-dammed lakes dominate the record of glacial lake outburst floods in Alaska, and this large decrease in ice-dammed lake presence has overall decreased the hazards from these lakes. Extending the record back to the 1970s, Alaska has experienced a decrease of nearly 70% in the number of ice-dammed lakes present.

While initial results showed an apparent increase in the number of documented ice-dammed lake drainages from 1985 to 2020, I had to address the observational bias in the satellite record of increasing temporal resolution with the introduction of Landsat 8 in 2013 and Sentinel-2 in 2015. When accounting for the increase in imagery availability, I found no significant change in the frequency of events over time. This result should motivate a re-evaluation of previous studies and caution future studies looking at multi-temporal changes, requiring that observational bias must be addressed.

An inventory of ice-marginal lake outlines (Chapter 2) and ice-dammed lake drainage events (Chapter 3) between the years 1984 and 2020 is critical for being able to predict the future impacts of climate change on glacial lakes and associated hazards in Alaska. Future studies could use models that invert for ice thickness to detect overdeepenings beneath glaciers to identify

potential glacial lake locations in the future, as well as use glacier models to determine whether the number of ice-dammed lakes will continue to decrease, or if an increase will occur as complex basins start of deglaciate (e.g., Linsbauer et al., 2016; Colonia et al., 2017; Furian et al., 2021).

Similar to a loss of ice-dammed lakes decreasing GLOF hazards in Alaska, the abundance of rock glaciers in Colorado will likely help buffer the impacts of climate change in alpine basins. I documented the presence of ice within the Lake Agnes rock glacier, as well as its impact on basin hydrology (Chapter 4). The rock glacier regulates stream temperatures, limiting the temperature of mixed-source streams to 3.5 °C, while the non-rock glacier stream reached a maximum of 13.5 °C. These temperatures, in addition to maintaining flow throughout the summer, help buffer the predicted impacts of warming air temperatures on cold-water alpine species. However, as rock glacier ice is buffered, yet not immune, to the impacts of a warming climate (Jones et al., 2019), the question remains: how long will these features persist? Is it a matter of decades or centuries? Long term velocity and hydrological monitoring, more detailed geophysical surveys, and internal structure verification of the rock glacier could help constrain the volume of ice present and the rate at which this ice is being lost. Future studies could explore the regional spatial variation in ice presence (e.g., InSAR to detect rock glacier movement as an inference of ice presence), long term hydrological trends (e.g., is an increase in late season discharge seen outside the Green Lakes Valley?), and the biological communities in and around rock glaciers.

While extreme events have increased globally and climate change has created profound and irreversible changes to the cryosphere, the results presented in this dissertation provide a small glimmer of hope for a slightly less dire future, at least for the time being. Decreased

hazards from glacial lakes in Alaska and the buffering effect of rock glaciers in alpine basins give us time to learn, adapt, and hopefully minimize the impacts of changes to the cryosphere in a warming world.

REFERENCES

Allen, S., Frey, H., and Huggel, C.: Assessment of Glacier and Permafrost Hazards in Mountain Regions - Technical Guidance Document, GAPHAZ, https://doi.org/10.13140/RG.2.2.26332.90245, 2017.

Amani, M., Ghorbanian, A., Ahmadi, S. A., Kakooei, M., Moghimi, A., Mirmazloumi, S. M., Moghaddam, S. H. A., Mahdavi, S., Ghahremanloo, M., Parsian, S., Wu, Q., and Brisco, B.: Google Earth Engine Cloud Computing Platform for Remote Sensing Big Data Applications: A Comprehensive Review, IEEE Journal of Selected Topics in Applied Earth Observations and Remote Sensing, 13, 5326–5350, https://doi.org/10.1109/JSTARS.2020.3021052, 2020.

Anderson, L. S. and Anderson, R. S.: Modeling debris-covered glaciers: Response to steady debris deposition, Cryosphere, 10, 1105–1124, https://doi.org/10.5194/tc-10-1105-2016, 2016.

Anderson, R. S., Anderson, L. S., Armstrong, W. H., Rossi, M. W., and Crump, S. E.: Glaciation of alpine valleys: The glacier – debris-covered glacier – rock glacier continuum, Geomorphology, 311, 127–142, https://doi.org/10.1016/j.geomorph.2018.03.015, 2018.

Anderson, S. P., Walder, J. S., Anderson, R. S., Kraal, E. R., Cunico, M., Fountain, A. G., and Trabant, D. C.: Integrated hydrologic and hydrochemical observations of Hidden Creek Lake jokulhlaups, Kennicott Glacier, Alaska, Journal of Geophysical Research, 108, 1–19, https://doi.org/10.1029/2002JF000004, 2003.

Barnett, T. P., Adam, J. C., and Lettenmaier, D. P.: Potential impacts of a warming climate on water availability in snow-dominated regions, Nature, 438, 303–309, https://doi.org/10.1038/nature04141, 2005.

Baroni, C., Carton, A., Seppi, R., Ferrata, V., and Pavia, I.-: Distribution and Behaviour of Rock Glaciers in the Adamello – Presanella Massif (Italian Alps), Permafrost and Periglacial Processes, 259, 243–259, https://doi.org/10.1002/ppp.497, 2004.

Barsch, D.: Rock-glaciers: indicators for the present and former geoecology in high mountain environments, Springer Science & Business Media, 1996.

Benn, D. I., Wiseman, S., and Hands, K. A.: Growth and drainage of supraglacial lakes on debrismantled Ngozumpa Glacier, Khumbu Himal, Nepal, Journal of Glaciology, 47, 626–638, https://doi.org/10.3189/172756501781831729, 2001.

Berthling, I.: Geomorphology Beyond confusion : Rock glaciers as cryo-conditioned landforms, Geomorphology, 131, 98–106, https://doi.org/10.1016/j.geomorph.2011.05.002, 2011.

Bodin, X., Krysiecki, J. M., Schoeneich, P., Le Roux, O., Lorier, L., Echelard, T., Peyron, M., and Walpersdorf, A.: The 2006 Collapse of the Bérard Rock Glacier (Southern French Alps), Permafrost and Periglacial Processes, 28, 209–223, https://doi.org/10.1002/ppp.1887, 2017.

Bogen, J., Xu, M., and Kennie, P.: The impact of pro-glacial lakes on downstream sediment delivery in Norway, Earth Surface Processes and Landforms, 40, 942–952, https://doi.org/10.1002/esp.3669, 2015.

Box, J. E., Colgan, W. T., Wouters, B., Burgess, D. O., Neel, S. O., Thomson, L. I., and Mernild, S. H.: Global sea-level contribution from Arctic land ice : 1971 – 2017, Environmental Research Letters, 13, 2018.

Brencher, G., Handwerger, A. L., and Munroe, J. S.: InSAR-based characterization of rock glacier movement in the Uinta Mountains, Utah, USA, Cryosphere, 15, 4823–4844, https://doi.org/10.5194/tc-15-4823-2021, 2021.

Brighenti, S., Hotaling, S., Finn, D. S., Fountain, A. G., Hayashi, M., Herbst, D., Saros, J. E., Tronstad, L. M., and Millar, C. I.: Rock glaciers and related cold rocky landforms: Overlooked climate refugia for mountain biodiversity, Global Change Biology, 27, 1504–1517, https://doi.org/10.1111/gcb.15510, 2021.

Brun, F., Wagnon, P., Berthier, E., Jomelli, V., Maharjan, S. B., Shrestha, F., and Kraaijenbrink, P. D. A.: Heterogeneous Influence of Glacier Morphology on the Mass Balance Variability in High Mountain Asia, Journal of Geophysical Research: Earth Surface, 124, 1331–1345, https://doi.org/10.1029/2018JF004838, 2019.

Buckel, J., Otto, J. C., Prasicek, G., and Keuschnig, M.: Glacial lakes in Austria - Distribution and formation since the Little Ice Age, Global and Planetary Change, 164, 39–51, https://doi.org/10.1016/j.gloplacha.2018.03.003, 2018.

Burger, K. C., Jr, J. J. D., and Giardino, J. R.: Engineering geomorphology of rock glaciers, Geomorphology, 1999.

Caine, N.: Recent hydrologie change in a Colorado alpine basin: An indicator of permafrost thaw?, Annals of Glaciology, 51, 130–134, https://doi.org/10.3189/172756411795932074, 2010.

Capps, D. M., Wiles, G. C., Clague, J. J., and Luckman, B. H.: Tree-ring dating of the nineteenth-century advance of Brady Glacier and the evolution of two ice-marginal lakes, Alaska, Holocene, 21, 641–649, https://doi.org/10.1177/0959683610391315, 2011.

Carrivick, J. L. and Quincey, D. J.: Progressive increase in number and volume of ice-marginal lakes on the western margin of the Greenland Ice Sheet, Global and Planetary Change, 116, 156–163, https://doi.org/10.1016/j.gloplacha.2014.02.009, 2014.

Carrivick, J. L. and Tweed, F. S.: Proglacial lakes : character, behaviour and geological importance, Quaternary Science Reviews, 78, 34–52, https://doi.org/10.1016/j.quascirev.2013.07.028, 2013.

Carrivick, J. L. and Tweed, F. S.: A global assessment of the societal impacts of glacier outburst fl oods, Global and Planetary Change, 144, 1–16, 2016.

Chen, F., Zhang, M., Guo, H., Allen, S., Kargel, J., Haritashya, U., and Watson, C. S.: Annual 30-meter Dataset for Glacial Lakes in High Mountain Asia from 2008 to 2017, Earth System Science Data Discussions, 4275164, 1–29, https://doi.org/10.5194/essd-2020-57, 2021.

Clague, J. J. and Evans, S. G.: A review of catastrophic drainage of moraine-dammed lakes in British Columbia, Quaternary Science Reviews, 19, 1763–1783, https://doi.org/10.1016/S0277-3791(00)00090-1, 2000.

Colombo, N., Salerno, F., Gruber, S., Freppaz, M., Williams, M., Fratianni, S., and Giardino, M.: Review: Impacts of permafrost degradation on inorganic chemistry of surface fresh water, Global and Planetary Change, 162, 69–83, https://doi.org/10.1016/j.gloplacha.2017.11.017, 2018.

Colonia, D., Torres, J., Haeberli, W., Schauwecker, S., Braendle, E., Giraldez, C., and Cochachin, A.: Compiling an Inventory of Glacier-Bed Overdeepenings and Potential New Lakes in De-Glaciating Areas of the Peruvian Andes: Approach, First Results, and Perspectives for Adaptation to Climate Change, Water, 9, https://doi.org/10.3390/w9050336, 2017.

Colonia, D., Torres, J., Haeberli, W., Schauwecker, S., Braendle, E., Giraldez, C., and Cochachin, A.: Compiling an Inventory of Glacier-Bed Overdeepenings and Potential New Lakes in De-Glaciating Areas of the Peruvian Andes: Approach , First Results , and Perspectives for Adaptation to Climate Change, Water, 9, https://doi.org/10.3390/w9050336, 2017.

Cook, S. J. and Quincey, D. J.: Estimating the volume of Alpine glacial lakes, Earth Surface Dynamics,

559–575, https://doi.org/10.5194/esurf-3-559-2015, 2015.

Cook, S. J., Kougkoulos, I., Edwards, L. A., Dortch, J., and Hoffmann, D.: Glacier change and glacial lake outburst flood risk in the Bolivian Andes, The Cryosphere, 10, 2399–2413, https://doi.org/10.5194/tc-10-2399-2016, 2016.

Dall'Asta, E., Forlani, G., Roncella, R., Santise, M., Diotri, F., and Morra, U.: Unmanned Aerial Systems and DSM matching for rock glacier monitoring, ISPRS Journal of Photogrammetry and Remote Sensing, 127, 102–114, https://doi.org/10.1016/j.isprsjprs.2016.10.003, 2017.

Dorava, J. M. and Milner, A. M.: Role of lake regulation on glacier fed rivers in enhancing salmon productivity: The Cook Inlet watershed south central Alaska, USA, Hydrological Processes, 14, 3149–3159, https://doi.org/10.1002/1099-1085(200011/12)14:16/17<3149::AID-HYP139>3.0.CO;2-Y, 2000.

Emmer, A.: Glacier Retreat and Glacial Lake Outburst Floods (GLOFs), in: Oxford Research Encyclopedia of Natural Hazard Science, 1–37, https://doi.org/10.1093/acrefore/9780199389407.013.275, 2017.

Emmer, A., Merkl, S., and Mergili, M.: Spatiotemporal patterns of high-mountain lakes and related hazards in western Austria, Geomorphology, 246, 602–616, https://doi.org/10.1016/j.geomorph.2015.06.032, 2015.

Emmer, A., Harrison, S., Mergili, M., Allen, S., Frey, H., and Huggel, C.: 70 years of lake evolution and glacial lake outburst floods in the Cordillera Blanca (Peru) and implications for the future, Geomorphology, 365, 107178, https://doi.org/10.1016/j.geomorph.2020.107178, 2020.

Farinotti, D., Huss, M., Fürst, J. J., Landmann, J., Machguth, H., Maussion, F., and Pandit, A.: A consensus estimate for the ice thickness distribution of all glaciers on Earth, Nature Geoscience, 12, 168–173, https://doi.org/10.1038/s41561-019-0300-3, 2019.

Farinotti, D., Huss, M., Fürst, J. J., Landmann, J., Machguth, H., Maussion, F., and Pandit, A.: A consensus estimate for the ice thickness distribution of all glaciers on Earth, Nature Geoscience, 12, 168–173, https://doi.org/10.1038/s41561-019-0300-3, 2019.

Fegel, T. S., Baron, J. S., Fountain, A. G., Johnson, G. F., and Hall, E. K.: Biogeosciences signatures of glaciers and rock glaciers, Journal of Geophysical Research, 919–932, https://doi.org/10.1002/2015JG003236.Received, 2016.

Field, H., Armstrong, W., and Huss, M.: Topography exerts primary control on the rate of Gulf of Alaska ice-marginal lake area change over the Landsat record, The Cryosphere Discussions, 1–34, https://doi.org/10.5194/tc-2020-366, 2021.

Florentine, C., Skidmore, M., Speece, M., Link, C., and Shaw, C. A.: Geophysical analysis of transverse ridges and internal structure at Lone Peak Rock Glacier, Big Sky, Montana, USA, Journal of Glaciology, 60, 453–462, https://doi.org/10.3189/2014JoG13J160, 2014.

Fujita, K., Sakai, A., Nuimura, T., Yamaguchi, S., and Sharma, R. R.: Recent changes in Imja Glacial Lake and its damming moraine in the Nepal Himalaya revealed by in situ surveys and multi-temporal ASTER imagery, Environmental Research Letters, 4, https://doi.org/10.1088/1748-9326/4/4/045205, 2009.

Furian, W., Loibl, D., and Schneider, C.: Future glacial lakes in High Mountain Asia: An inventory and assessment of hazard potential from surrounding slopes, Journal of Glaciology, https://doi.org/10.1017/jog202118, 2021.

Gardelle, J., Arnaud, Y., and Berthier, E.: Contrasted evolution of glacial lakes along the Hindu Kush

Himalaya mountain range between 1990 and 2009, Global and Planetary Change, 75, 47–55, https://doi.org/10.1016/j.gloplacha.2010.10.003, 2011.

Geiger, S. T., Daniels, J. M., Miller, S. N., and Nicholas, J. W.: Influence of Rock Glaciers on Stream Hydrology in the La Sal Mountains, Utah, Arctic, Antarctic, and Alpine Research, 46, 645–658, https://doi.org/10.1657/1938-4246-46.3.645, 2014.

Giardino, J. R. and Vitek, J.: The significance of rock glaciers in the glacial- periglacial landscape continuum, Journal of Quaternary Science, 3, 97–103, 1988.

Gilbert, R.: Drainings of ice-dammed Summit Lake, British Columbia, Inland waters directorate, scientific series, 1–17, 1972.

Glasser, N. F., Holt, T. O., Evans, Z. D., Davies, B. J., Pelto, M., and Harrison, S.: Recent spatial and temporal variations in debris cover on Patagonian glaciers, Geomorphology, 273, 202–216, https://doi.org/10.1016/j.geomorph.2016.07.036, 2016.

Granato, G. E., Ries, K. G. I., and Steeves, P. A.: Compilation of streamflow statistics calculated from daily mean streamflow data collected during water years 1901-2015 for selected U.S. Geological Survey streamgages, U.S. Geological Survey Open-File Report 2017-1108, 17, 2017.

Gruber, S. and Haeberli, W.: Permafrost in steep bedrock slopes and its temperature-related destabilization following climate change, Journal of Geophysical Research, 112, 1–10, https://doi.org/10.1029/2006JF000547, 2007.

Haeberli, W.: Die Basis-Temperatur der winterlichen Schneedecke als moglicher Indikator fur die Verbreitung von Permafrost in den Alpen, in: Glazialgeol, 1973.

Haeberli, W.: Creep of mountain permafrost: internal structure and flow of alpine rock glaciers, Mitteilungen der Versuchsanstalt fur Wasserbau, Hydrologie und Glaziologie an der Eidgenossischen Technischen Hochschule Zurich, 1985.

Haeberli, W., Hallet, B., Arenson, L., Elconin, R., Humlum, O., Kääb, A., Kaufmann, V., Ladanyi, B., Matsuoka, N., Springman, S., and Mühll, D. V.: Permafrost creep and rock glacier dynamics, Permafrost and Periglacial Processes, 17, 189–214, https://doi.org/10.1002/ppp.561, 2006.

Haeberli, W., Hallet, B., Arenson, L., Elconin, R., Humlum, O., and Ka, A.: Permafrost Creep and Rock Glacier Dynamics, Permafrost and Periglacial Processes, 214, 189–214, https://doi.org/10.1002/ppp, 2006.

Hansen, J., Ruedy, R., Sato, M., and Lo, K.: Global Surface Temperature Change, Reviews of Geophysics, 1–29, https://doi.org/10.1029/2010RG000345.1.INTRODUCTION, 2010.

Harrington, J. S., Hayashi, M., and Kurylyk, B. L.: Influence of a rock glacier spring on the stream energy budget and cold-water refuge in an alpine stream, Hydrological Processes, 31, 4719–4733, https://doi.org/10.1002/hyp.11391, 2017.

Harrington, J. S., Mozil, A., Hayashi, M., and Bentley, L. R.: Groundwater flow and storage processes in an inactive rock glacier, Special Issue Canadian Geophysical Union, 3070–3088, https://doi.org/10.1002/hyp.13248, 2018.

Harrison, S., Whalley, B., and Anderson, E.: Relict rock glaciers and protalus lobes in the British Isles : implications for Late Pleistocene mountain geomorphology and palaeoclimate, Journal of Quaternary Science, 23, 287–304, https://doi.org/10.1002/jqs, 2008.

Harrison, S., Kargel, J. S., Huggel, C., Reynolds, J., Shugar, D. H., Betts, R. A., Emmer, A., Glasser, N.,

Haritashya, U. K., Klimeš, J., Reinhardt, L., and Schaub, Y.: Climate change and the global pattern of moraine-dammed glacial lake outburst floods, The Cryosphere, 12, 1195–1209, 2018.

Herreid, S. and Pellicciotti, F.: The state of rock debris covering Earth's glaciers, Nature Geoscience, https://doi.org/10.1038/s41561-020-0615-0, 2020.

Hotaling, S., Foley, M. E., Zeglin, L. H., Finn, D. S., Tronstad, L. M., Giersch, J. J., Muhlfeld, C. C., and Weisrock, D. W.: Microbial assemblages reflect environmental heterogeneity in alpine streams, Global Change Biology, 25, 2576–2590, https://doi.org/10.1111/gcb.14683, 2019.

How, P., Messerli, A., Mätzler, E., Santoro, M., Wiesmann, A., Caduff, R., Langley, K., Bojesen, M. H., Paul, F., Kääb, A., and Carrivick, J. L.: Greenland-wide inventory of ice marginal lakes using a multi-method approach, Scientific Reports, 11, 1–13, https://doi.org/10.1038/s41598-021-83509-1, 2021.

Hudson, R. and Fraser, J.: The Mass Balance (or Dry Injection) Method, Management, 9, 6–12, 2005.

Huggel, C., Kääb, A., Haeberli, W., and Teysseire, P.: Remote sensing based assessment of hazards from glacier lake outbursts : A case study in the Swiss Alps, Canandian Geotechnical Journal, 39, 3160330, https://doi.org/10.1139/t01-099, 2002.

Hugonnet, R., McNabb, R., Berthier, E., Menounos, B., Nuth, C., Girod, L., Farinotti, D., Huss, M., Dussaillant, I., Brun, F., and Kääb, A.: Accelerated global glacier mass loss in the early twenty-first century, Nature, 592, 726–731, https://doi.org/10.1038/s41586-021-03436-z, 2021.

Huss, M., Bookhagen, B., Huggel, C., Jacobsen, D., Bradley, R. S., Clague, J. J., Vuille, M., Buytaert, W., Cayan, D. R., Greenwood, G., Mark, B. G., Milner, A. M., Weingartner, R., and Winder, M.: Toward mountains without permanent snow and ice, Earth's Future, 5, 418–435, https://doi.org/10.1002/2016EF000514, 2017.

Ilyashuk, B. P., Ilyashuk, E. A., Psenner, R., Tessadri, R., and Koinig, K. A.: Rock Glacier Outflows May Adversely Affect Lakes: Lessons from the Past and Present of Two Neighboring Water Bodies in a Crystalline- Rock Watershed, Environmental Science and Technology, 48, 6192–6200, https://doi.org/10.1021/es500180c, 2014.

Immerzeel, W. W., Lutz, A. F., Andrade, M., Bahl, A., Biemans, H., Bolch, T., Hyde, S., Brumby, S., Davies, B. J., Elmore, A. C., Emmer, A., Feng, M., Fernández, A., Haritashya, U., Kargel, J. S., Koppes, M., Kraaijenbrink, P. D. A., Kulkarni, A. V., Mayewski, P. A., Nepal, S., Pacheco, P., Painter, T. H., Pellicciotti, F., Rajaram, H., Rupper, S., Sinisalo, A., Shrestha, A. B., Viviroli, D., Wada, Y., Xiao, C., Yao, T., and Baillie, J. E. M.: Importance and vulnerability of the world's water towers, Nature, 577, 364–369, https://doi.org/10.1038/s41586-019-1822-y, 2020.

Isaak, D. J., Young, M. K., Nagel, D. E., Horan, D. L., and Groce, M. C.: The cold-water climate shield: Delineating refugia for preserving salmonid fishes through the 21st century, Global Change Biology, https://doi.org/10.1111/gcb.12879, 2015.

Jacquemart, M., Loso, M., Leopold, M., Welty, E., Berthier, E., Hansen, J. S. S., Sykes, J., and Tiampo, K.: What drives large-scale glacier detachments? Insights from Flat Creek glacier, St. Elias Mountains, Alaska, Geology, 48, 703–707, https://doi.org/10.1130/G47211.1, 2020.

Jacquet, J., McCoy, S. W., McGrath, D., Nimick, D. A., Fahey, M., O'Kuinghttons, J., Friesen, B. A., and Leidich, J.: Hydrologic and geomorphic changes resulting from episodic glacial lake outburst floods: Rio Colonia, Patagonia, Chile, Geophysical Research Letters, 44, 854–864, https://doi.org/10.1002/2016GL071374, 2017.

Jakob, L., Gourmelen, N., Ewart, M., and Plummer, S.: Ice loss in High Mountain Asia and the Gulf of Alaska observed by CryoSat-2 swath altimetry between 2010 and 2019, The Cryosphere, 1–29,

https://doi.org/10.5194/tc-2020-176, 2021.

Janke, J. R.: Long-term flow measurements (1961-2002) of the Arapaho, Taylor, and Fair rock glaciers, Front Range, Colorado, Physical Geography, 26, 313–336, https://doi.org/10.2747/0272-3646.26.4.313, 2005.

Janke, J. R.: Photogrammetric Analysis of Front Range Rock Glacier Flow Rates Photogrammetric Analysis of Front Range Rock Glacier Flow Rates By, Methods, 515–526, 2005.

Janke, J. R.: Colorado Front Range Rock Glaciers: Distribution of Topographic Characteristics, Arctic and Alpine Research, 39, 74–83, 2007.

Janke, J. R., Ng, S., and Bellisario, A.: An inventory and estimate of water stored in firn fields, glaciers, debris-covered glaciers, and rock glaciers in the Aconcagua River Basin, Chile, Geomorphology, 296, 142–152, https://doi.org/10.1016/j.geomorph.2017.09.002, 2017.

Johnson, G., Chang, H., and Fountain, A.: Rock glaciers of the contiguous United States: GIS inventory and spatial distribution patterns, 1–26, 2020.

Jones, D., Harrison, S., Anderson, K., and Betts, R. A.: Mountain rock glaciers contain globally significant water stores, Scientific Reports, 8, 1–10, https://doi.org/10.1038/s41598-018-21244-w, 2018.

Jones, D., Harrison, S., Anderson, K., and Whalley, W. B.: Rock glaciers and mountain hydrology : A review, Earth-Science Reviews, 193, 66–90, https://doi.org/10.1016/j.earscirev.2019.04.001, 2019.

Jones, K. W. and Wolken, G. J.: Valdez glacier ice-dammed lake: June 2018 glaical lake outburst flood, State of Alaska Department of Natural Resources Division of Geological & Geophysical Surveys, 2019.

Kaufman, D. S. and Manley, W. F.: Pleistocene Maximum and Late Wisconsinan glacier extents across Alaska, U.S.A., Developments in Quaternary Science, 2, 9–27, https://doi.org/10.1016/S1571-0866(04)80182-9, 2004.

Kienholz, C., Pierce, J., Hood, E., Amundson, J. M., Wolken, G. J., Jacobs, A., Hart, S., Wikstrom Jones, K., Abdel-Fattah, D., Johnson, C., and Conaway, J. S.: Deglacierization of a Marginal Basin and Implications for Outburst Floods, Mendenhall Glacier, Alaska, Frontiers in Earth Science, 8, 1–21, https://doi.org/10.3389/feart.2020.00137, 2020.

King, O., Bhattacharya, A., Bhambri, R., and Bolch, T.: Glacial lakes exacerbate Himalayan glacier mass loss, Scientific Reports, 9, 1–9, https://doi.org/10.1038/s41598-019-53733-x, 2019.

Klein, J. A., Tucker, C. M., Nolin, A. W., Hopping, K. A., Reid, R. S., Steger, C., Grêt-Regamey, A., Lavorel, S., Müller, B., Yeh, E. T., Boone, R. B., Bourgeron, P., Butsic, V., Castellanos, E., Chen, X., Dong, S. K., Greenwood, G., Keiler, M., Marchant, R., Seidl, R., Spies, T., Thorn, J., and Yager, K.: Catalyzing Transformations to Sustainability in the World's Mountains, Earth's Future, 547–557, https://doi.org/10.1029/2018EF001024, 2019.

Langston, G., Bentley, L. R., Hayashi, M., Mcclymont, A., and Pidlisecky, A.: Internal structure and hydrological functions of an alpine proglacial moraine, Hydrological Processes, 25, 2967–2982, https://doi.org/10.1002/hyp.8144, 2011.

Larsen, C. F., Burgess, E., Arendt, A. A., O'Neel, S., Johnson, A. J., and Kienholz, C.: Surface melt dominates Alaska glacier mass balance, Geophysical Research Letters, 42, 5902–5908, https://doi.org/10.1002/2015GL064349, 2015.

Larsen, D. J., Crump, S. E., and Blumm, A.: Alpine glacier resilience and Neoglacial fluctuations linked to Holocene snowfall trends in the western United States, Science Advances, 6,

https://doi.org/10.1126/sciadv.abc7661, 2020.

Leopold, M., Williams, M. W., Caine, N., Völkel, J., and Dethier, D.: Internal structure of the Green Lake 5 rock glacier, Colorado Front Range, USA, Permafrost and Periglacial Processes, 22, 107–119, https://doi.org/10.1002/ppp.706, 2011.

Leopold, M., Lewis, G., Dethier, D., Caine, N., and Williams, M. W.: Cryosphere: ice on Niwot Ridge and in the Green Lakes Valley, Colorado Front Range, Plant Ecology and Diversity, 8, 625–638, https://doi.org/10.1080/17550874.2014.992489, 2015.

Linsbauer, A., Frey, H., Haeberli, W., Machguth, H., Azam, M. F., and Allen, S.: Modelling glacier-bed overdeepenings and possible future lakes for the glaciers in the Himalaya – Karakoram region, Annals of Glaciology, 57, 119–130, https://doi.org/10.3189/2016AoG71A627, 2016.

Liu, L., Millar, C. I., Westfall, R. D., and Zebker, H. A.: Surface motion of active rock glaciers in the Sierra Nevada, California, USA: Inventory and a case study using InSAR, Cryosphere, 7, 1109–1119, https://doi.org/10.5194/tc-7-1109-2013, 2013.

Marcer, M., Cicoira, A., Cusicanqui, D., Bodin, X., Echelard, T., Obregon, R., and Schoeneich, P.: Rock glaciers throughout the French Alps accelerated and destabilised since 1990 as air temperatures increased, Communications Earth and Environment, 2, 1–11, https://doi.org/10.1038/s43247-021-00150-6, 2021.

Martin, H. E. and Whalley, W. B.: Rock glaciers: part 1: rock glacier morphology: classification and distribution, Progress in Physical Geography: Earth and Environment, 11, 260–282, https://doi.org/10.1177/030913338701100205, 1987.

Mathews, W. H.: Two Self-Dumping Ice-Dammed Lakes in British Columbia, Geographical Review, 55, 46, https://doi.org/10.2307/212854, 1965.

Mathews, W. H. and Clague, J. J.: The record of jokulhlaups from Summit Lake, northwestern British Columbia, Canadian Journal of Earth Sciences, 30, 499–508, https://doi.org/10.1139/e93-039, 1993.

Maurer, H. and Hauck, C.: Instruments and methods: Geophysical imaging of alpine rock glaciers, Journal of Glaciology, 53, 110–120, https://doi.org/10.3189/172756507781833893, 2007.

Maurer, J. M., Schaefer, J. M., Rupper, S., and Corley, A.: Acceleration of ice loss across the Himalayas over the past 40 years, Science Advances, 5, https://doi.org/10.1126/sciadv.aav7266, 2019.

Meerhoff, E., Castro, L. R., Tapia, F. J., and Pérez-Santos, I.: Hydrographic and Biological Impacts of a Glacial Lake Outburst Flood (GLOF) in a Patagonian Fjord, Estuaries and Coasts, 42, 132–143, https://doi.org/10.1007/s12237-018-0449-9, 2018.

Melkonian, A. K., Willis, M. J., and Pritchard, M. E.: Satellite-derived volume loss rates and glacier speeds for the Juneau Icefield, Alaska, Journal of Glaciology, 60, 743–760, https://doi.org/10.3189/2014JoG13J181, 2014.

Melkonian, A. K., Willis, M. J., and Pritchard, M. E.: Stikine icefield mass loss between 2000 and 2013/2014, Frontiers in Earth Science, 4, 1–12, https://doi.org/10.3389/feart.2016.00089, 2016.

Menounos, B., Anslow, F., Bevington, A., Onwukwe, C., Townend, J., Heathfield, D., Shea, J., Darychuk, S., Shugar, D., Flowers, G., and Jackson, P.: Cryospheric response to the June, 2021 Heat Dome, in: AGU Fall Meeting Abstracts, C54C-06, 2021.

Merz, K., Maurer, H., Rabenstein, L., Buchli, T., Springman, S. M., and Zweifel, M.: Multidisciplinary geophysical investigations over an alpine rock glacier, Geophysics, 81, WA147–WA157, https://doi.org/10.1190/geo2015-0157.1, 2016.

Millar, C. I. and Westfall, R. D.: Distribution and Climatic Relationships of the American Pika (Ochotona princeps) in the Sierra Nevada and Western Great Basin , U.S.A.; Periglacial Landforms as Refugia in Warming Climates, Arctic, Antarctic, and Alpine Research, 42, 76–88, https://doi.org/10.1657/1938-4246-42.1.76, 2010.

Miller, J. A., Whitehead, R. L., Gingerich, S. B., Oki, D. S., and Olcott, P. G.: Ground Water Atlas of the United States - Segment 13 - Alaska, Hawaii, Puerto Rico and the U.S. Virgin Islands, 4–5 pp., 1999.

Milner, A. M., Robertson, A. L., Monaghan, K. A., Veal, A. J., and Flory, E. A.: Colonization and development of an Alaskan stream community over 28 years, Frontiers in Ecology and the Environment, 6, 413–419, https://doi.org/10.1890/060149, 2008.

Milner, A. M., Khamis, K., Battin, T. J., Brittain, J. E., Barrand, N. E., Füreder, L., Cauvy-Fraunié, S., Gíslason, G. M., Jacobsen, D., Hannah, D. M., Hodson, A. J., Hood, E., Lencioni, V., Ólafsson, J. S., Robinson, C. T., Tranter, M., and Brown, L. E.: Glacier shrinkage driving global changes in downstream systems, Proceedings of the National Academy of Sciences of the United States of America, 114, 9770–9778, https://doi.org/10.1073/pnas.1619807114, 2017.

Monnier, S. and Kinnard, C.: Reconsidering the glacier to rock glacier transformation problem: New insights from the central Andes of Chile, Geomorphology, 238, 47–55, https://doi.org/10.1016/j.geomorph.2015.02.025, 2015.

Mote, P. W., Li, S., Lettenmaier, D. P., Xiao, M., and Engel, R.: Dramatic declines in snowpack in the western US, npj Climate and Atmospheric Science, 1, 2, https://doi.org/10.1038/s41612-018-0012-1, 2018.

Muhlfeld, C. C., Cline, T. J., Giersch, J. J., Peitzsch, E., Florentine, C., Jacobsen, D., and Hotaling, S.: Specialized meltwater biodiversity persists despite widespread deglaciation, Proceedings of the National Academy of Sciences of the United States of America, 117, https://doi.org/10.1073/pnas.2001697117, 2020.

Munroe, J. S.: Distribution, evidence for internal ice, and possible hydrologic significance of rock glaciers in the Uinta Mountains, Utah, USA, Quaternary Research (United States), 90, 50–65, https://doi.org/10.1017/qua.2018.24, 2018.

Neal, E. G.: Hydrology and glacier-lake outburst floods (1987-2004) and water quality(1998-2003) of the Taku River near Juneau, Alaska, US Geological Scientific Investigations Report, 1–38, 2007.

Nie, Y., Sheng, Y., Liu, Q., Liu, L., Liu, S., Zhang, Y., and Song, C.: A regional-scale assessment of Himalayan glacial lake changes using satellite observations from 1990 to 2015, Remote Sensing of Environment, 189, 1–13, https://doi.org/10.1016/j.rse.2016.11.008, 2017.

Nitze, I., Grosse, G., Jones, B. M., Romanovsky, V. E., and Boike, J.: Remote sensing quantifies widespread abundance of permafrost region disturbances across the Arctic and Subarctic, Nature Communications, 1–11, https://doi.org/10.1038/s41467-018-07663-3, 2018.

Alaska GDL Main Page: https://www.weather.gov/aprfc/gdlMain, last access: 7 June 2022.

Nolin, A. W.: Recent advances in remote sensing of seasonal snow, Journal of Glaciology, 56, 1141–1150, https://doi.org/10.3189/002214311796406077, 2010.

O'Connor, J. E., Clague, J. J., Walder, J. S., Manville, V., and Beebee, R. A.: Outburst Floods, https://doi.org/10.1016/b978-0-12-818234-5.00007-9, 2020.

Obu, J., Westermann, S., Bartsch, A., Berdnikov, N., Christiansen, H. H., Dashtseren, A., Delaloye, R., Elberling, B., Etzelmüller, B., Kholodov, A., Khomutov, A., Kääb, A., Leibman, M. O., Lewkowicz, A.

G., Panda, S. K., Romanovsky, V., Way, R. G., Westergaard-Nielsen, A., Wu, T., Yamkhin, J., and Zou, D.: Northern Hemisphere permafrost map based on TTOP modelling for 2000–2016 at 1 km2 scale, Earth-Science Reviews, 193, 299–316, https://doi.org/10.1016/j.earscirev.2019.04.023, 2019.

Onarheim, I. H., Eldevik, T., Smedsrud, L. H., and Stroeve, J. C.: Seasonal and regional manifestation of Arctic sea ice loss, Journal of Climate, 31, 4917–4932, https://doi.org/10.1175/JCLI-D-17-0427.1, 2018.

Östrem, G.: Ice Melting under a Thin Layer of Moraine, and the Existence of Ice Cores in Moraine Ridges, Geografiska Annaler, 41, 228–230, https://doi.org/10.1080/20014422.1959.11907953, 1959.

Otto, J.: Proglacial Lakes in High Mountain Environments: Landform and Sediment Dynamics in Recently Deglaciated Alpine Landscapes, in: Geography of the Physical Environment, edited by: Heckmann, T. and Morche, D., Springer Nature Switzerland, https://doi.org/10.1007/978-3-319-94184-4, 2019.

Patel, K.: As record-setting heat blasts Pakistan, a glacial lake floods village, The Washington Post, 2022.

Patel, K.: Second glacier avalanche in a week shows dangers of a warming climate, The Washington Post, 2022.

Pelto, M., Capps, D., Clague, J. J., and Pelto, B.: Rising ELA and expanding proglacial lakes indicate impending rapid retreat of Brady Glacier, Alaska, Hydrological Processes, 27, 3075–3082, https://doi.org/10.1002/hyp.9913, 2013.

Pepin, N., Bradley, R. S., Diaz, H. F., Baraer, M., Caceres, E. B., Forsythe, N., Fowler, H., Greenwood, G., Hashmi, M. Z., Liu, X. D., Miller, J. R., Ning, L., Ohmura, A., Palazzi, E., Rangwala, I., Schöner, W., Severskiy, I., Shahgedanova, M., Wang, M. B., Williamson, S. N., and Yang, D. Q.: Elevation-dependent warming in mountain regions of the world, Nature Climate Change, 5, 424–430, https://doi.org/10.1038/nclimate2563, 2015.

Perkins-Kirkpatrick, S. E. and Lewis, S. C.: Increasing trends in regional heatwaves, Nature Communications, 11, 1–8, https://doi.org/10.1038/s41467-020-16970-7, 2020.

Petersen, E. I., Levy, J. S., Holt, J. W., and Stuurman, C. M.: New insights into ice accumulation at Galena Creek Rock Glacier from radar imaging of its internal structure, Journal of Glaciology, 66, 1–10, 2020.

Phillis, M.: Warming world creates hazard for Alpine glaciers, Phys.org, 2022.

Post, A. and Mayo, L. R.: Glacier Dammed Lakes and Outburst Floods in Alaska, Hydrologic Investigations Atlas HA-455, USGS, 1971.

Potter, N. J.: Ice-Cored Rock Glacier, Galena Creek, Northern Absaroka Mountains, Wyoming, Geological Society of America Bulletin, 1972.

Pronk, J. B., Bolch, T., King, O., Wouters, B., and Benn, D. I.: Proglacial Lakes Elevate Glacier Surface Velocities in the Himalayan Region, 1–36, 2021.

Rangecroft, S., Harrison, S., and Anderson, K.: Rock glaciers as water stores in the Bolivian Andes: An assessment of their hydrological importance, Arctic, Antarctic, and Alpine Research, 47, 89–98, https://doi.org/10.1657/AAAR0014-029, 2015.

Refsnider, K. A. and Brugger, K. A.: Rock Glaciers in Central Colorado, U.S.A., as Indicators of Holocene Climate Change, Arctic, Antarctic, and Alpine Research, 39, 127–136, https://doi.org/10.1657/1523-0430(2007)39[127:RGICCU]2.0.CO;2, 2007.

Reynolds, J. M.: On the formation of supraglacial lakes on debris-covered glaciers, IAHS-AISH

Publication, 153–161, 2000.

RGIK: IPA Action Group Rock glacier inventories and kinematics (version 4.1), International Permafrost Association, 1–13, 2022.

Richardson, S. D. and Reynolds, J. M.: An overview of glacial hazards in the Himalayas, Quaternary International, 66, 31–47, 2000.

Rick, B., McGrath, D., Armstrong, W., and Mccoy, S. W.: Dam type and lake location characterize ice-marginal lake area change in Alaska and NW Canada between 1984 and 2019, Cryosphere, 16, 297–314, https://doi.org/10.5194/tc-16-297-2022, 2022.

Rounce, D. R., Watson, C. S., and McKinney, D. C.: Identification of Hazard and Risk for Glacial Lakes in the Nepal Himalaya Using Satellite Imagery from 2000 – 2015, Remote Sensing, 9, https://doi.org/10.3390/rs9070654, 2017.

Salerno, F., Thakuri, S., D'Agata, C., Smiraglia, C., Manfredi, E. C., Viviano, G., and Tartari, G.: Glacial lake distribution in the Mount Everest region: Uncertainty of measurement and conditions of formation, Global and Planetary Change, 92–93, 30–39, https://doi.org/10.1016/j.gloplacha.2012.04.001, 2012.

Santos, J. and Córdova, C.: Little Ice Age glacial geomorphology and sedimentology of Portage Glacier, South-Central Alaska, Finisterra, 44, 95–108, https://doi.org/10.18055/finis1380, 2009.

Scambos, T. A., Dutkiewicz, M. J., Wilson, J. C., and Bindschadler, R. A.: Application of image cross-correlation to the measurement of glacier velocity using satellite image data, Remote Sensing of Environment, 42, 177–186, https://doi.org/10.1016/0034-4257(92)90101-O, 1992.

Shugar, D., Jacquemart, M., Shean, D., Bhushan, S., Upadhyay, K., Sattar, A., Schwanghart, W., McBride, S., Wyk, de V. M. Van, Mergili, M., Emmer, A., Deschamps-Berger, C., McDonnell, M., Bhambri, R., Allen, S., Berthier, E., Carrivick, J. L., Clague, J., Dokukin, M., Dunning, S. A., Frey, H., Gascoin, S., Haritashya, U. K., Huggel, C., Kääb, A., Kargel, J. S., Kavanaugh, J. L., Lacroix, P., Petley, D., Rupper, S., Azam, M. F., Cook, S. J., Dimri, A. P., Eriksson, M., Farinotti, D., Fiddes, J., Gnyawali, K. R., Harrison, S., Jha, M., Koppes, M., Kumar, A., Leinss, S., Majeed, U., Mal, S., Muhuri, A., Noetzli, J., Paul, F., Rashid, I., Sain, K., Steiner, J., Ugalde, F., Watson, C. S., and Westoby, M. J.: A massive rock and ice avalanche caused the 2021 disaster at Chamoli, Indian Himalaya, Science, 373, 300–306, 2021.

Shugar, D. H., Burr, A., Haritashya, U. K., Kargel, J. S., Watson, C. S., Kennedy, M. C., Bevington, A. R., Betts, R. A., Harrison, S., and Strattman, K.: Rapid worldwide growth of glacial lakes since 1990, Nature Climate Change, 10, 939–945, https://doi.org/10.1038/s41558-020-0855-4, 2020.

Solomina, O. N., Bradley, R. S., Hodgson, D. A., Ivy-Ochs, S., Jomelli, V., Mackintosh, A. N., Nesje, A., Owen, L. A., Wanner, H., Wiles, G. C., and Young, N. E.: Holocene glacier fluctuations, Quaternary Science Reviews, 111, 9–34, https://doi.org/10.1016/j.quascirev.2014.11.018, 2015.

Solomina, O. N., Bradley, R. S., Jomelli, V., Geirsdottir, A., Kaufman, D. S., Koch, J., McKay, N. P., Masiokas, M., Miller, G., Nesje, A., Nicolussi, K., Owen, L. A., Putnam, A. E., Wanner, H., Wiles, G., and Yang, B.: Glacier fluctuations during the past 2000 years, Quaternary Science Reviews, 149, 61–90, https://doi.org/10.1016/j.quascirev.2016.04.008, 2016.

Song, C., Sheng, Y., Wang, J., Ke, L., Madson, A., and Nie, Y.: Heterogeneous glacial lake changes and links of lake expansions to the rapid thinning of adjacent glacier termini in the Himalayas, Geomorphology, 280, 30–38, https://doi.org/10.1016/j.geomorph.2016.12.002, 2017.

Streletskiy, D. A., Shiklomanov, N. I., Little, J. D., Nelson, F. E., Brown, J., Nyland, K. E., and Klene, A. E.: Thaw Subsidence in Undisturbed Tundra Landscapes, Barrow, Alaska, 1962–2015, Permafrost and

Periglacial Processes, 28, 566–572, https://doi.org/10.1002/ppp.1918, 2017.

Stroeve, J. and Notz, D.: Changing state of Arctic sea ice across all seasons, Environmental Research Letters, 13, https://doi.org/10.1088/1748-9326/aade56, 2018.

Sturm, B. M. and Benson, S.: A history of jokulhlaups from Strandline Lake, Alaska, U.S.A., Journal of Glaciology, 31, 1985.

Tronstad, L. M., Hotaling, S., Giersch, J. J., Wilmot, O. J., and Finn, D. S.: Headwaters fed by subterranean ice: potential climate refugia for mountain stream communities?, bioRxiv, https://doi.org/10.1101/788273, 2019.

Tweed, F. S. and Carrivick, J. L.: Deglaciation and proglacial lakes, Geology Today, 31, 96–102, 2015.

Tweed, F. S. and Russell, A. J.: Controls on the formation and sudden drainage of glacier-impounded lakes: Implications for jökulhlaup characteristics, Progress in Physical Geography, 23, 79–110, https://doi.org/10.1191/030913399666727306, 1999.

Veh, G., Korup, O., Specht, S. Von, Roessner, S., and Walz, A.: Unchanged frequency of moraine-dammed glacial lake outburst floods in the Himalaya, Nature Climate Change, 9, https://doi.org/10.1038/s41558-019-0437-5, 2019.

Veh, G., Korup, O., and Walz, A.: Hazard from Himalayan glacier lake outburst floods, Proceedings of the National Academy of Sciences of the United States of America, 117, 907–912, https://doi.org/10.1073/pnas.1914898117, 2020.

Veh, G., Lützow, N., Kharlamova, V., Petrakov, D., Hugonnet, R., and Korup, O.: Trends, breaks, and biases in the frequency of reported glacier lake outburst floods, Earth's Future, https://doi.org/10.1029/2021ef002426, 2022.

Wahrhaftig, C. and Cox, A.: Rock Glaciers in the Alaska Range, Bulletin of the Geological Society of America, 70, 383–436, 1959.

Walder, J. S. and Costa, J. E.: Outburst floods from glacier-dammed lakes: The effect of mode of lake drainage on flood magnitude, Earth Surface Processes and Landforms, 21, 701–723, https://doi.org/10.1002/(SICI)1096-9837(199608)21:8<701::AID-ESP615>3.0.CO;2-2, 1996.

Wallis, G. P., Waters, J. M., Upton, P., and Craw, D.: Transverse Alpine Speciation Driven by Glaciation, Trends in Ecology and Evolution, 31, 916–926, https://doi.org/10.1016/j.tree.2016.08.009, 2016.

Wang, S. J. and Zhou, L. Y.: Integrated impacts of climate change on glacier tourism, Advances in Climate Change Research, 10, 71–79, https://doi.org/10.1016/j.accre.2019.06.006, 2019.

Wang, X., Liu, S., Ding, Y., Guo, W., Jiang, Z., Lin, J., and Han, Y.: An approach for estimating the breach probabilities of moraine-dammed lakes in the Chinese Himalayas using remote-sensing data, Natural Hazards and Earth System Science, 12, 3109–3122, https://doi.org/10.5194/nhess-12-3109-2012, 2012.

Wang, X., Ding, Y., Liu, S., and Jiang, L.: Changes of glacial lakes and implications in Tian Shan , central Asia , based on remote sensing data from 1990 to 2010, Environmental Research Letters, 8, 11p, https://doi.org/10.1088/1748-9326/8/4/044052, 2013.

Wang, X., Guo, X., Yang, C., Liu, Q., Wei, J., Zhang, Y., Liu, S., Zhang, Y., Jiang, Z., and Tang, Z.: Glacial lake inventory of High Mountain Asia (1990–2018) derived from Landsat images, Earth System Science Data Discussions, 1–23, https://doi.org/10.5194/essd-2019-212, 2020.

Welling, J., Árnason, T., and Ólafsdóttir, R.: Implications of climate change on nature-based tourism

demand: A segmentation analysis of glacier site visitors in southeast Iceland, Sustainability (Switzerland), 12, https://doi.org/10.3390/su12135338, 2020.

White, S. E.: Rock Glacier Studies in the Colorado Front Range, 1961 to 1968, Arctic and Alpine Research, 3, 43–64, https://doi.org/10.2307/1550382, 1971.

Wicky, J. and Hauck, C.: Air Convection in the Active Layer of Rock Glaciers, Frontiers in Earth Science, 8, 1–17, https://doi.org/10.3389/feart.2020.00335, 2020.

Wilcox, A. C., Wade, A. A., and Evans, E. G.: Drainage events from a glacier-dammed lake, Bear Glacier, Alaska: Remote sensing and field observations, Geomorphology, 220, 41–49, https://doi.org/10.1016/j.geomorph.2014.05.025, 2014.

Wiles, G. C., Barclay, D. J., and Calkin, P. E.: Tree-ring-dated "Little Ice Age" histories of maritime glaciers from western Prince William Sound, Alaska, Holocene, 9, 163–173, https://doi.org/10.1191/095968399671927145, 1999.

Williams, M. W., Knauf, M., Caine, N., Liu, F., and Verplanck, P. L.: Geochemistry and Source Waters of Rock Glacier Outflow , Colorado Front Range, Permafrost and Periglacial Processes, 17, 13–33, https://doi.org/10.1002/ppp.535, 2006.

Wolfe, D. F. G., Kargel, J. S., and Leonard, G. J.: Glacier-dammed ice-marginal lakes of Alaska, 263–295 pp., https://doi.org/10.1007/978-3-540-79818-7, 2014.

Worni, R., Huggel, C., and Stoffel, M.: Glacial lakes in the Indian Himalayas — From an area-wide glacial lake inventory to on-site and modeling based risk assessment of critical glacial lakes, Science of the Total Environment, The, 468–469, S71–S84, https://doi.org/10.1016/j.scitotenv.2012.11.043, 2013.

Zemp, M., Huss, M., Thibert, E., Eckert, N., Mcnabb, R., Huber, J., Barandun, M., Machguth, H., Nussbaumer, S. U., Thomson, L., Paul, F., Maussion, F., Kutuzov, S., Cogley, J. G., Asia, C., Zealand, N., Canada, W., and Zealand, N.: Global glacier mass changes and their contributions to sea-level rise from 1961 to 2016, Nature, https://doi.org/10.1038/s41586-019-1071-0, 2019.

Zhang, G., Yao, T., Xie, H., Wang, W., and Yang, W.: An inventory of glacial lakes in the Third Pole region and their changes in response to global warming, Global and Planetary Change, 131, 148–157, https://doi.org/10.1016/j.gloplacha.2015.05.013, 2015.

Zhang, M., Chen, F., and Tian, B.: An automated method for glacial lake mapping in High Mountain Asia using Landsat 8 imagery, Journal of Mountain Science, 15, 13–24, https://doi.org/10.1007/s11629-017-4518-5, 2018.

Zheng, G., Allen, S. K., Bao, A., Ballesteros-Cánovas, J. A., Huss, M., Zhang, G., Li, L., Yuan, Y., Jiang, L., Yu, T., Chen, W., and Stoffel, M.: Increasing risk of glacial lake outburst floods from future Third Pole deglaciation, Nature Climate Change, in press, https://doi.org/10.1038/s41558-021-01028-3, 2021.

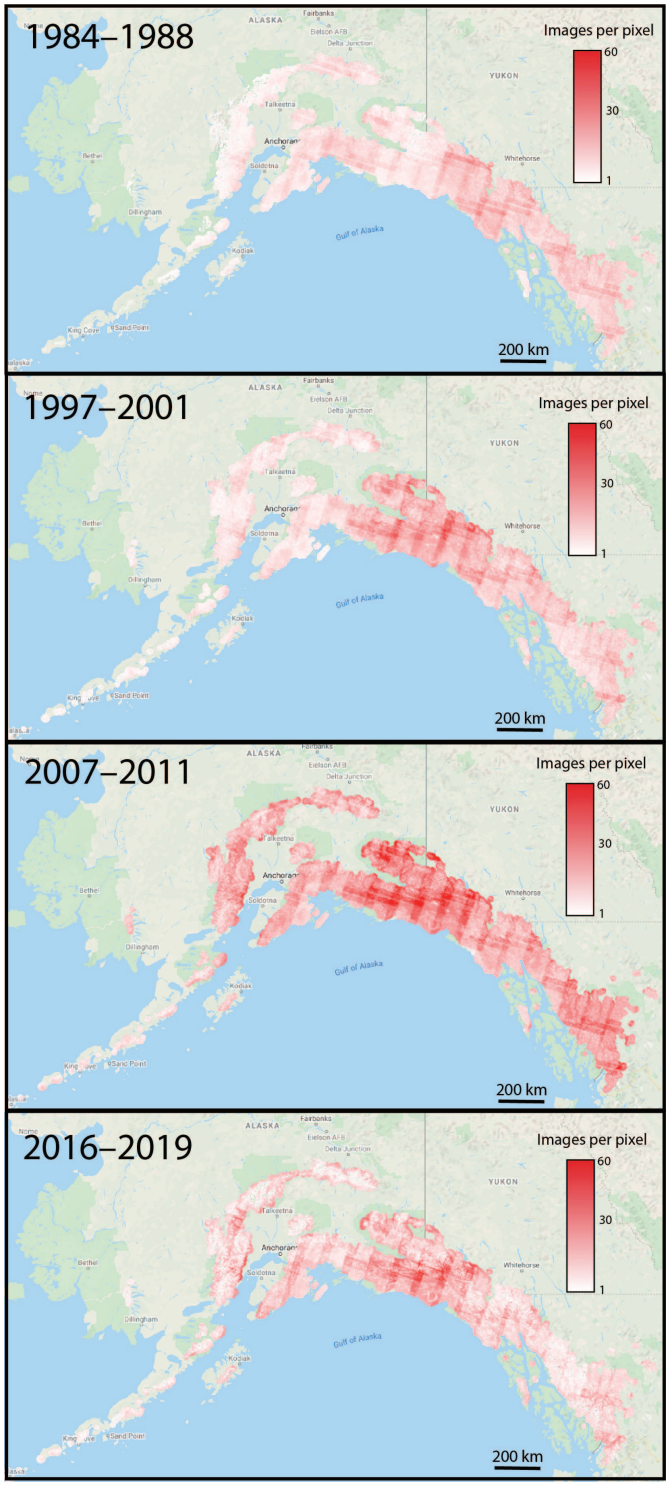

Fig. A1. Images per pixel per time period for each mosaic (median of each pixel value) used in analysis. Maps created in © Google Earth Engine (Gorelick et al., 2017).

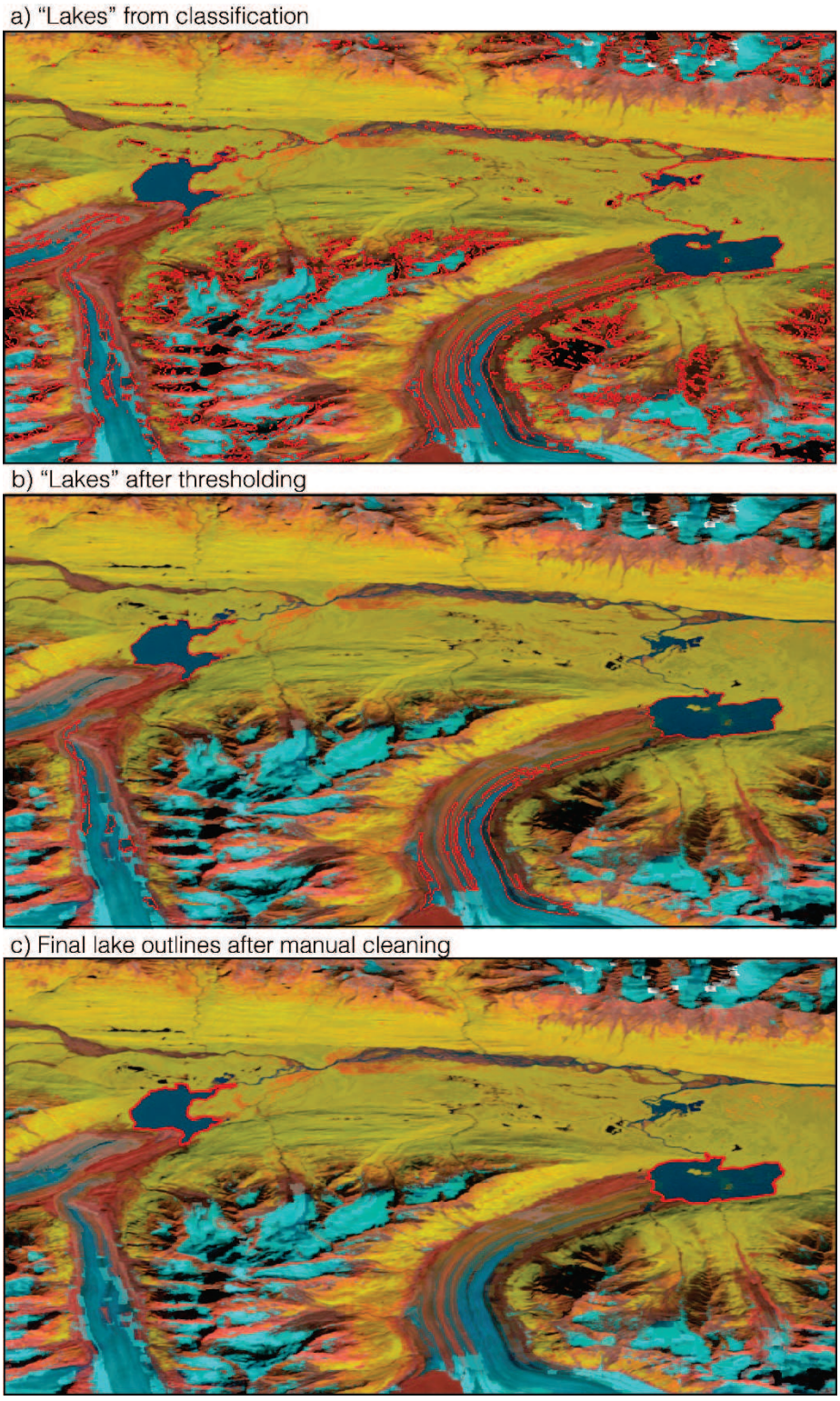

Fig. A2. Example of lake polygons after supervised classification (a), after applying slope, area, distance, and length:area ratio thresholds (b), and after manual verification. Polygon outlines are in red. False color images using Landsat bands for shortwave infrared (SWIR), near infrared (NIR), and red.

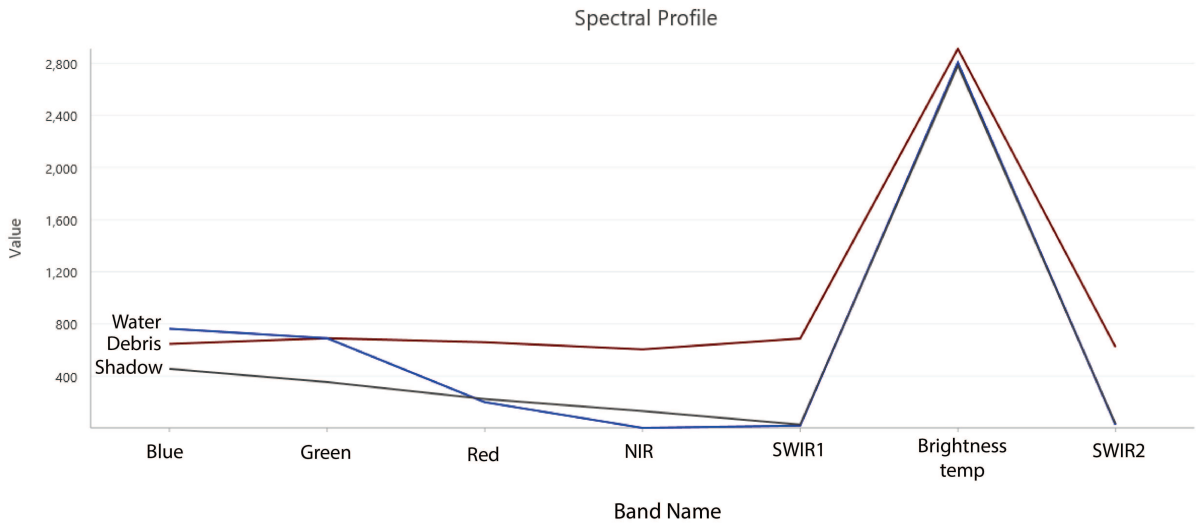

Fig. A3. Spectral comparison of water, mountain shadow, and a debris band.

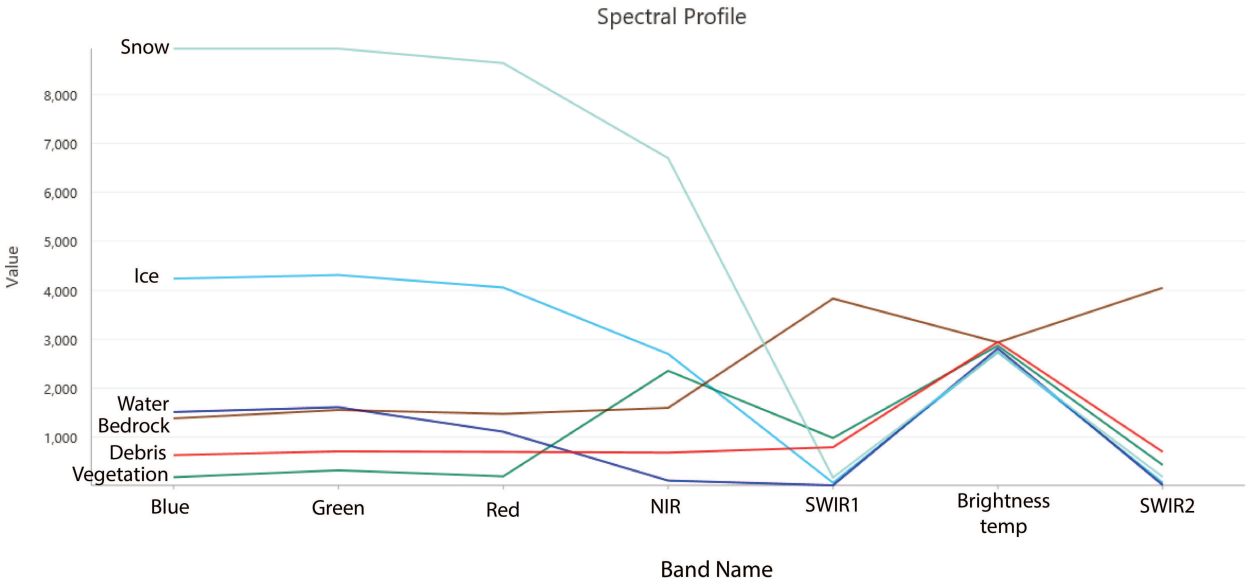

Fig. A4. Example spectral profiles for each landcover type (snow, ice, water, bedrock, debris, and vegetation) used in supervised classification.

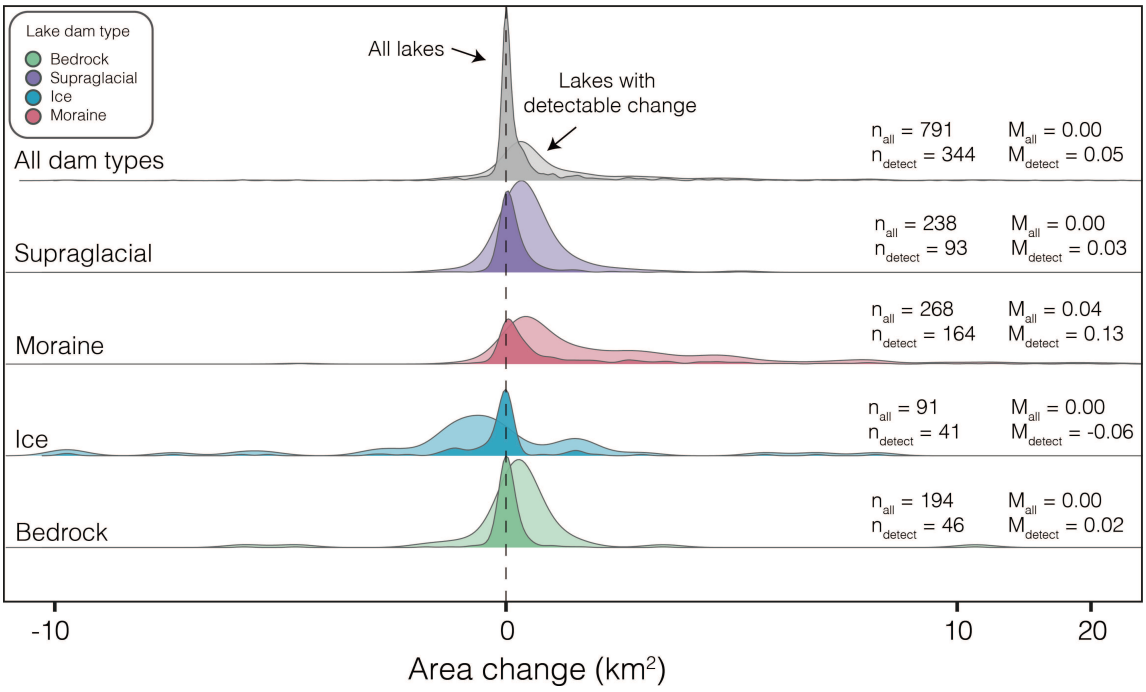

Fig. A5. Smoothed density distribution (normalized to 1 for each dam type) of absolute lake area change for all lakes (dark curves) and lakes with detectable change (light curves) for each dam type, with number of lakes (n) and median lake area change (M).

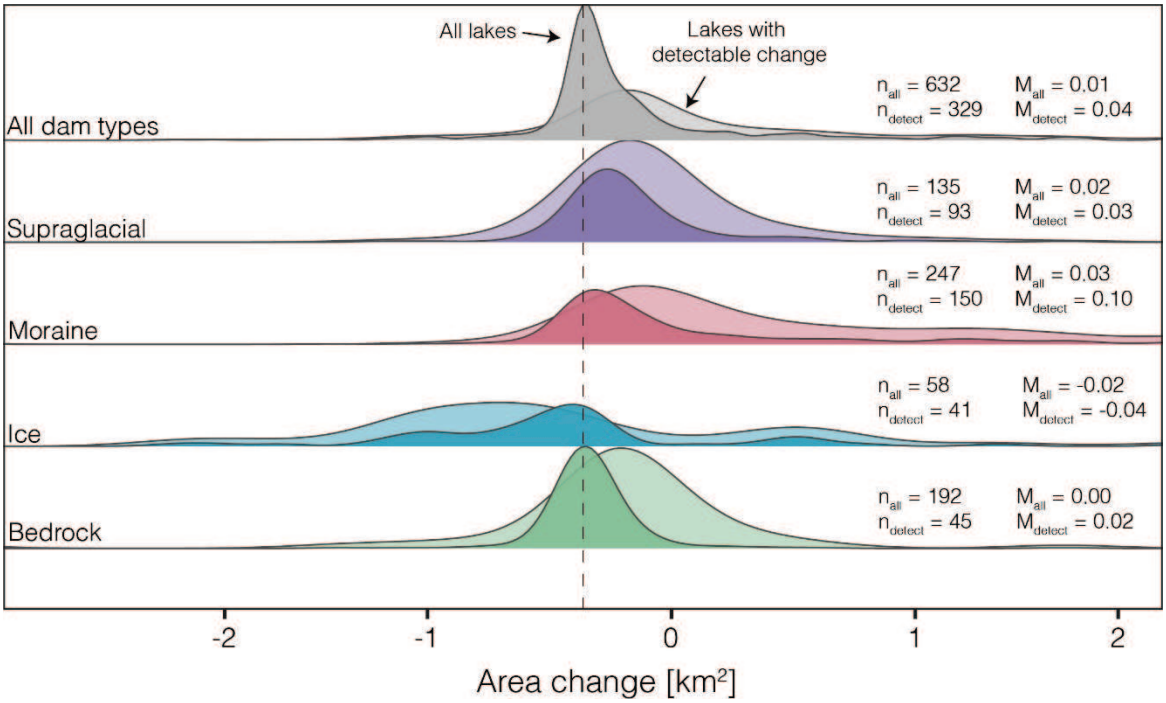

Fig. A6. Smoothed density distribution (normalized to 1 for each dam type) of absolute lake area change for all lakes with an area less than 10 km^2 in 2016–2019 (dark curves) and lakes with detectable change (light curves) for each dam type, with number of lakes (n) and median lake area change (M). Note that the x-axis has been limited to –2 and 2 km^2.

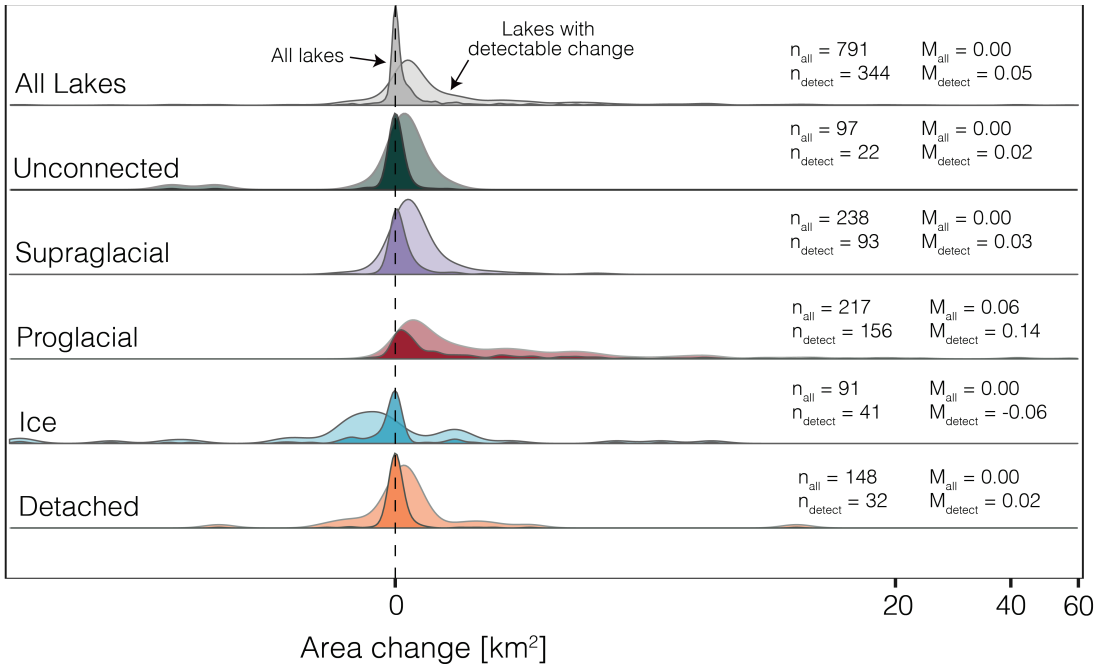

Fig. A7. Distribution of lake area change (km^2) for all lakes (dark curves) and lakes with detectable change (light curves) for each topological position, with number of lakes (n) and median lake area change (M).

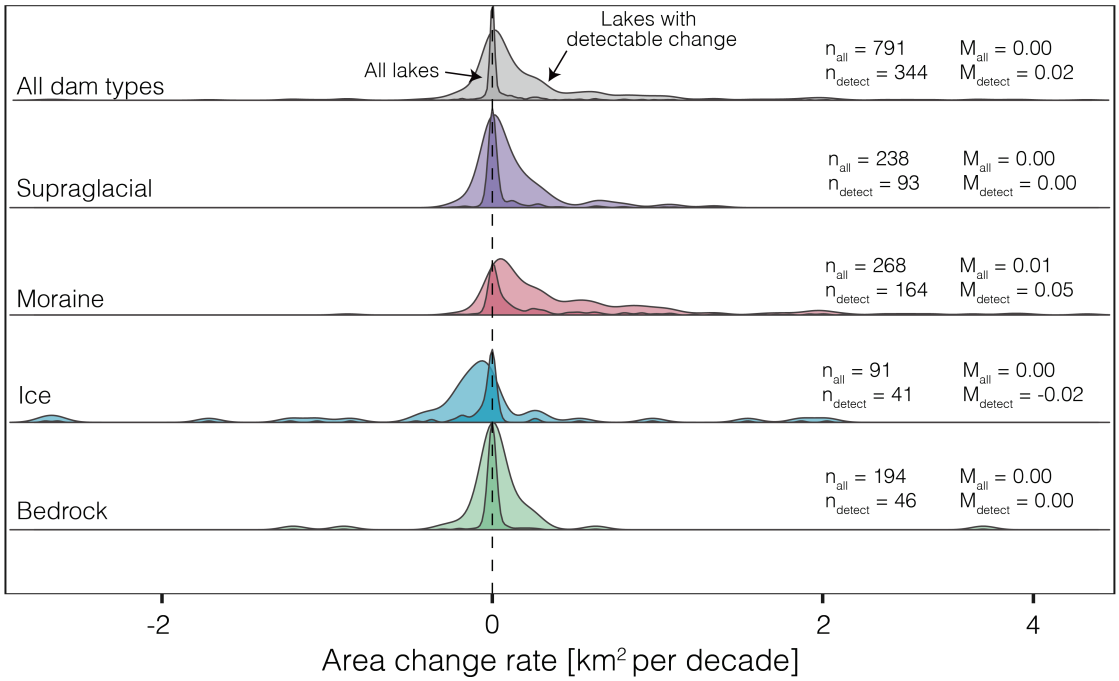

Fig. A8. Distribution of lake area change rate (km^2 per decade) for all lakes (dark curves) and lakes with detectable change (light curves) for each dam type, with number of lakes (n) and median lake area change (M).

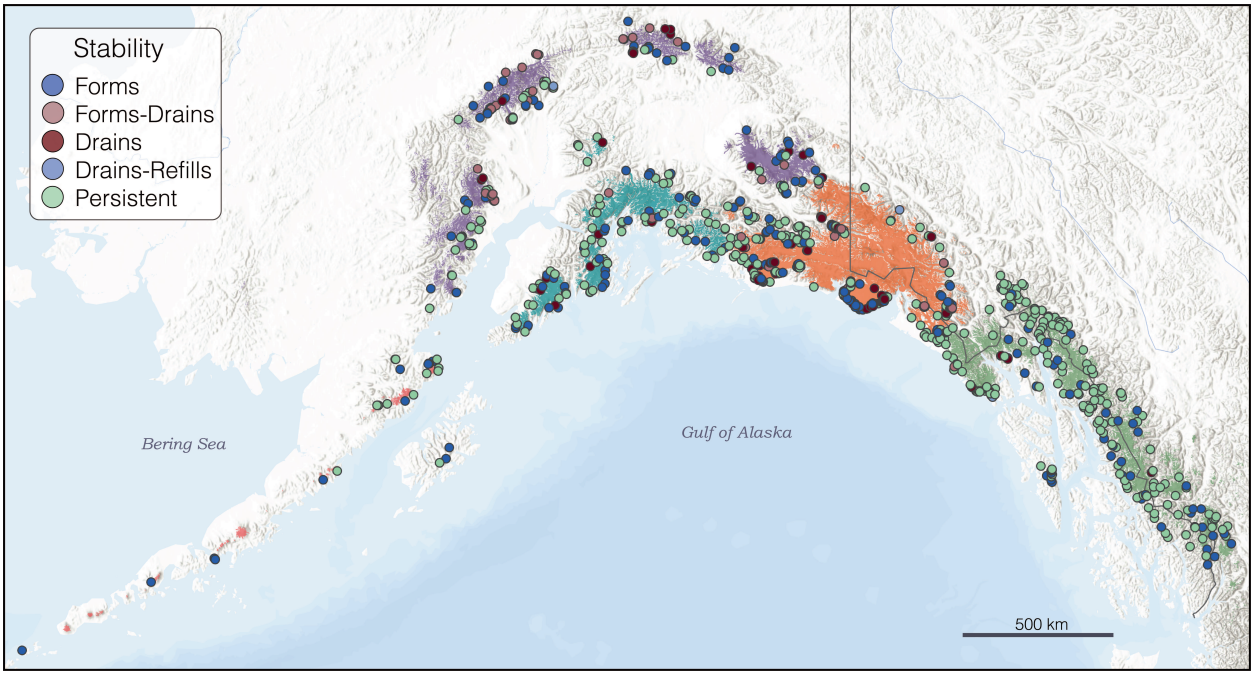

Fig. A9. Lake stability distribution across Alaska. Each dot represents an individual lake. Colored areas refer to the RGI subregions (see Fig. 1) (basemap provided by ESRI, 2021).

Table A1. Attributes of the 19 lakes with area greater than 10 km^2.

LakeID	GlacierName	Area 1984-1988(km^2)	Area 1997-2001(km^2)	Area 2007-2011(km^2)	Area 2016-2019(km^2)	Position	Dam Type	Elevation (m)	<2 m asl	PiedmontBasin	O2Region	Stability	Area Change 1984-2016(km^2)	Change Rate (km^2/decade)
RGI60-01.10006n50	Colony Glacier	25.43	26.35	26.73	27.71	proglacial	moraine	62.00	N	Y	4	Persistent	2.28	0.71
RGI60-01.13538n432	Tana Glacier	1.45	2.93	1.93	13.31	proglacial	moraine	481.00	N	N	5	Persistent	11.86	3.71
RGI60-01.13531n428	Miles Glacier	31.62	40.07	31.22	40.26	proglacial	moraine	39.00	N	Y	5	Persistent	8.64	2.70
RGI60-01.14883n431	Steller Glacier	21.98	16.32	17.15	12.78	ice	ice	132.00	N	N	5	Persistent	-9.20	-2.88
RGI60-01.14883n430	Steller Glacier	10.11	15.77	15.95	22.58	proglacial	moraine	8.00	N	Y	5	Persistent	12.48	3.90
RGI60-01.16545n457	Lowell Glacier	7.52	11.19	18.47	22.51	proglacial	moraine	514.00	N	Y	5	Persistent	14.99	4.68
RGI60-01.13635n325	Bering Glacier	91.19	87.38	143.11	131.82	proglacial	moraine	0.00	Y	Y	5	Persistent	40.63	12.70
RGI60-01.09471n48	Excelsior Glacier	7.94	11.59	14.74	17.31	proglacial	moraine	0.25	Y	Y	4	Persistent	9.37	2.93
RGI60-01.17803n310	Bear Glacier	7.98	10.57	17.08	18.61	proglacial	moraine	0.00	Y	Y	4	Persistent	10.63	3.32
RGI60-01.12645n433	East Yakutat Glacier	53.84	61.52	62.84	96.61	proglacial	moraine	28.00	N	Y	5	Persistent	42.77	13.37
RGI60-01.13696n454	Malaspina Glacier	30.08	43.43	72.51	87.03	proglacial	moraine	1.80	Y	Y	5	Persistent	56.95	17.80
RGI60-01.21081n455	Alsek Lake	45.75	55.64	61.95	69.27	proglacial	moraine	21.00	N	Y	6	Persistent	23.52	7.35
RGI60-01.01514n459	Twin Glacier Lake	12.04	12.44	12.54	12.53	proglacial	moraine	6.00	N	Y	6	Persistent	0.49	0.15
RGI60-01.04532n319	NA	4.74	5.36	6.83	11.07	proglacial	moraine	105.00	N	Y	6	Persistent	6.33	1.98
RGI60-01.03741n51	Great Glacier	11.60	12.83	13.58	13.60	proglacial	moraine	18.00	N	Y	6	Persistent	1.99	0.62
RGI60-01.01522n703	Llewellyn Glacier	4.82	7.30	9.73	11.34	proglacial	moraine	702.00	N	N	6	Persistent	6.52	2.04
RGI60-01.20748n688	NA	12.58	24.95	29.05	30.41	proglacial	moraine	193.00	N	N	6	Persistent	17.83	5.57
RGI60-01.20985n434	Grand Plateau Glacier	25.27	33.05	39.07	44.94	proglacial	moraine	22.00	N	Y	6	Persistent	19.67	6.15
RGI60-01.12397n47	Barrier Glacier	74.36	79.45	82.67	85.35	detached	bedrock	346.00	N	N	2	Persistent	10.99	3.44

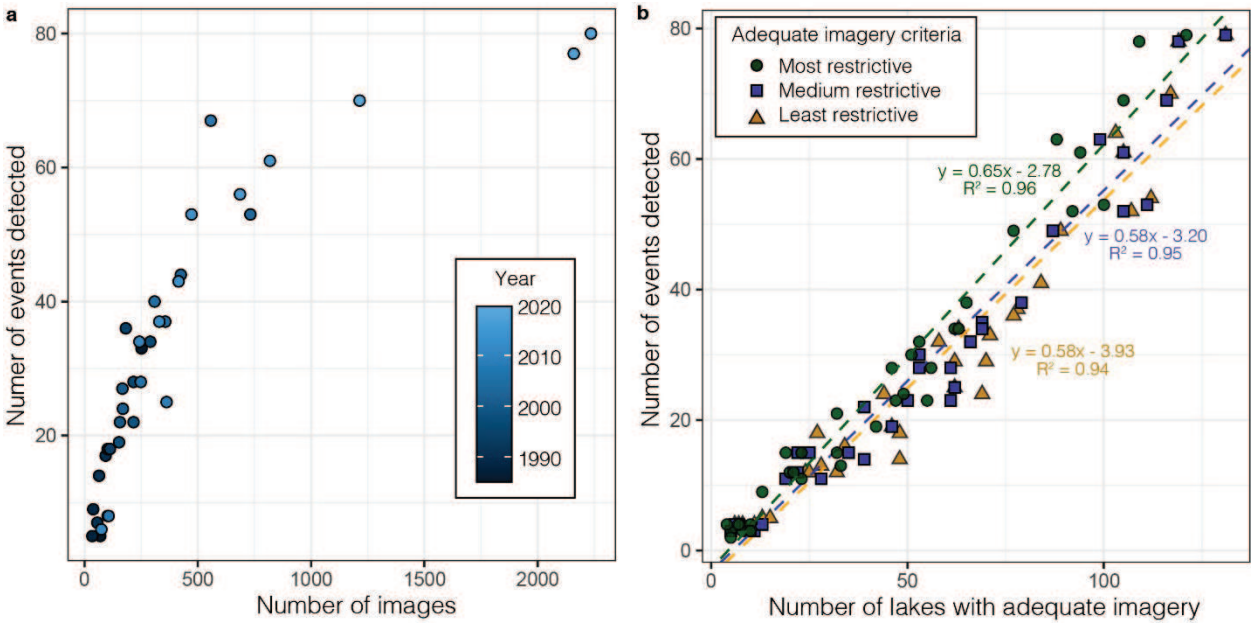

Fig. B1. Correlation between the number of images available each year, number of lakes with adequate imagery, and the number of drainage events detected. **a,** Relationship between the total number of images available and number of drainage events detected colored by year, and **b,** relationship between the number of events detected and the number of lakes with adequate imagery for the three different criteria (see Fig. B3).

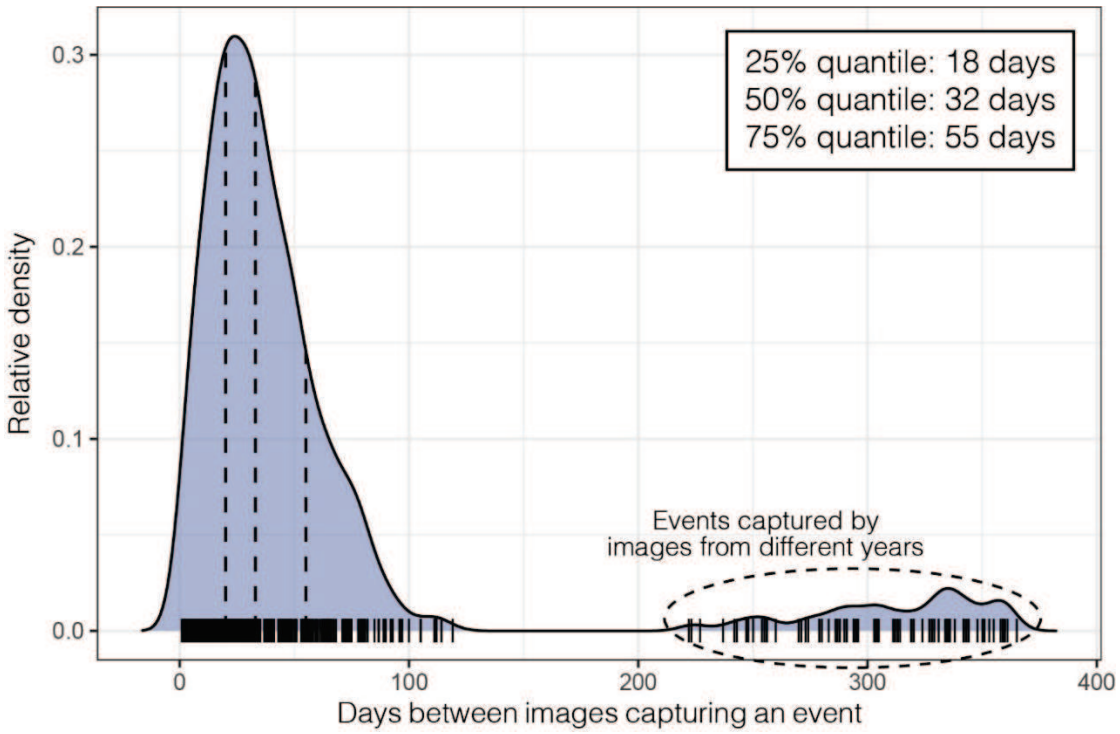

Fig. B2. Empirical probability density function of number of days between images which captured a lake drainage event. Black ticks represent an individual event, and dashed lines represent the 25%, 50%, and 75% quantiles.

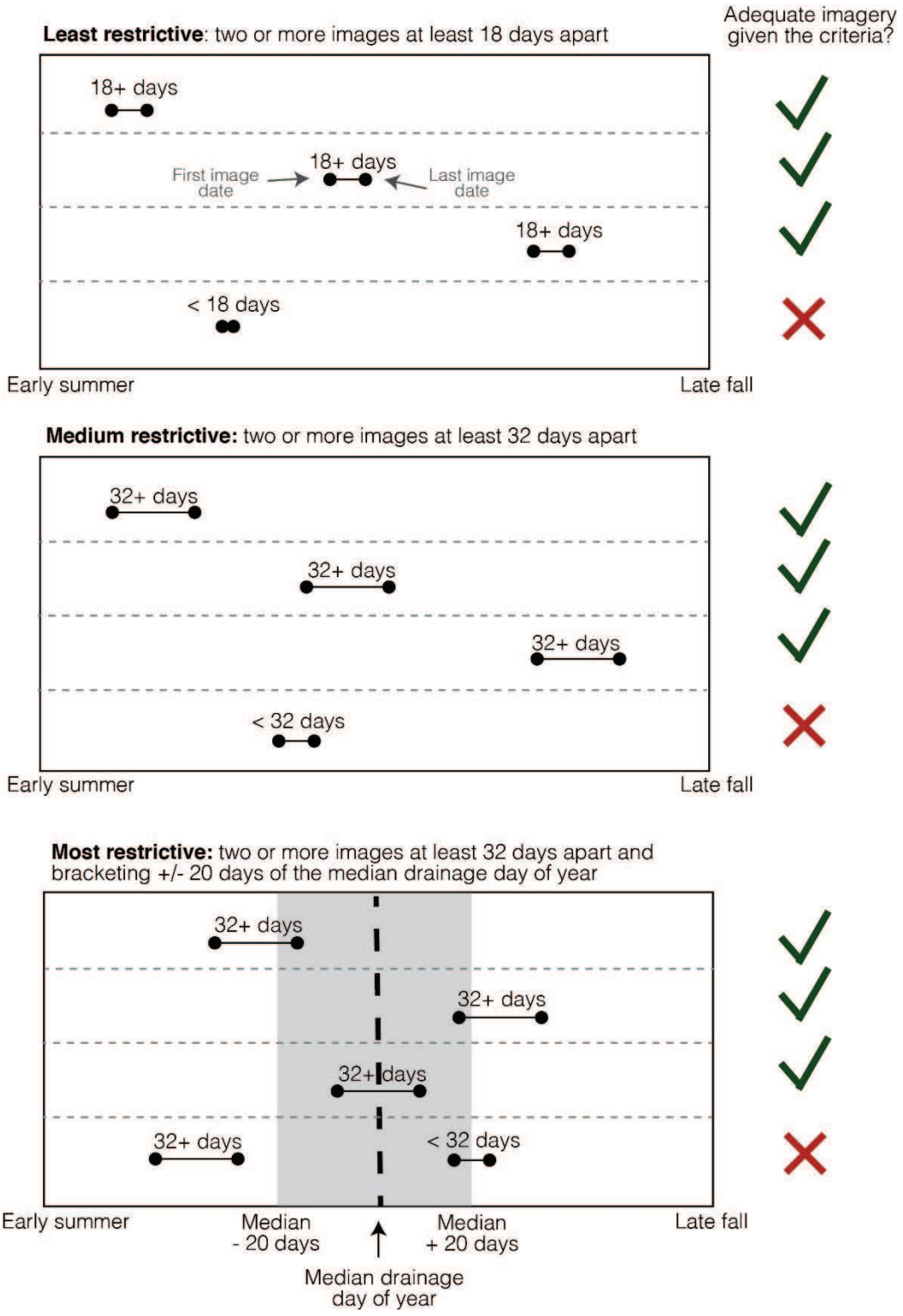

Fig. B3. Visual representation of the three different criteria used to define whether a lake had adequate imagery to detect an event in any given year. The three criteria includes the least restrictive criteria (at least two images that are 18 or more days apart), the medium restrictive criteria (at least two images that are 32 or more days apart), and the most restrictive (two images at least 32 or more days apart, taking the timing of the images into consideration).

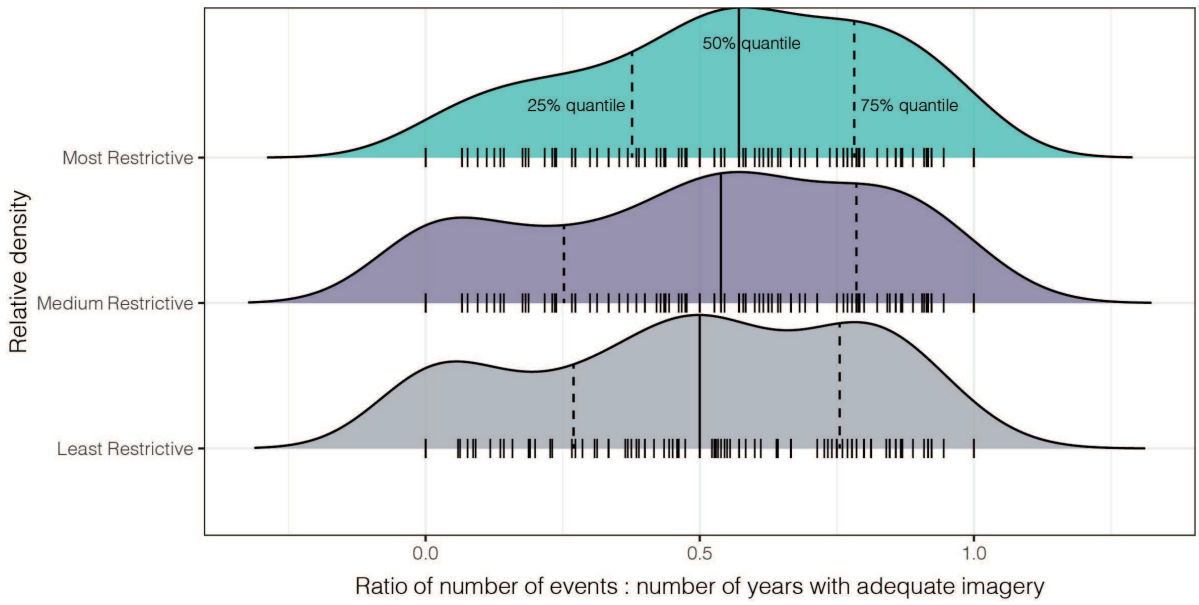

Fig. B4. Smoothed density distribution of the ratio of number of events to the number of years with adequate imagery given the three different criteria (see Fig. B3). Black ticks represent individual lakes and vertical lines represent the 25%, 50%, and 75% quantiles. A value of 0.5 indicates that a lake drained 50% of all years where adequate imagery was detected.

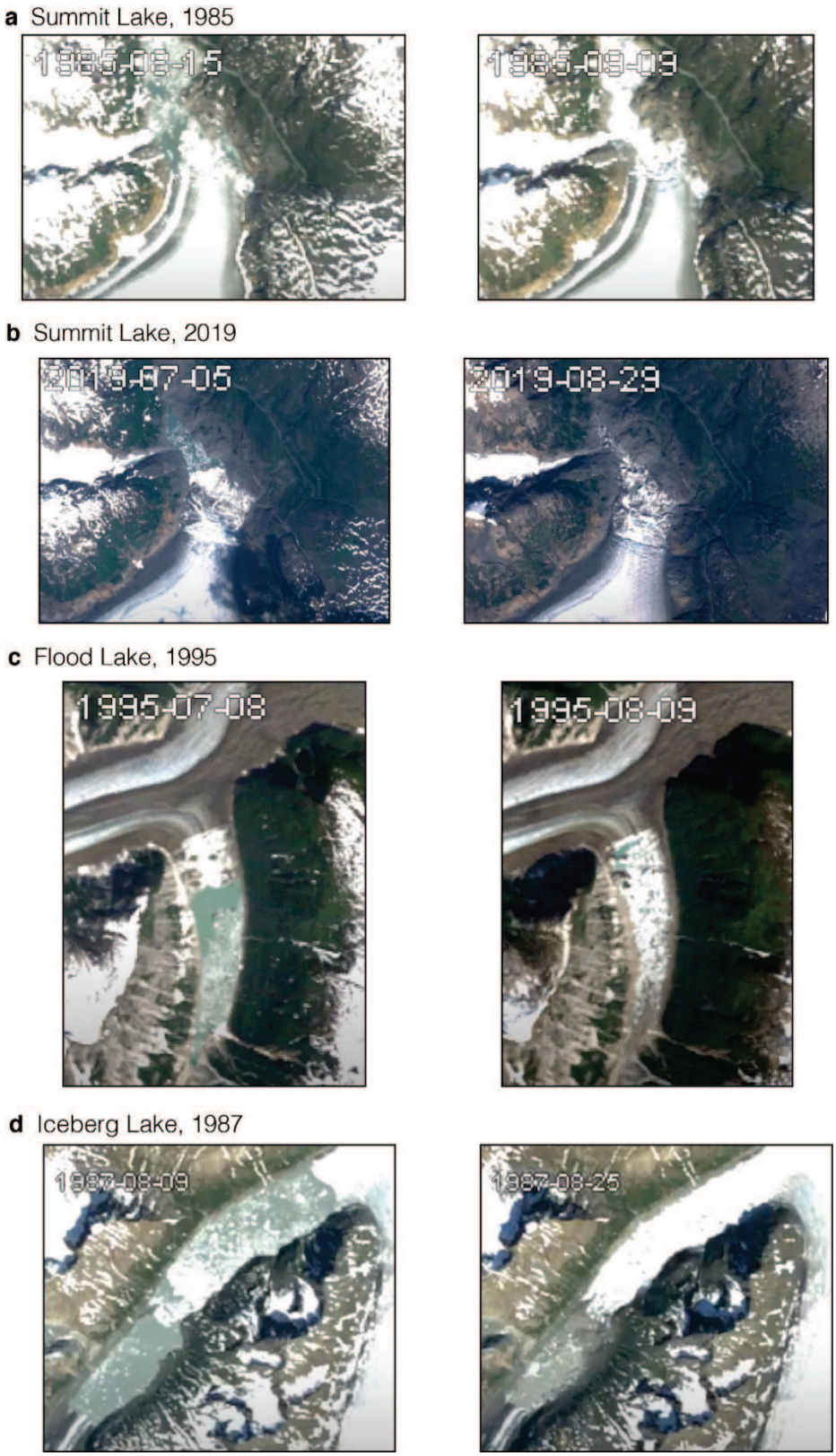

Fig. B5. Example of what lakes look like before (left) and after (right) a drainage event at **a, b,** Summit Lake, **c,** Flood Lake, and **d,** Iceberg Lake.

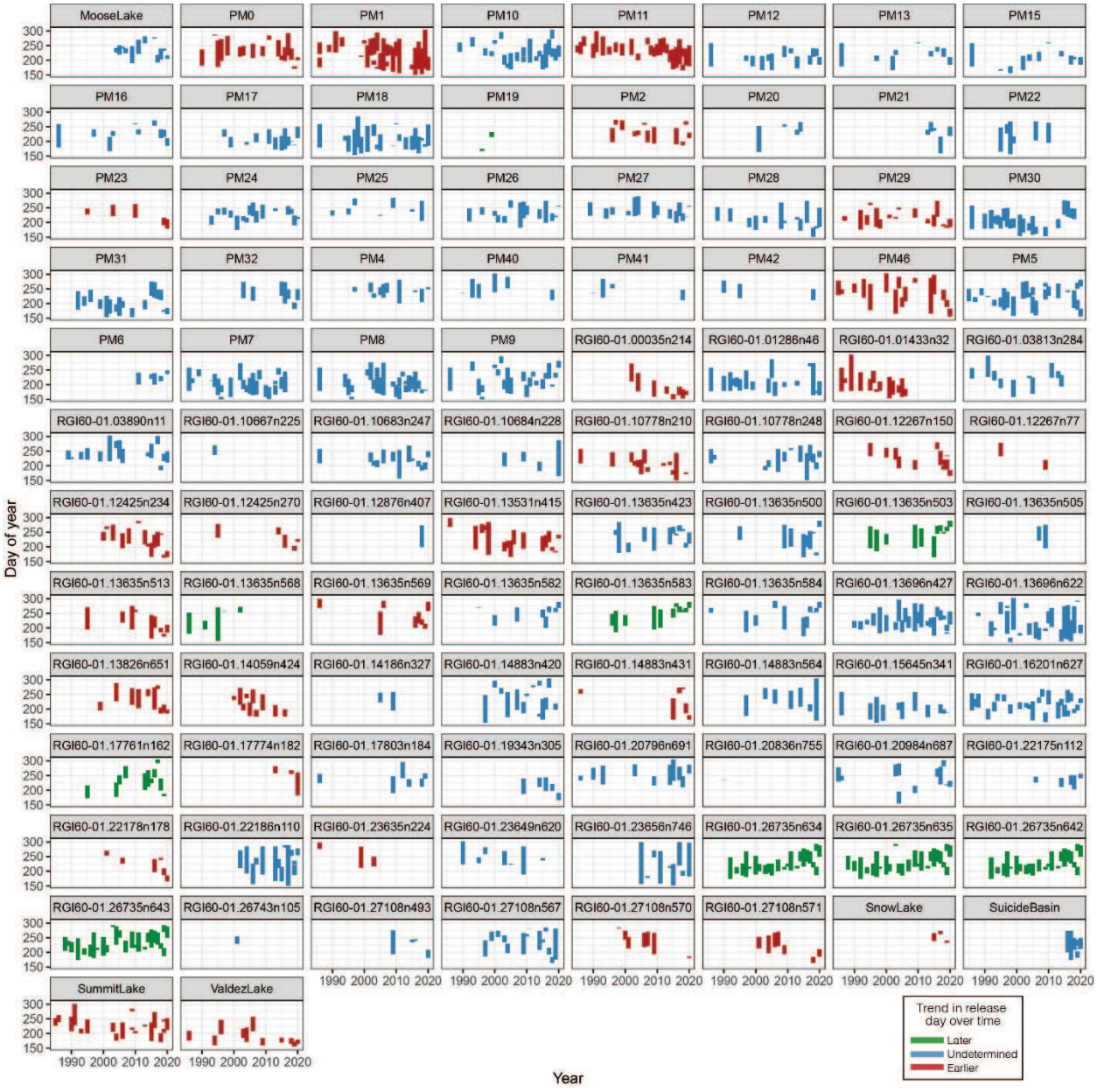

Fig. B6. Lake drainage events documented for each individual lake. Segments signify the last date a lake was full to the first day it was drained, colored by whether the lake had an earlier release over time (red), later release over time (green), or and indistinguishable trend (blue).

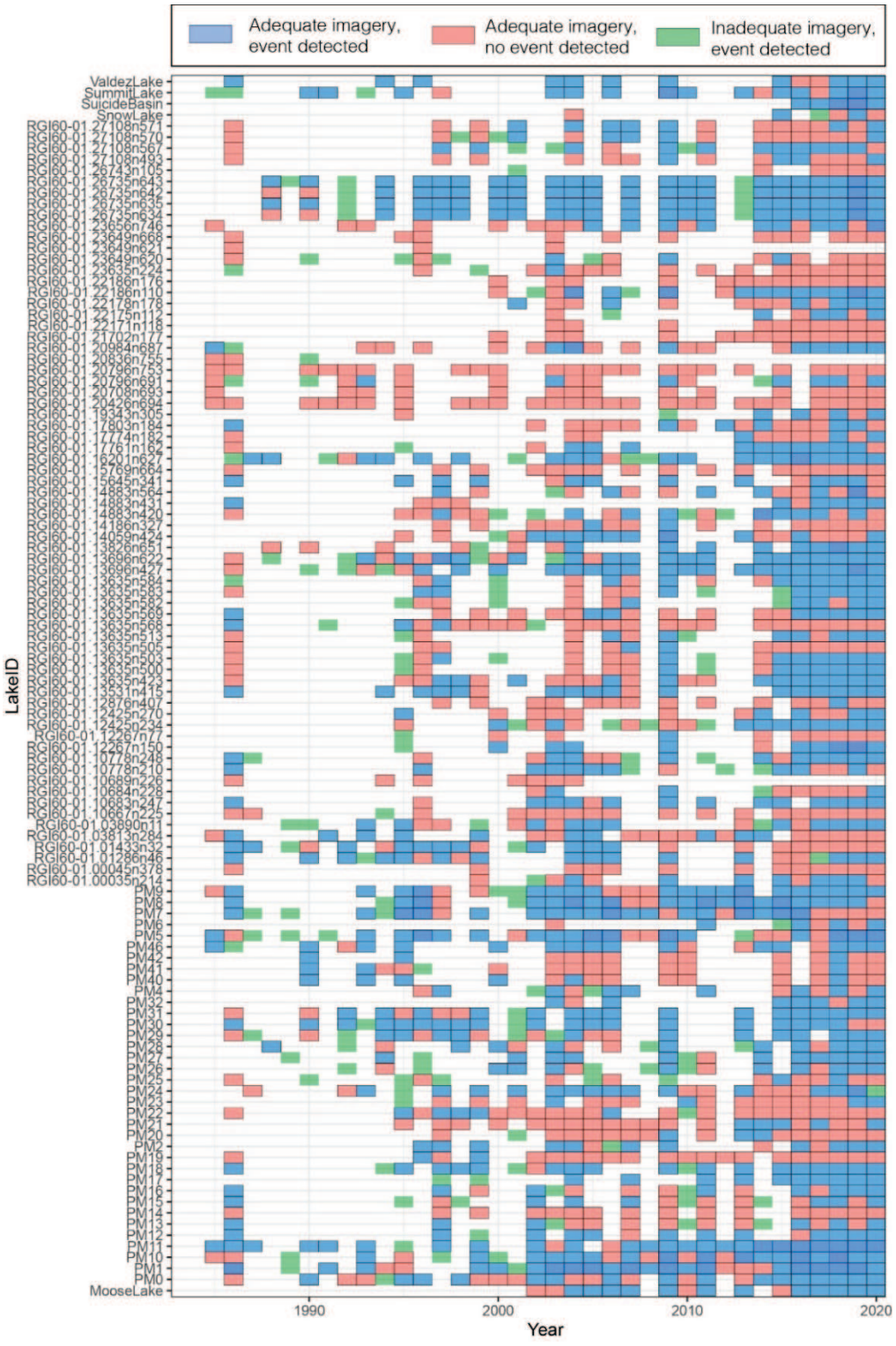

Fig. B7. Imagery availability and drainage event detection. Lakes and years in which there was adequate imagery and an event detected (blue), adequate imagery and no event detected (red), and inadequate imagery yet an event detected (green) given the middle ground criteria of two images at least 32 or more days apart (Fig. B3). White space represents years without adequate imagery and no events detected.

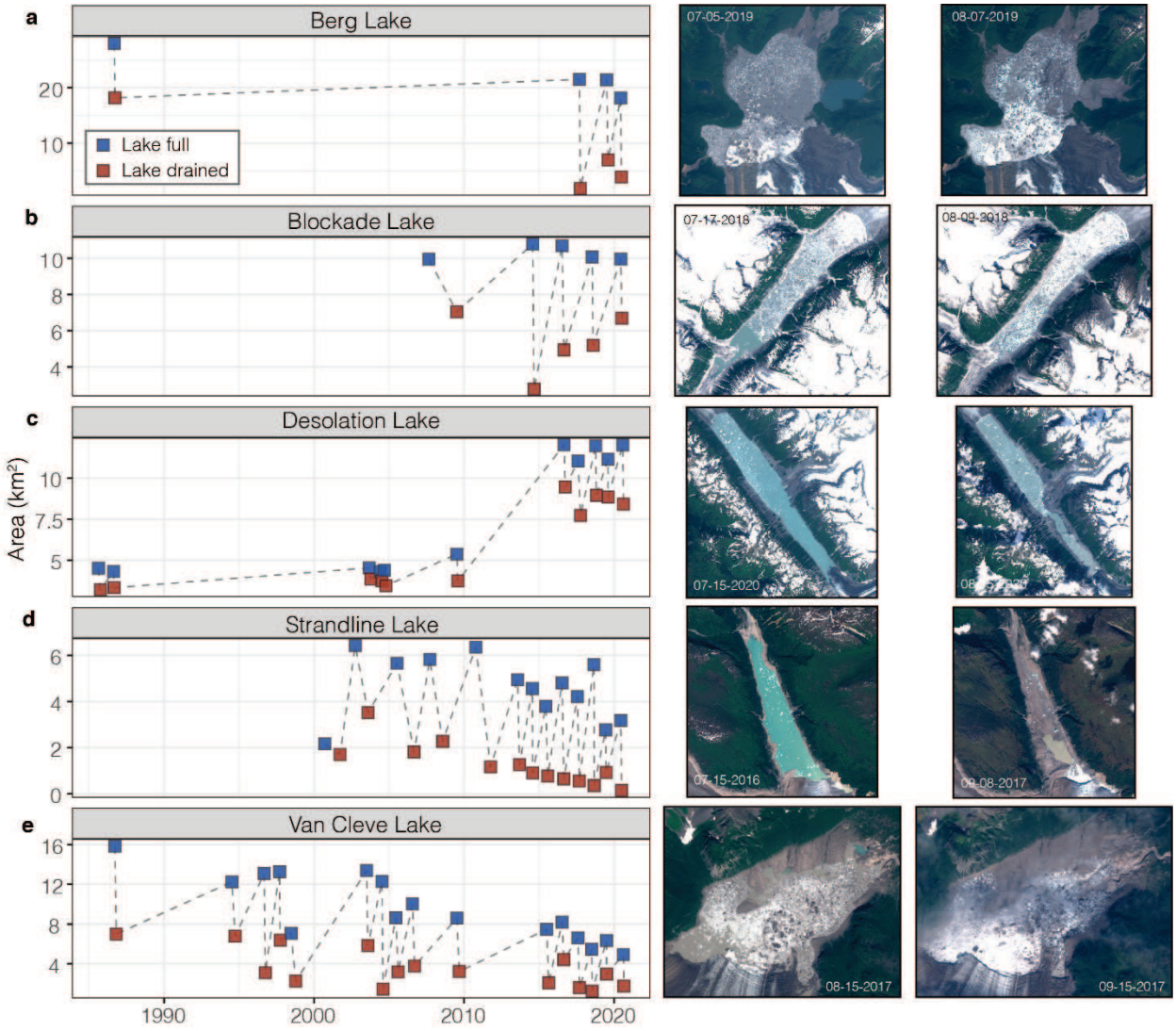

Fig. B8. Lake area before and after a drainage event for the five largest ice-dammed lakes. **a,** Berg Lake, **b,** Blockade Lake, **c,** Desolation Lake, **d,** Strandline Lake, and **e,** Van Cleve Lake and examples of imagery before and after an event.

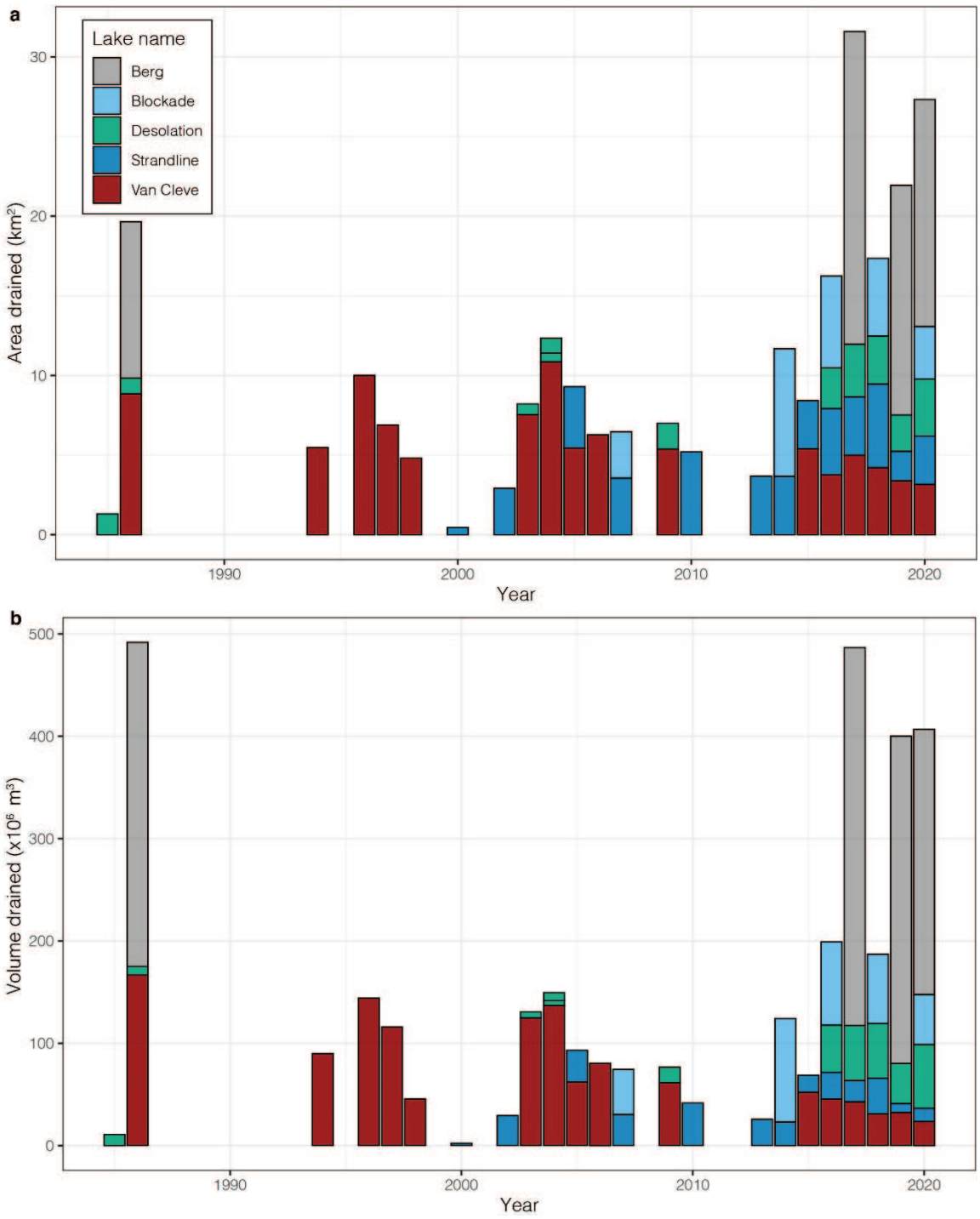

Fig. B9. Estimated area and volume for drainage events from the five largest lakes. **a,** Total area and **b,** volume drained per year from the five largest ice-dammed lakes (see Fig. B6).

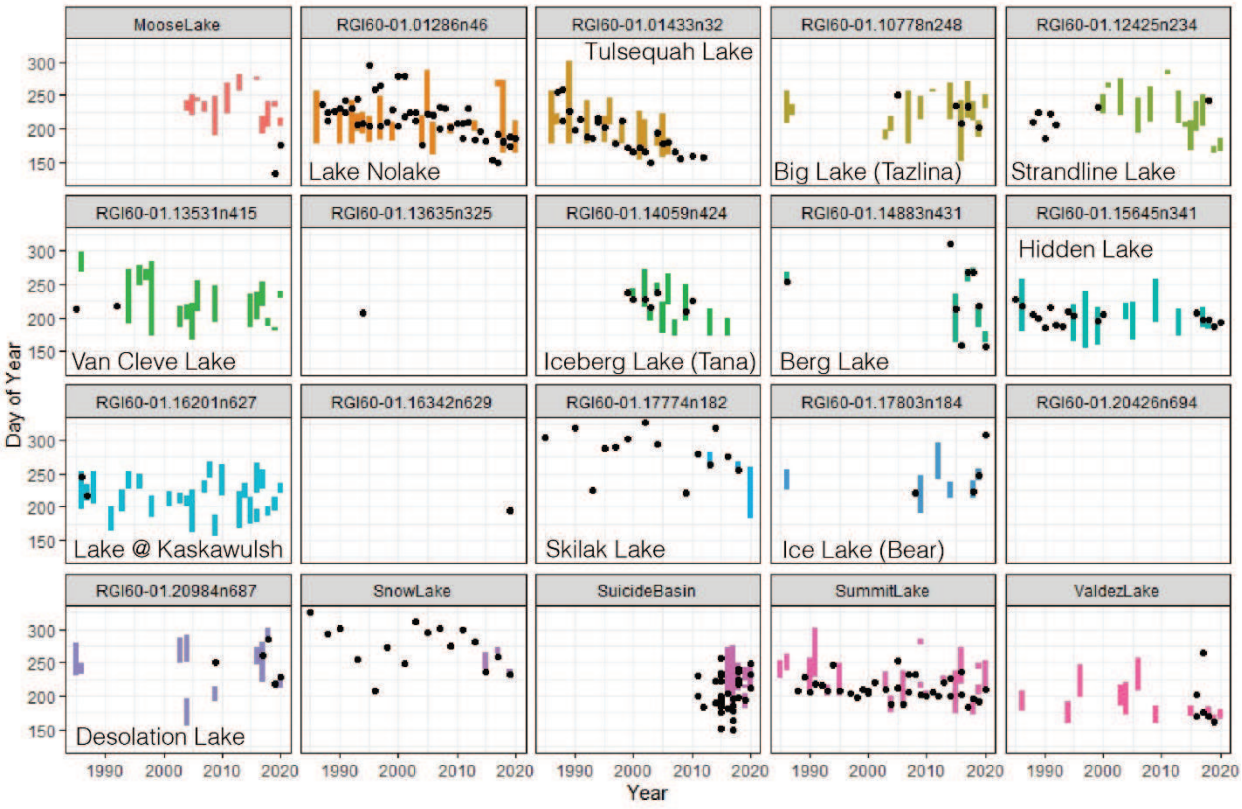

Fig. B10. Comparison between events documented in this study and previously recorded events. Segments signify the last date a lake was full to the first day it was drained identified in satellite imagery, and black dots represent the observed lake release date previously compiled by Veh et al. (2022).

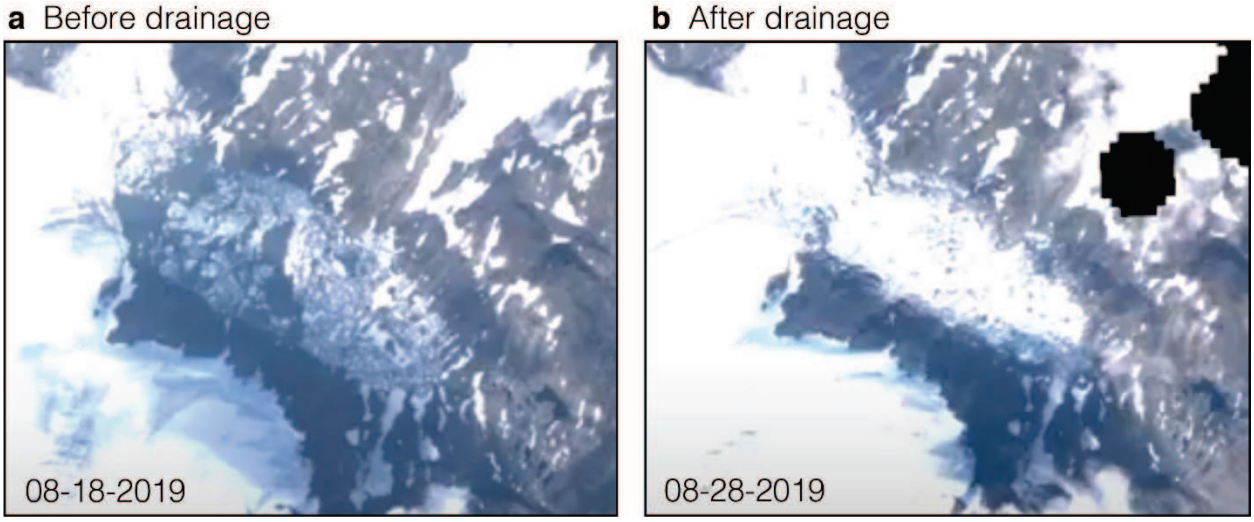

Fig. B11. Example of a difficult to detect Snow Lake drainage event. Example of **a,** before and **b,** after a visible drainage event at Snow Lake in 2019. Images were taken ten days apart. This event resulted in $350,000 in damages (Alaska GDL, 2022).

Table B1. Table with corresponding lake IDs for numbered lakes in Fig. 3.2. IDs beginning with "RGI" indicate the ID of lakes identified by Rick et al. (2022) and IDs beginning with "PM" indicate lakes identified from the Post and Mayo (1971) dataset.

St. Elias Mountains		Alaska Ranges		W Chugach Mountains		N Coast Ranges	
Lake Number	**Lake ID**	**Lake Number**	**Lake ID**	**Lake Number**	**Lake ID**	**Lake Number**	**Lake ID**
1	RGI60-01.12876n407	1	RGI60-01.26743n105	1	RGI60-01.17761n162	1	RGI60-01.20836n755
2	RGI60-01.13635n568	2	PM19	2	RGI60-01.10778n248	2	PM30
3	PM20	3	RGI60-01.22186n110	3	RGI60-01.17803n184	3	PM31
4	RGI60-01.13635n583	4	PM15	4	RGI60-01.10684n228	4	RGI60-01.23656n746
5	PM6	5	PM9	5	RGI60-01.10683n247	5	RGI60-01.20796n691
6	RGI60-01.26735n642	6	RGI60-01.22175n112	6	MooseLake	6	RGI60-01.03890n11
7	RGI60-01.26735n634	7	PM16	7	PM0	7	RGI60-01.01286n46
8	RGI60-01.13635n503	8	PM13	8	ValdezLake	8	RGI60-01.20984n687
9	PM22	9	PM12	9	PM2	9	PM40
10	RGI60-01.26735n635	10	PM18	10	PM1	10	RGI60-01.03813n284
11	RGI60-01.26735n643	11	PM10	11	RGI60-01.10778n210	11	SummitLake
12	RGI60-01.13635n423	12	PM7	12	RGI60-01.23635n224	12	PM29
13	RGI60-01.14883n564	13	PM17	13	SnowLake	13	PM41
14	RGI60-01.13635n582	14	PM8	14	RGI60-01.17774n182	14	PM42
15	RGI60-01.13635n584	15	RGI60-01.15645n341			15	PM46
16	PM5	16	PM11			16	PM32
17	PM26	17	RGI60-01.12267n150			17	RGI60-01.01433n32
18	RGI60-01.13696n427	18	RGI60-01.12425n270			18	SuicideBasin
19	PM24	19	RGI60-01.19343n305				
20	PM25	20	RGI60-01.12425n234				
21	RGI60-01.16201n627	21	RGI60-01.22178n178				
22	RGI60-01.13696n622	22	RGI60-01.00035n214				
23	PM4	23	RGI60-01.12267n77				
24	RGI60-01.14883n420						
25	PM27						
26	RGI60-01.27108n567						
27	PM28						
28	RGI60-01.13635n500						
29	RGI60-01.23649n620						
30	RGI60-01.13826n651						
31	RGI60-01.14883n431						
32	RGI60-01.13635n569						
33	RGI60-01.13531n415						
34	PM23						
35	RGI60-01.13635n513						
36	PM21						
37	RGI60-01.14186n327						
38	RGI60-01.27108n493						
39	RGI60-01.27108n571						
40	RGI60-01.27108n570						
41	RGI60-01.13635n505						
42	RGI60-01.14059n424						

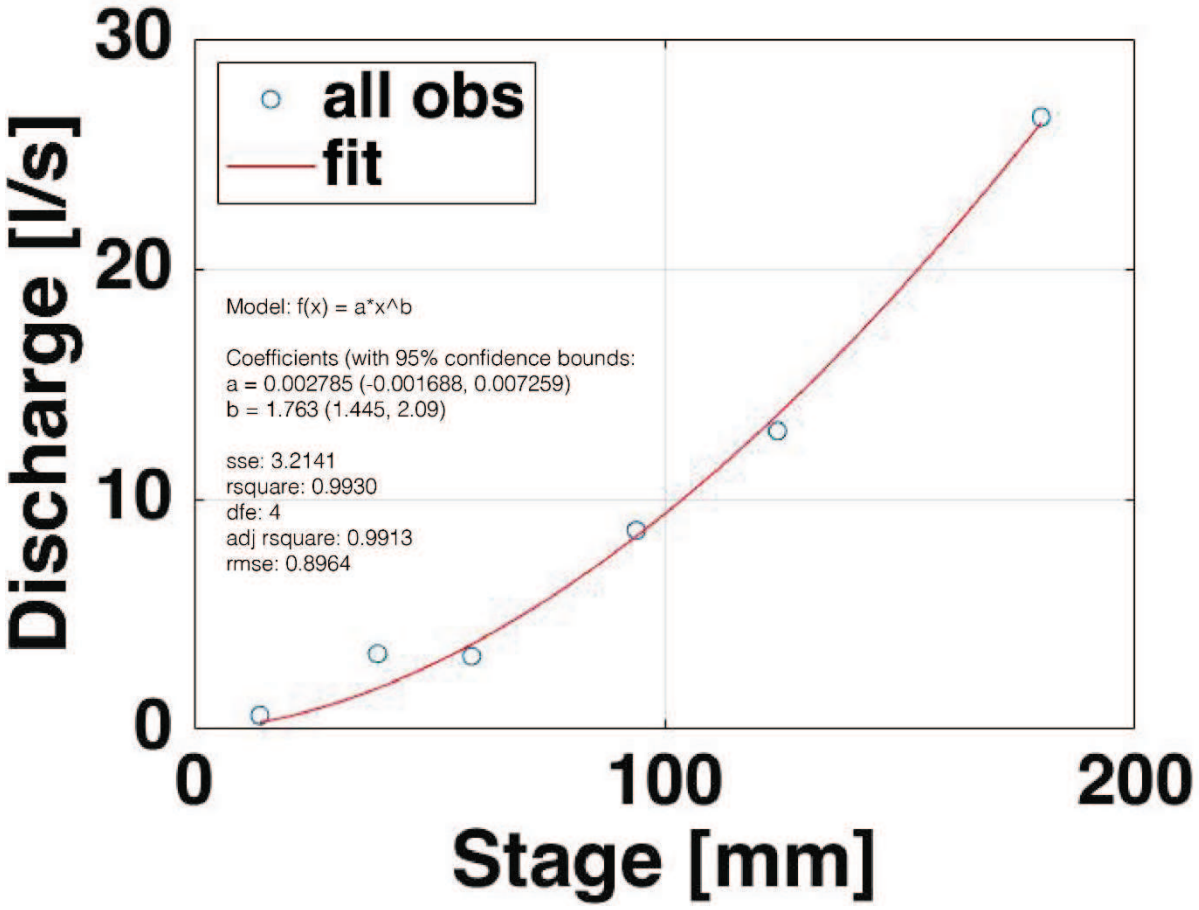

Fig. C1. Rating curve for the stream gauge located in Stream 3 and associated model output.

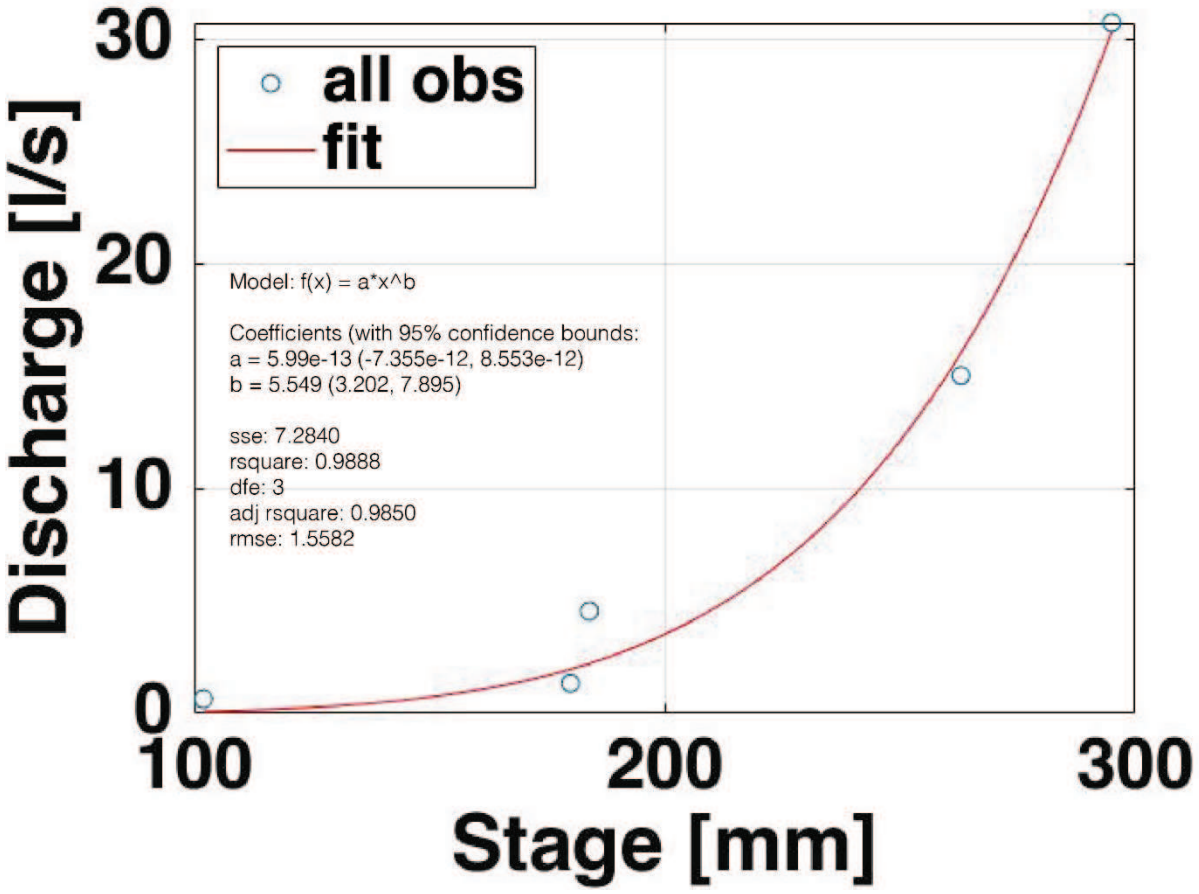

Fig. C2. Rating curve for the stream gauge located in Stream 6 and associated model output.

APPENDIX D: DATA AVAILABILITY

The ice-marginal lake inventory is available for download at:

Brianna Rick and Daniel McGrath. 2021. Multi-decadal Glacial Lake Inventory in the Alaska Region between 1984 and 2019. Arctic Data Center. https://doi.org/10.18739/A2MK6591G

An interactive map of the lake inventory in Chapter 2 can be found at https://briannarick.github.io/dataviz/AKmapNov152021.html

The full ice-dammed lake drainage event dataset from Chapter 3 is available at https://www.hydroshare.org/resource/930f35f1a68949cb9963903b95caadea/

The Google Earth Engine script for Chapter 3 is available at https://code.earthengine.google.com/b42773bcd3832d4889d3953f2fe07f2a

An interactive map of rock glaciers in Colorado can be found at https://briannarick.github.io/dataviz/RGmap_Colorado.html